Disrupting the Repeat Domain in Zebrafish Premelanosome Protein (Pmela) to Probe an Evolutionary Puzzle and Model Pigmentary Glaucoma

by

Elizabeth Dorothy Hodges

A thesis submitted in partial fulfillment of the requirements for the degree of

Master of Science

Department of Biological Sciences

University of Alberta

Abstract

The premelanosome protein (PMEL) is a functional amyloid that provides a scaffold for the even distribution of melanin and provides structure for the organelle that contains them, the melanosome. Mutations in this protein cause a plethora of phenotypes that extend beyond affecting strictly pigmentation. Dominantly inherited, non-synonymous point mutations in the repeat domain of the premelanosome protein (PMEL) cause pigmentary glaucoma in humans.

To better appreciate PMEL's biology and molecular complexity, we first positioned PMEL within an evolutionary context by comparing species, various mutations, and other related genes (GPNMB, TMEM130). We focused our attention on PMEL's repeat domain, because it is the location of many of the human mutations and is a known contributor to the functional amyloid structure. We hypothesize that PMEL's repeat domain is necessary for normal pigmentation and ocular anatomy and function. To assess this, lab members mutated the repetitive domain in zebrafish PMEL.

Prior to the collaborative efforts presented in this thesis, existing animal models with PMEL mutations were null mutants that exhibit recessive inheritance. Due to poor primary sequence conservation (despite functional conservation) in PMEL's repeat domain, the point mutations observed in humans are difficult to model in animals. Our lab generated zebrafish with an in-frame deletion within the repeat domain to test the hypothesis that the repeat domain is required for melanosome function. We compare this new mutant (with a perturbation restricted to the repeat region) to wildtype and a *pmela* null (or strong hypomorph) mutant.

This new mutant contrasts the aforementioned *pmela* null mutant zebrafish in that it is predicted to produce (modified) premelanosome protein. Moreover, we observed dominant inheritance with a phenotype in heterozygous animals. Both mutations cause larval melanosomal

and ocular phenotypes. Neither of the adult zebrafish mutants had ocular phenotypes when clinically evaluated with optical coherence tomography (OCT) and rebound tonometry. Use of rebound tonometry in zebrafish is described, and numerous baseline measures were taken. This provides an easy tool to assess intraocular pressure, a hallmark of glaucoma, in zebrafish models.

In conclusion, we found that disrupting the repeat region was sufficient to cause pigmentary and ocular pathology in zebrafish and, curiously, through mechanisms that did not align perfectly with the previously described loss of function mutations. This new repeat domain mutant provides a tool to look at the effect of the repeat region on ocular development and *in vivo* fibril structure.

Preface

This thesis is an original work by Elizabeth Hodges. The research project of which this thesis is a part, received animal research ethics approval from the University of Alberta Animal Care and Use Committee: Biosciences, Animal Use Protocol 00000077, under the auspices of the Canadian Council on Animal Care.

Chapter one is modified from Chrystal *et al.* "Functional Domains and Evolutionary History of the PMEL and GPNMB Family Proteins" (2021). This work was done collaboratively between Dr. Allison's and Dr. Walter's labs primarily written by Drs. Paul Chrystal and W. Ted Allison. I contributed to the production of figures 1-1, 1-2, 1-13 (and the writing concerning 1-13), and Tables 1-1 through 1-4. I also supervised a student, Justin Jensen, who produced figures 1-8 through 1-12 and contributed to interpretation and writing associated with those elements. All authors participated in editing the manuscript and interpreting the data.

The figures and writing in Chapters 2, 3 and 4 are my own with the exception of parts of figure 2-1 which was modified from Chapter 1, figures 2-7 and 2-8 where the optical coherence tomography images were acquired by Dr. Nicole Noel, and figures 2-2 and 2-10 which were produced by Drs. Paul Chrystal and W. Ted Allison, respectively.

Acknowledgements

Many people helped with various aspects of this thesis including all, but not limited to, members of the Allison lab, Walter Lab, and Science Animal Support Services at the University of Alberta. More specifically, Arlene Oatway and Kacie Norton for the preparation of the electron microscopy samples, Chiye Kim for her advice on quantifying the electron microscopy images, Nicole Noel for performing the OCT imaging, and Susanna Ogle/Harvest Pointe Veterinary Hospital for her help and the use of their Tonovet plus, my graduate committee, Debbie McKenzie and Daniel Barreda for their interest, encouragement, and suggestions, and Branko Braam and Wenqing Zhuang for their continued help in trying to get a servonull running for zebrafish eyes.

Special thank you to all specifically working on this research with me: W. Ted Allison, I was truly inspired to see your creativity seamlessly pivot with the pandemic and always felt the much needed support and direction from you and Michael Walter with this project. I am very grateful to have experienced the effective and positive learning environment you have both fostered. Paul Chrystal, Tim Footz, Justin Jensen, and Lance Doucette for their patience with me at the bench top or laptop, advice, and hard work and interest in creating many parts of this work.

This work was made possible through grants from the Alberta Innovates Prion Research Institute, Fighting Blindness Canada, and my Graduate Excellence Scholarships

Table of Contents

List of Tables

List of Figures

List of Figures

List of Abbreviations

ACD - amyloidosis cutis dyschromica

ADAM - a disintegrin and metalloprotease

ALS - amyotrophic lateral sclerosis

ANOVA - analysis of variance

AUP - animal use protocol

BACE2 - β-site amyloid precursor protein cleaving enzyme 2

BLAST - Basic Local Alignment Search Tool

BLASTp – protein BLAST

BLOSUM - blocks substitution matrix

BS – bootstrap

C - carboxy

CAF - core amyloid fragment

cDNA -complementary DNA

Ch - chromosome

CRISPR - clustered regularly interspaced short palindromic repeats

Cyt – cytosomal portion, or cytoplasmic domain

DIN – drug identification number

DNA - Deoxyribonucleic acid

dpf – days post fertilization

Ex - example

e.g. - example given

et al. - et alia (latin for with others)

E-value - expected-value

GPNMB - glycoprotein nonmetastatic melanoma protein B

i.e. - id est (latin for that is)

Id – identification

IOP -intraocular pressure

KLD – kringle like domain

OCT -optical coherence tomography

MITF - melanocyte-inducing transcription factor

MCOA – multiple congenital ocular anomalies

mmHg -millimeters of mercury (unit of pressure)

MUC2 – mucin 2

MUSCLE - multiple sequence comparison by log-expectation

MS222 -tricaine methanesulfonate

n/a - not applicable

NCBI – national center for biotechnology information

N - amino

NTR – N terminal region

PDS – pigment dispersion syndrome

PG – pigmentary glaucoma

PMEL - premelanosome protein

Pmela - zebrafish premelanosome protein A

Pmelb - zebrafish premelanosome protein B

PMEL - human premelanosome protein gene

Pmel - general animal premelanosome protein gene

pmela - zebrafish premelanosome protein A gene

pmelb – zebrafish premelanosome protein B gene

PTHR – PANTHER - protein annotation through evolutionary relationship

PKD – polycystic kidney disease domain

RADAR - rapid automated detection of repeats

RPE – retinal pigmented epithelium

RPT – repeat domain

SINE – short interspersed nuclear element

SP – signal peptide

tBLASTn – translate nucleotide BLAST

TM – transmembrane domain

TMEM -transmembrane

WT – wildtype

ZFIN – zebrafish information network

Goals of this Thesis

Given the interest not only from an evolutionary and amyloid biology perspective (discussed in Chapter 1), but also the role in human disease, the functionality of the repeat region of the premelanosome protein (PMEL) warrants further investigation *in vivo*. We sought to test the hypothesis that the repeat region of PMEL is necessary from the organelle (melanosome) to the organ (eye) level.

In Chapter 2, we employed zebrafish as a model as it allowed us to manipulate *pmela* in a targeted fashion that limited perturbations to the repeat region. Quantifying melanosome characteristics in the retinal pigmented epithelium served as a proxy for Pmel fibril formation in zebrafish melanosomes. Larval ocular phenotypes were similar to what has been described in other zebrafish *pmela* mutants. Intriguingly, unique heterozygote phenotypes in the repeat domain mutant question whether there is some toxicity or novel function due to disturbance in the repeat region of the *pmela*. A more dominant inheritance is in line with many previously described mutations in this gene. The adult mutant fish were clinically assessed to see if they reflected the human disease phenotype of glaucoma.

In Chapter 3, I describe my efforts to develop a minimally invasive measure of intraocular pressure. This could be used for phenotype screening as well as in longitudinal research studies using zebrafish. I provided numerous baseline measurements which will hopefully aid veterinarians already using this equipment. The overall goal was to contribute a tool to improve phenotyping of glaucoma-like characters in the powerful zebrafish model.

Chapter 1.
Functional Domains and Evolutionary History of the PMEL and GPNMB Family Proteins

This Chapter is modified from:

Chrystal PW[1], T Footz[1], **ED Hodges**, JA Jensen, MA Walter*, WT Allison*. 2021. Functional domains and evolutionary history of the PMEL and GPNMB family proteins. *Molecules*. 26(12): 3529.

[1]co-first authors. *co-corresponding authors.

doi: 10.3390/molecules26123529.

- Highlighted in *Molecules* listed as a *Feature Paper.*

Author Contributions: Formal analysis, P.W.C., T.F., J.A.J. and **E.D.H.**; writing—original draft preparation, P.W.C., T.F., **E.D.H.** and W.T.A.; visualization, P.W.C., T.F., J.A.J. and **E.D.H.**; supervision, M.A.W. and W.T.A. and funding acquisition, M.A.W. and W.T.A. All authors contributed to writing—review and editing. All authors have read and agreed to the published version of the manuscript.

In particular, **E.D.H.** contributed to this chapter via the production of figures 1-1, 1-2, 1-13 (and the writing concerning 1-13) and Tables 1-1, 1-2, 1-3, and 1-4 in addition to supervising a student, J.A.J., who produced figures 1-8, 1-9, 1-10, 1-11, and 1-12. She also participated in editing the manuscript and interpreting the data.

1.1 Abstract

The ancient paralogs premelanosome protein (*PMEL)* and glycoprotein nonmetastatic melanoma protein B (*GPNMB)* have independently emerged as intriguing disease loci in recent years. Both proteins possess common functional domains and variants that cause a shared spectrum of overlapping phenotypes and disease associations: melanin-based pigmentation, cancer, neurodegenerative disease and glaucoma. Surprisingly, these proteins have yet to be shown to physically or genetically interact within the same cellular pathway. This juxtaposition inspired us to compare and contrast this family across a breadth of species to better understand the divergent evolutionary trajectories of two related, but distinct, genes. In this study, we investigated the evolutionary history of *PMEL* and *GPNMB* in clade-representative species and identified *TMEM130* as the most ancient paralog of the family. By curating the functional domains in each paralog, we identified many commonalities dating back to the emergence of the gene family in basal metazoans. *PMEL* and *GPNMB* have gained functional domains since their divergence from *TMEM130*, including the core amyloid fragment (CAF) that is critical for the amyloid potential of PMEL. Additionally, the *PMEL* gene has acquired the enigmatic repeat domain (RPT), composed of a variable number of imperfect tandem repeats; this domain acts in an accessory role to control amyloid formation. Our analyses revealed the vast variability in sequence, length and repeat number in homologous RPT domains between craniates, even within the same taxonomic class. We hope that these analyses inspire further investigation into a gene family that is remarkable from the evolutionary, pathological and cell biology perspectives.

1.2 Introduction

In recent years, the disease-causing genes *GPNMB* (Glycoprotein nonmetastatic melanoma protein B) (i.e., HGFIN, NMB and Osteoactivin) and *PMEL* (premelanosome protein) (i.e., PMEL17, SILV, MMP115 and gp100) have generated increased interest from disparate biomedical fields. *GPNMB* and *PMEL* are related genes that encode for proteins with a common functional domain architecture: a signal peptide, core amyloid fragment, Kringle-like domain and a single transmembrane domain [1]. Consistent with this common architecture, both have also been implicated in the same diverse biological roles via their association with phenotypic presentation and disease, i.e., cancer [2–6], glaucoma [7–9], neurodegenerative disease [10–13],

melanin-based pigmentation [14–17] and amyloid formation/amyloidosis [18–22]. It is therefore surprising that these related proteins with a strikingly similar suite of functional domains have yet to be identified as interacting in, or being partially redundant in, any biological process or pathway.

PMEL is a single-pass Type I transmembrane glycoprotein expressed in pigmented melanocytes, retinal pigmented epithelium and the substantia nigra [5]. This protein is processed through several complex steps of O-linked glycosylation and ADAM/BACE2/proprotein convertase/γ-secretase proteolytic cleavages [23–30] and shuttled to stage I melanosomes. Mature PMEL fragments assemble into striated amyloid fibrils within stage II melanosomes, elongating the organelles and providing a scaffold for eumelanin deposition, driving melanosome maturation [24,25,31–33]. In this role, PMEL represents a protein of significant interest as a functional amyloid (discussed further in references [20,34]). Amyloid has historically been studied in relation to its toxicity and association with degenerative neuropathies such as Alzheimer's and Parkinson's disease. How the PMEL amyloid is tolerated within cells is therefore of major therapeutic interest [34,35].

PMEL mutations have been selected in domesticated animals for at least a century [36] thanks to desirable changes in coats and plumage colors. However, it was not until the 1990s that molecular genetic analyses have identified the allele in *Pmel* responsible for the autosomal recessive, progressive greying fur of the Silver mouse [37,38]. Since then, a panoply of striking pigmentation patterns has been associated with mutations of the *pmel* gene (Figure 1-1). The majority of these represent recessive, loss-of-function mutations that give rise to hypopigmentation phenotypes [9,38–42]. However, dominant, missense mutations have also been described, suggestive of gain-of-function (GOF) pathology [16,17,43–45]. These dominantly inherited mutations sometimes cause more severe phenotypes, including ocular anterior segment dysgenesis (Figure 1-1) and deafness [46–51]. In humans, autosomal dominant pigmentary glaucoma is caused by missense *PMEL* mutations (Figure 1-1), providing a tantalizing suggestion that GOF mutations in a (usually) strictly regulated functional amyloid can lead to retinal neuropathy [9].

Like PMEL, the GPNMB protein undergoes glycosylation and proteolytic cleavage to produce the mature peptide [52–55]. GPNMB also localizes to melanosomes [54,56,57], is transcriptionally regulated by the Melanocyte-Inducing Transcription Factor (MITF) [58–61]

and, when mutated, can lead to hypopigmented lesions and pigmentary glaucoma in mice (Figure 1-2) [7,8,18,19]. Surprisingly, there has been no functional evidence of the amyloid-forming roles of GPNMB, owing to the post-transcriptional modification of its PKD domain [62]. Human mutations of *GPNMB* cause recessive and semi-dominant amyloidosis cutis dyschromica [18,63–66], a condition characterized by amyloid deposition in the papillary dermis; remarkably though, the GPNMB protein is not a constituent of amyloid deposits [18]. Furthermore, *GPNMB* is more broadly expressed than PMEL and has been implicated in a broad array of biological processes outside of pigmentation.

GPNMB is highly expressed in the nervous system, kidney nephrons, macrophages, dendritic cells and astrocytes [52,61,67–70]. A major role appears to be as a negative regulator of inflammation [71,72], and the breakdown of the ocular immune privilege is hypothesized to be the cause of *Gpnmb*-associated glaucoma in mice [73,74]. GPNMB is required for the differentiation of osteoblasts [58,67,75–80], and the protein localizes to the plasma membrane, as well as is cleaved in some cell types to act as a matricellular protein regulating extracellular matrix remodeling [53–55,58,81–88]. Most strikingly, the heightened expression of *GPNMB* has been associated with amyotrophic lateral sclerosis (ALS) [10,11], Parkinson's disease [12,89,90] and Alzheimer's Disease [91], all of which have pathogenic amyloids as major components of the disease progression. Perhaps counterintuitively, elevated levels of GPNMB are neuroprotective in Parkinson's and ALS models, and the protein has not been described as a component of amyloid plaques [92–94].

Despite apparent differences in protein functions, the *GPNMB* and *PMEL* genes are putative paralogs that arose from an ancient common ancestor. In this paper, we synthesized the existing literature and performed new bioinformatic comparisons to help situate these (and future) comparisons of *PMEL* and *GPNMB* in the correct framework. We identified the enigmatic *TMEM130* as the most ancient paralog in the protein family, from which *PMEL* and *GPNMB* evolved in early craniate radiation. We then compare-and-contrasted their protein domains across a diversity of metazoans to identify the characteristic motifs unique to each gene. Of particular interest, the *PMEL*-specific repeat (RPT) domain, a key accessory domain to amyloid formation, was thoroughly analyzed across clade-representative species to interrogate the most highly conserved features of the domain. We hope that this work will stimulate interest

in this important protein family, further elucidating the overlapping but divergent roles of GPNMB and PMEL and encouraging investigations into the functions of TMEM130.

1.3. Methods

Animal Ethics

Zebrafish were maintained and bred using typical husbandry methods and with the approval of the Animal Care and Use Committee at the University of Alberta (protocol AUP00000077). Zebrafish mutants *pmela*^{ua5022} described previously as larvae [9] was assigned as ZFIN ID: ZDB-ALT-191119-1.

Identification of PKAT Family Homologs

PKAT (PKD- and KLD-Associated Transmembrane) homologs were identified via tblastn searches of the NCBI (https://blast.ncbi.nlm.nih.gov/Blast.cgi) and ENSEMBL (https://uswest.ensembl.org/Multi/Tools/Blast?db=core) genome assembly databases. For *E. muelleri*, the BLAST search was performed at https://spaces.facsci.ualberta.ca/ephybase/.The query sequence was human TMEM130, GPNMB or the PMEL PKD domain. All default parameters were maintained, including BLOSUM62 and an E-value cut-off of 0.05. For predicted/uncharacterized loci, a reciprocal blastp to the human assembly was performed. Percentage homology between paralogs was reported as the sequence identity/sequence length calculated after Clustal Omega alignment.

Annotating PKAT Protein Domain Architecture and Intron–Exon Architecture

Human TMEM130 (ENST00000416379.6), GPNMB (NP_001005340.1) and PMEL (ENST00000548493.5) protein sequences were analyzed with the InterPro Scan web client (https://www.ebi.ac.uk/interpro/search/sequence) [95] to receive domain predictions. Schematic representations of these domains were created in CorelDRAW X7. Exon length was determined by uploading genomic DNA sequences of each gene into Geneious software and exporting the exon length information. Schematics representing the protein domain boundaries were created in CorelDRAW X7.

Production of Cladogram/Phylograms

The clade names and branching structure of Figure 1-4 were derived from the NCBI Taxonomy Browser, building a phylip-formatted tree with selected taxa at https://www.ncbi.nlm.nih.gov/Taxonomy/CommonTree/wwwcmt.cgi. The phylogram from Figure 1-6 was created using clade-representative protein sequences. Sequences were uploaded to MEGA X, and phylogeny was inferred using the Maximum Likelihood method and Whelan and Goldman + Frequency model. One thousand bootstrap iterations were performed, and Trichoplax tmem130 was chosen as the outgroup. Color of the monophyletic groups was added in Photoshop v22.1.

Synteny Analysis

One hundred genes upstream and downstream (or until the end of the chromosome) of the lamprey PKAT outparalogs were downloaded from the NCBI genome assembly (kPetMar1.pri). The gene identity tracks were then compared against the human Ch7 and Ch12 (GRCh38.p13), chicken Ch2 and Ch33 (GRCg6a) and skate Ch2 and Ch46 (sAmbRad1.pri). Genes shared with any of the other species were used as evidence of paralogous regions. The schematic representation figure was produced in Photoshop v22.1

Functional Domain Alignments

Representative protein sequences for each gene in each major clade were chosen from the annotated and curated organismal lists at Ensembl (https://uswest.enseml.org/index.html) or NCBI (https://www.ncbi.nlm.nih.gov/) where possible. For incompletely annotated genes, BLASTp and tBLASTn [96' searched of the NCBI database (http://blast.ncbi.nlm.nih.gov/Blast.cgi) were performed to identify representative gene entries or unannotated gene fragments in whole genome shotgun contigs. Protein sequences were alligned in Geneious Prime 2020.1.2, created by Biomatters (https://www.geneious.com using the MUSCLE algoritm and manual editing.

RPT Domain Identification and Comparison

Rapid Automated Detection of Repeats (RADAR) (https://www.ebi.ac.uk/Tools/pfa/radar/) [97,98] was used to identify repetitive regions in the

premelanosome (*Pmel*) protein amino acid sequences prior to aligning repeats via similarity by hand. The corresponding cDNA of each protein repeat was aligned to correspond with the amino acids, polarity color coding was selected and consensus sequences and sequence logos were made in Geneious Prime.

1.2 Results and Discussion

Mutations of PMEL or GPNMB Cause an Overlapping Spectrum of Pathologies but Highlight the Disparate Functional Roles of Each Protein

Many mutations have been described in the *PMEL* gene from a variety of animals, owing to the striking pigmentary changes that result (Figure 1-1). Correlating genotypes to phenotypes reveals that missense mutations in *PMEL* homologs typically exhibit a dominant inheritance pattern (Table 1-1 and the references therein). For example, the dominant inheritance of the pigment phenotypes in white chicken, Charolais cattle and Silver dapple horses are caused by missense mutations in *PMEL*. This contrasts the recessive pigmentation phenotypes in the Silver/*Pmel*$^{-/-}$ mouse and two alleles of zebrafish, which harbor nonsense mutations (Table 1-1). This correlation is also apparent in human dominantly inherited pigmentary glaucoma associated with missense mutations in *PMEL* (Table 1-2 and the references therein). The exceptions to this trend include a variable expansion of the SINE intron insertion within Merle dogs that is a dominantly inherited nonsense mutation. This overall pattern suggests that nonsense mutations in *PMEL* homologs are often better-tolerated and require two mutant alleles for detectable phenotypes. However, the phenotype–genotype correlation for pigmentation defects is not retained across the ocular phenotypes associated with *PMEL* mutation, which have been described in zebrafish (recessive), horses (recessive), dogs (recessive) and humans (dominant). In contrast, the human disease amyloidosis cutis dyschromica (Figure 1-2) is caused by *GPNMB* mutations with both recessive and semi-dominant inheritance patterns described (Table 1-3 and the references therein). Causal mutations can be either nonsense or missense, and the symptoms include generalized hypopigmented skin mottled with hyperpigmented macules [18]. While no detectable phenotype has been described in zebrafish *gpnmb* mutants, murine *Gpnmb*, *Tryp1* double-homozygotes develop pigment dispersion, pigmentary glaucoma and iris atrophy (Table 1-4) without reported dermal amyloidosis [8,74]. These murine phenotypes highlight an

intriguing overlap between *Gpnmb* and *Pmel*, as the mutations in each can result in pigmentary and ocular defects.

TMEM130, GPNMB and PMEL form a Protein Family and Share a Common Protein Domain Architecture

GPNMB and *PMEL* have long been recognized as outparalogs (genes arising from an ancient duplication event (for review, see reference [99]) and studied together as a gene family. However, *TMEM130* is also a recognized member of the PANTHER melanocyte protein PMEL-17-related (PTHR11861) family (http://www.pantherdb.org) but remains poorly studied. If *TMEM130* does indeed represent a third member of the gene family, then comparisons of the three genes could provide insight as to how *PMEL* and *GPNMB* evolved different functions. Despite being predicted homologs, the MUSCLE alignment of the full-length human sequences (Table 5 and Table 6) demonstrated the limited sequence identity of *PMEL* to the other members at either the cDNA level (38.7% vs. *TMEM130* and 33.2% vs. *GPNMB*) or the protein level (13.7% vs. TMEM130 and 24.9% vs. GPNMB). We therefore opted to investigate the similarities at the level of the shared domain architecture. The sequences for human TMEM130 (ENST00000416379.6), GPNMB (ENST00000647578.1) and PMEL (ENST00000548493.5) proteins were run through InterPro Scan to identify the functional domains based on the database signatures [95]. As expected, the GPNMB and PMEL proteins displayed a conserved protein domain architecture: (1) an N-terminal secretory pathway targeting signal (signal peptide, SP), (2) a large non-cytoplasmic (luminal) region containing an immunoglobulin-like polycystic kidney domain (PKD) and (3) a single Type I transmembrane domain with a short, C-terminal cytosolic domain (Figure 1-3A and Table 7).

The InterPro Scan analysis does not annotate the highly conserved Kringle-like domain (KLD) that has been previously characterized in *GPNMB* and *PMEL* [100,101]; this domain, (named after the triple-loop fold Kringle domain) lies downstream of the PKD (Figure 1-3A dashed line) and contains six highly conserved cysteine residues that are critical for forming the disulphide bonds of mature PMEL dimers [100]. However, the InterPro Scan analysis does identify a disordered (low complexity) region unique to PMEL. This region corresponds to the enigmatic PMEL repeat domain (RPT), which is sufficient to form fibrils outside of the normal physiological conditions [21,102,103] but is dispensable for amyloid formation in vivo

[22,104,105]. Instead, the most recent data suggests that the RPT is an essential accessory domain required for physiological amyloid packing [22]; this is consistent with the absence of a RPT domain in GPNMB, which does not contribute to melanosome amyloid [62].

An analysis of the human TMEM130 domain architecture revealed that, despite being considerably shorter than the other two family members (435 residues vs. 588 GPNMB and 661 PMEL), TMEM130 has a strikingly similar domain architecture (Figure 1-3B and Table 7). The signal peptide, PKD and transmembrane domains were present and conserved in order with the other two proteins. Furthermore, a KLD was resolved via multiple sequence alignment (see section 3.6)). Despite lacking identifiable homology in the region between the SP and PKD domains, this analysis strongly supports the inclusion of TMEM130 as a member of the same protein family. Consistently, all three proteins were identified as "melanocyte protein PMEL-17-related family members". This nomenclature is based upon the previous naming convention of PMEL (PMEL-17) and is outdated. We therefore propose the use of "PKD- and KLD-Associated Transmembrane (PKAT) protein family" for this interesting protein family. This name reflects the highly conserved domain architecture of the three human gene members and remains inclusive of species-specific paralogs (inparalogs) that arise during gene duplication events (see section 3.3).

The PKAT Family Genes Are Distantly Related Paralogs and TMEM130 Represents the Most Ancient Homolog

The conservation of the domain architecture between all three PKAT members suggests that these genes are either related by descent (homologs) or arose via convergent evolution. To investigate if there is support for homology, we first investigated when each gene arose. Using the human PKD domains, we can identify hundreds of potential homologs from the ENSEMBL and NCBI databases using translated nucleotide (tblastn) searches. A selection of these hits has been used as representatives of major animal clades and was included in all subsequent analyses (Table 8). The first evidence of putative *tmem130* orthologs was discovered in Placozoa (*T. adhaerens*) and *Cnidaria* (*P. damicornis* and *N. vectensis*), but no regions of significant sequence identity can be detected in the early metazoan genome assemblies of *Porifera* (*E. mulleri*) and *Ctenophora* (*P. bachei*) [106,107]. In more derived species, including the *Protostomia*, *Hemichordata* and *Echinodermata*, *tmem130* orthologs can also be identified (Figure 1-4);

however, no *gpnmb* or *pmel* orthologs were identified in any of the invertebrate clades examined. These data suggest that *tmem130* is the most ancient of the PKAT family genes and originated in early eumetazoans prior to the divergence of *Cnidaria*, Placozoa and *Ctenophora.*

Orthologs of all three PKAT family members were identified in cartilaginous fish (*A. radiata* and *C. milli*), and all subsequent *Gnathostomes* that were analyzed (Figure 1-4). Assuming the PKAT genes are homologs then this pattern suggests that two rounds of *TMEM130* duplication followed by neo- or sub-functionalization [108,109] gave rise to vertebrate *TMEM130*, *GPNMB* and *PMEL*, with the final of the four paralogs being lost. This proposal is consistent with the two rounds of whole-genome duplications (1R and 2R, Figure 1-4) that occurred during early vertebrate evolution [110–112]. While the exact timing of the 2R duplication is still contested [113–117], the inheritance pattern of the PKAT gene family favors the 2R duplication occurring prior to the divergence of the Cyclostomata: *gpnmb* and *pmel* orthologs discovered in lamprey (*P. marinus*) and hagfish (*E. burgeri*). Intriguingly, no evidence for the *tmem130* orthologs were discovered in the early *Chordates* lancelet (*B. belcheri*) or tunicate (*C. intestinalis*), nor in the Cyclostomes, suggesting an independent *tmem130* gene loss in these species [118] or incomplete genome sequences that prevent orthologs from being identified. The *tmem130* orthologs were also absent from several protostome species assemblies that we probed (e.g., *C. elegans* WBcel235 and *Octopus vulgaris* ASM395772v1), despite orthologs existing in other members of the clade. In conjunction with the absence of *tmem130* in basal chordates, these data suggest that *TMEM130* has been lost independently multiple times throughout animal evolution. Conversely, duplication of the PKAT genes was also apparent. Two *gpnmb* and two *pmel* orthologs were discovered in the lamprey, presumably via a segmental duplication similar to that which gave rise to the six lamprey hox clusters compared to the four found in most tetrapods [119]. Furthermore, zebrafish (and other teleosts) possess two recent *PMEL* inparalogs (*pmela* and *pmelb*) but only one copy of the other PKAT genes, likely because of the teleost-specific genome duplication event (3R, Figure 1-4) and subsequent rapid gene loss [120–123]. Taken together, these data support a paralogous relationship between the PKAT family genes and demonstrate that *TMEM130* is the most ancient, eumetazoan gene from which the other two genes evolved. It has not escaped our notice that the emergence of *GPNMB* and *PMEL* also coincides with the evolution of the complex, camera-style eye. Considering the

ocular phenotypes that arise when these genes are mutated, it seems plausible that these two events are related.

To further interrogate the paralogous relationship of the PKAT genes, we next examined the intron–exon structure of the clade-representative genes. The exon length (bps) from the PKAT genomic DNA sequences was correlated with the functional domains that they encoded. When displayed graphically, several features were apparent that supported a shared origin (Figure 1-5). A signal peptide domain was detected in all the sequences examined and was encoded by the first two exons of the gene. In 27/31 genes, the majority of the SP was encoded within an initial, small (< 110 bp) exon. The Kringle-like domain was encoded by two exons in 30/31 genes examined, and the exon lengths were conserved by ± 5% in most of the clade representatives: *TMEM130* 85 bp (9/11) and 203 bp (9/11), *GPNMB* 103 bp (7/10) and 206 bp (7/10) and PMEL 106 bp (6/10) and 206 bp (9/10). This analysis also supported an ancient homology, because the close similarities of the exon sizes between these three genes were consistent with them arising from a common origin.

Interestingly, this comparison of gene architectures revealed differences between the genes that speak to the evolution and divergence of the gene family. Firstly, the PKD domain was encoded by two exons in 9/11 of the *TMEM130* genes examined but within a single exon in *GPNMB* and *PMEL* (Figure 1-5). This suggests that there was a loss of the intron from the PKD after the 1R genome duplication and prior to the divergence of *GPNMB* and *PMEL* as novel genes. Furthermore, there were multiple exons introduced upstream of the PKD in the *GPNMB* and *PMEL* genes that were absent from *TMEM130*. These exons (ex2-5) showed particularly high conservations ± 5% of the exon length in both *GPNMB* (153 bp (7/10), 144 bp (6/10), 174 bp (6/10) and 159 bp (5/10)) and *PMEL* (135 bp (6/10), 147 bp (9/10), 141 bp (6/10) and 16 2bp (10/10)), respectively, supportive of a shared origin. In *PMEL*, these exons encoded for the N-terminal region and core amyloid fragment, which was critical for the formation of amyloid filaments [1]. It was therefore surprising that the exon length was conserved in this region in GPNMB that does not form amyloids; however, this apparent contradiction may be due to a lack of protein residue conservation between the two. Finally, the RPT domain, which is found only in *PMEL* orthologs, was encoded within either one or two exons in the species examined without any discernable patterns between the species.

TMEM130 Is a Sister Group of Both GPNMB and PMEL

With evidence of a paralogous relationship between the PKAT family genes, we next produced a Maximum Likelihood phylogenetic tree based on the whole-protein sequence alignment of the clade representative sequences. TMEM130 was the most ancient paralog detected (Figure 1-4) and was selected as an outgroup for tree construction, and the *Trichoplax* sequence was used as the most basal PKAT sequence that was identified. Within our model, there are three strongly supported monophyletic groups that correlated to TMEM130, GPNMB and PMEL (Figure 1-6). In our phylogram, TMEM130 formed a sister group with both GPNMB and PMEL.

Intriguingly, sea lamprey possesses four inparalogs: *pmel*, *pmel-like*, *gpnmb* and *gpnmb-like* but no putative *tmem130* ortholog. These inparalogs cannot confidently be separated into the three clades and, instead, form a separate, paraphyletic group of their own (Figure 1-6, bracket). Unexpectedly, gpnmb and pmel-like are predicted to be more closely related to each other, whereas pmel and gpnmb-like are separately more closely related to each other, suggesting that these inparalogs may be incorrectly annotated. To test whether lamprey *gpnmb-like* (XP_032831262.1) and *pmel-like* (XP_032807179.1*)* were named incorrectly, we examined the chromosomal synteny of up to 100 genes upstream and downstream of the lamprey PKAT genes, making comparisons to the homologous chromosomal regions (paralogons) of both GPNMB and PMEL in three Gnathostomes: human, chicken and thorny skate (Table 1-9). All four lamprey chromosomal regions have syntenic genes in common with *Gnathostome GPNMB* and *PMEL*; surprisingly, for each lamprey PKAT gene, there are more neighboring genes in common with the homologous *Gnathostome* GPNMB region than with the PMEL regions (Figure 1-7). Lamprey *gpnmb* and *pmel-like* possess the strongest signals, each with a higher ratio of genes syntenic with Gnathostome *GPNMB* than with *PMEL* (47/3 = 15.7 and 33/6 = 5.5, respectively). Conversely, lamprey *pmel* and *gpnmb-like* have a lower ratio of genes syntenic with Gnathostome *GPNMB* than with *PMEL* (22/16 = 1.4 and 25/10 = 2.5, respectively). Since these analyses demonstrate that the lamprey paralogons have mixtures of homologous genes relative to both the *GPNMB* and *PMEL* chromosomal regions (Table 9), it was therefore not possible to conclude what gene names ultimately should be applied to the lamprey inparalogs *pmel-like* and *gpnmb*-like via synteny analysis alone. However, Gpnmb-like does appear to possess an RPT domain (discussed in detail below), suggesting that it may be the canonical inparalog of *pmel*.

The PMEL RPT Domain Sequence Is Highly Divergent Between Species but Considerably Conserved Within Repeat Units of Most Species

Despite the poor overall sequence conservation between the PKAT family proteins, several functional domains have been described as being well-conserved between PMEL and GPNMB [124]. The conservation of functional domains is suggestive of a common function within the cell; however, this is not appreciated with the repeat domain between species. The repeat domain (RPT) is a low complexity region unique to PMEL, and in mammals, it contains a variable number of proline/serine/threonine-rich imperfect repeats [103]. The RPT domain is controversial with respect to its role in PMEL amyloid formation, having originally been shown to be sufficient for fibril formation in vitro [102,125] but also dispensable for the formation of fibrils containing the N-terminal region and PKD domains [104,105]. Recent studies have instead demonstrated that the RPT domain has an accessory role in amyloid formation, at least in the few species studied to date. The PMEL RPT domain undergoes the heavy O-glycosylation of Thr/Ser residues that are required to sustain the sheet-like architecture of melanosomal amyloids. Deletion of the RPT domain or pharmacological inhibition of O-glycosylation causes amyloid collapse. Conversely, replacement of the RPT domain with a region of the MUC2 gene (which is also highly O-glycosylated) can rescue the fibril architecture [22].

To investigate the evolutionary relationship between orthologous PMEL RPT domains, we used RADAR predictions [97,126] and manually curated these to predict the RPT domain sequences of each PMEL protein (Figures 1-8 through 1-12). Our results highlighted the high variability of the RPT domain in terms of the repeat unit length and repeat unit number between clade-representative organisms (Figure 1-8, c.f., thorny skate has seven 22-mer repeats vs. human has ten 13-mer repeats). These data also highlight the difficulty in accurately predicting the RPT domain sequence, since some organisms, like the common lizard, have a dearth of repeating residues per unit yet retain a similar chemical composition. Furthermore, even within a clade, there is much variability; for example, 11/11 mammalian proteins examined have 13-mer repeats, but these range from five repeat units in the Tasmanian devil to 16 units in sperm whale PMEL (Figure 1-9); in fish, the repeat unit length is highly variable, as exemplified by the difference between cod (11-mer length) and Pachon cavefish (26-mer length) (Figure 1-11).

The primary sequences of individual repeats are also drastically different between species. The human RPT contains two motifs that we noted are highly conserved amongst the repeats: GTT and PTXE; in contrast, the chicken RPT domain has a much more divergent TXXXTXX[DE] motif, despite also being a similar 12-mer-repeating unit. These striking differences in sequences are especially remarkable considering that the chicken RPT domain is sufficient to rescue the fibrilogenesis defects of human PMEL lacking a RPT domain, while the zebrafish RPT domain can provide a partial rescue [22]. These data suggest that, despite huge variations in RPT domain evolution, this region has a conserved protein function.

Despite the extremely poor sequence conservation between orthologous PMEL RPT domains, there are notable similarities. As discussed above, the repeat domain is highly O-glycosylated in vivo, and all of our clade representative sequences have threonine/serine residues evenly spaced to form a "[TS] ladder" (Figure 1-8, asterisks). The pharmacological inhibition of O-glycosylation using benzyl-2-acetamido-2-deoxy-α-D-galactopyranoside causes a collapsed PMEL amyloid [22], highlighting the importance of these residues. However, it is not currently known if the precise spacing of these residues is also important for their function. Furthermore, 7/10 of the RPT domains in fish lacked a clear [TS] adder (Figure 1-12). It would be interesting to determine if the PMEL amyloid structure of these species is more densely packed than those with clear [TS] ladders and whether the RPT domain of these fish can rescue the loss of the charged residues in PMEL fibril formation.

The glutamic acid residues in the *Pmel* RPT have been speculated to form hydrogen bonds similar to β-zippers of other amyloids in low-pH conditions [102]. However, the recently discovered accessory role of the PMEL RPT domain may instead implicate the regularly spaced, negatively charged residues with supporting the fibril arrangement of the amyloid. Evenly spaced glutamic acid/aspartic acid residues are a common feature of most (7/8) clade representative repeats (Figure 1-8), as well as most mammals (9/11) and fish (9/10) (Figures 1-9 & 1-12). However, this pattern of [ED] ladders is rarely observed in bird (Figure 1-10) and reptile (Figure 1-11) species, even when negatively charged residues are present. More work is required to determine the functional significance of these negatively mammalian RPT domains.

A Strong Evolutionary Pressure for Uniform Repeat Unit Sequence, Length and E/D Ladder Conservation Is Evident in Teleost Fish

An interesting observation made during the analysis of the RPT domain sequences was that some species had near-perfect repeating protein sequences. For example, the RPT domain of zebrafish (*Danio rerio*), blunt-snouted clingfish (*Gouania willdenowi*) and Atlantic herring (*Clupea harengus)* each possess many repeat units that are almost perfectly identical in amino acid sequence within the species. However, comparing the near-perfect regions between species reveals that these closely related species underwent considerable sequence divergences (Figure 1-13a). We therefore examined these species in more detail at the amino acid and nucleotide levels to determine whether the evolutionary mechanisms could be deduced from the sequences. Firstly, the repeat unit numbers are different between all three species, suggesting an expansion or contraction of the tandem repeats after their divergence. Secondly, the lengths of the repeats are different between species, with a 22-mer in zebrafish, a 17-mer in clingfish and 23-mer repeat in herring. This variability cannot be explained at the DNA level by a frameshift event (since the motif V/A DAAA is common to all three species; a frameshift would shift the codon and disrupt this motif in subsequent repeats). Instead, each clingfish repeat lacks a total of 15 nucleotides per unit at the beginning of each repeat and a 3-bp deletion surrounded by a highly conserved GATGC motif upstream and GCT motif downstream that is found in 23/25 of the repeats (Figure 1-13b). For these nucleotides to have been deleted in clingfish (or inserted in herring and zebrafish), these mutations would have had to occur multiple times over (once per repeat unit). A more parsimonious explanation is therefore that these changes occurred after the divergence of these species from the last common ancestor but before there was expansion of the number of repeat units. Alternatively, it could be explained by very strong purifying/positive selection pressure to return to a uniform repeat unit length and consistent sequence. This area of the genome could also be particularly prone to DNA duplication, gene conversion and mobile elements of unequal recombination/crossing over events.

One might speculate that these near-perfect repeat units confer an evolutionary advantage to the number of sequences from individual animals than are currently available would be required to test this hypothesis. Despite this divergence, these three species did have regularly spaced D/E ladders within all of the repeats, separated by speciation events.

1.5 Conclusion

The PKAT family of genes are linked by a common ancestor and share a common domain architecture. However, the functional roles of PMEL and GPNMB have few commonalities, whereas practically nothing is known about the most ancient member, TMEM130. In this manuscript, we investigated the commonalities in the mutant phenotypes, evolutionary origin and functional domains between GPNMB and PMEL and analyzed the major difference: the RPT domain. Furthermore, we established that TMEM130 is well-suited to serve as an outgroup for future analyses comparing PMEL and GPNMB functions. We hope that this analysis assists with improving the understanding of the PKAT family and encourages further investigations into their evolution and diversification to perform such disparate functions.

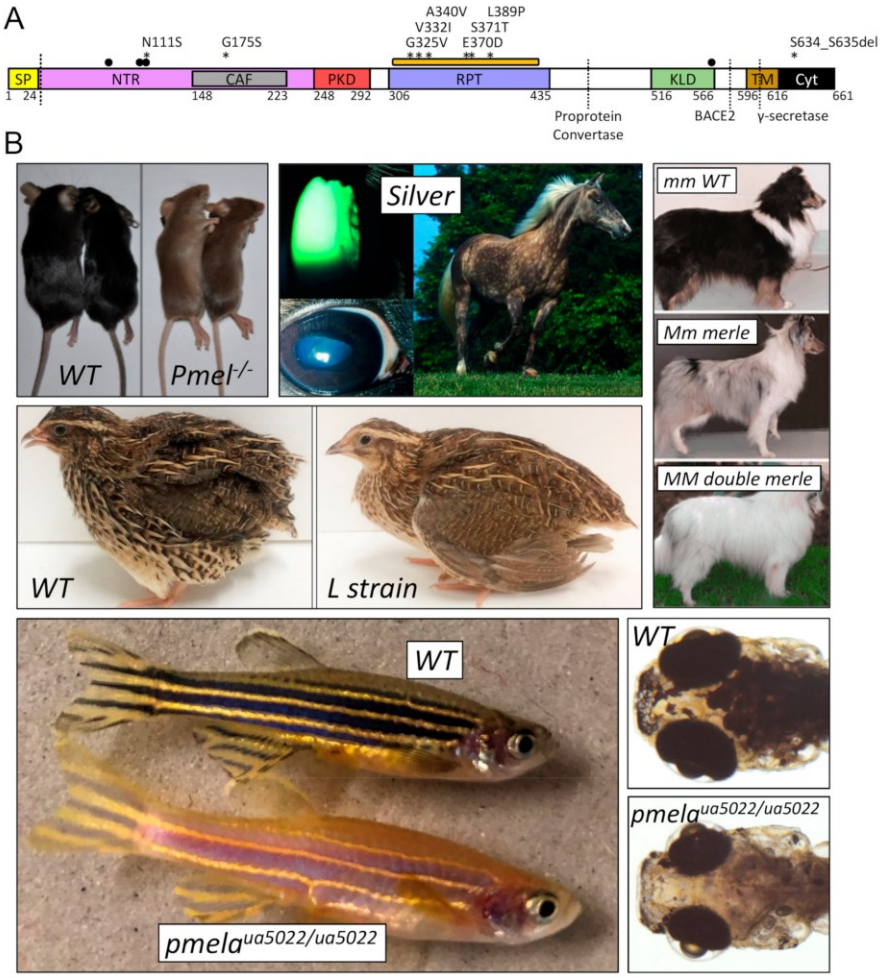

Figure 1-1. Human and animal mutations in PMEL result in hypopigmentation and ocular pathology. **(A)** Protein domain model for human premelanosome protein (PMEL) ENST00000548493.5 is shown, with residue positions determined from the alignments presented in [124]. Symbols at the top of the schematic indicate the location of: (1) human variants associated with pigment dispersion syndrome/pigmentary glaucoma [9] (asterisks), (2) N-linked glycosylation sites (black dots) and (3) the serine-/threonine-rich region of the RPT domain that is modified with O-linked glycosylation (orange rectangle). Various enzyme cleavage sites are depicted by dotted vertical lines. **(B)** Selected animal pigmentation and/or ocular defect images are reproduced below the model with permission. All phenotypes are caused by a mutation of the respective PMEL ortholog (see Table 1). From top-left to bottom-right: Pmel-/- null mouse with a subtle dilution of coat and tail colors [40]; Silver Rocky Mountain Horse with cataracts and mitotic pupils, ectropion uvea, dyscoria, lens subluxation and a shiny white mane and tail, in conjunction with a slightly diluted body color with "silver" dapples [47]; coat color defects in merle (Mm) and double-merle (MM) Shetland Sheepdogs [49]; Japanese "L strain" quail with yellowish plumage [42] and pmelaua5022/ua5022 zebrafish with reduced global pigmentation and ocular anomalies that include enlarged anterior segments, microphthalmia and eyes that are more spherical in shape, suggestive of high intraocular pressure, a hallmark of glaucoma.

Table 1-1. List of animal *Pmel* variants associated with disease with the domain designation, inheritance pattern and reported phenotype[1]

Domain	Animal	HGVS cDNA	HGVS Protein	Inheritance	Phenotype	Notes	Reference
SP	Cattle	NM_001080215.2: c.50_52del	NP_001073684.2: p.(Leu18del)	dominant	dilute coat	Highland/Galloway (c.64G > A) allele, interacts with MC1R (e) allele	Schmutz 2013
SP	Cattle	NM_001080215.2: c.64G > A	NP_001073684.2: p.(Gly22Arg)	dominant	dilute coat	Charolais (Dc) allele	Kühn 2007
NTR	Mouse	NM_021882.4: c.74_331del	NP_068682.2: p.(Gly25_Asn110del)	recessive	dilute coat and tail, loss of rod-shape in melanosomes (including uveal melanocytes and RPE cells)	null allele	Hellström 2011
NTR	Quail	XM_032441057.1: c.271T > G, 353G > A, 446G > A	XP_032296948.1: p.(Ser91Ala), (Arg118His), (Trp149Ter)	recessive	yellowish plumage	"L" strain	Ishishita 2018
PKD	Chicken	-	"del.280-284PTVT" relative to AY636124.1	dominant	grayish plumage	Smoky allele, modifies Dominant White mutation	Kerje 2004
RPT	Zebrafish	NM_001045330.1: c.1474G > T	NP_001038795.1: p.(Glu492Ter)	n/a	hypopigmented body and RPE, vision defects	"fading vision" (fdv) mutant	Schonthaler 2005
TM	Chicken	-	"ins.723-725WAP" relative to AY636124.1	dominant	white plumage	Dominant white allele, coincident with N399D variant upstream of RPT	Kerje 2004
TM	Chicken	-	"del.731-7135LGTAA" relative to AY636124.1	dominant	brown/khaki plumage	Dun allele, coincident with A35V, G105S, and R740C variants in NTR or Cyt domains	Kerje 2004
TM	Horse	NM_001163889.1: c.1849C > T	NP_001157361.1: p.(Arg617Cys)	dominant	silver mane and tail, body dapples, MCOA syndrome	Multiple Congenital Ocular Anomalies	Andersson 2013
Cyt	Dog	"SINE insertion in final intron"	(predicted to affect splicing)	dominant	merle (diluted) coat pattern, various auditory and ocular defects	variable oligo(dA) length affects phenotype	Clark 2006; Murphy 2018
Cyt	Mouse	NM_021882.4: c.1805insA	NP_068682.2: p.(Trp602Ter)	recessive	silver coat	reduction in melanocyte density	Martínez-Esparza 1999
Cyt	Zebrafish	NM_001045330.1: c.2426_2436del	NP_001038795.1: p.(Arg810fs)	recessive	global hypopigmentation, ocular defects	pmelaua5022 allele	Lahola-Chomiak 2018

[1] SP = signal peptide, NTR = N-terminal region, PKD = polycystic kidney disease domain, RPT = repeat domain, TM = transmembrane domain, Cyt = cytosomal portion, RPE = retinal pigmented epithelium and MCOA = multiple congenital ocular anomalies.

Table 1-2. List of published human *PMEL* mutations with the domain designation, inheritance pattern and reported phenotype[2].

Domain	HGVS cDNA	HGVS Protein	Inheritance	Phenotype	Notes	Reference
NTR	NM 001200054.1 c.332A	NP 001186983.1: p.(Asn111Ser)	putative dominant	PDS	singleton	Lahola-Chomiak 2018
CAF	NM 001200054.1 c.523G > A	NP 001186983.1: p.(Gly175Ser)	dominant	PDS / PG	13 member family	Lahola-Chomiak 2018
RPT	NM 001200054.1 c.974G > T	NP 001186983.1: p.(Gly325Val)	putative dominant	PDS / PG	singleton	Lahola-Chomiak 2018
RPT	NM 001200054.1 c.994G > A	NP 001186983.1: p.(Val332Ile)	putative dominant	PDS	singleton	Lahola-Chomiak 2018
RPT	NM 001200054.1 c.1019C > T	NP 001186983.1: p.(Ala340Val)	putative dominant	PDS / PG	2 member family	Lahola-Chomiak 2018
RPT	NM 001200054.1 c.1110G > C	NP 001186983.1: p.(Glu370Asp)	putative dominant	PDS / PG	singleton x3	Lahola-Chomiak 2018
RPT	NM 001200054.1 c.1112G > C	NP 001186983.1: p.(Ser371Thr)	putative dominant	PDS	singleton	Lahola-Chomiak 2018
RPT	NM 001200054.1 c.1166T > C	NP 001186983.1: p.(Leu389Pro)	putative dominant	PDS	singleton x3	Lahola-Chomiak 2018
Cyt	NM 001200054.1 c.1921_1926del	NP 001186983.1: p.(Ser641_Ser642del)	putative dominant	PDS / PG	singleton	Lahola-Chomiak 2018

[2] NTR = N-terminal region, CAF = core amyloid fragment, RPT = repeat domain, Cyt = cytosomal portion, PDS = pigment dispersion syndrome and PG = pigmentary glaucoma.

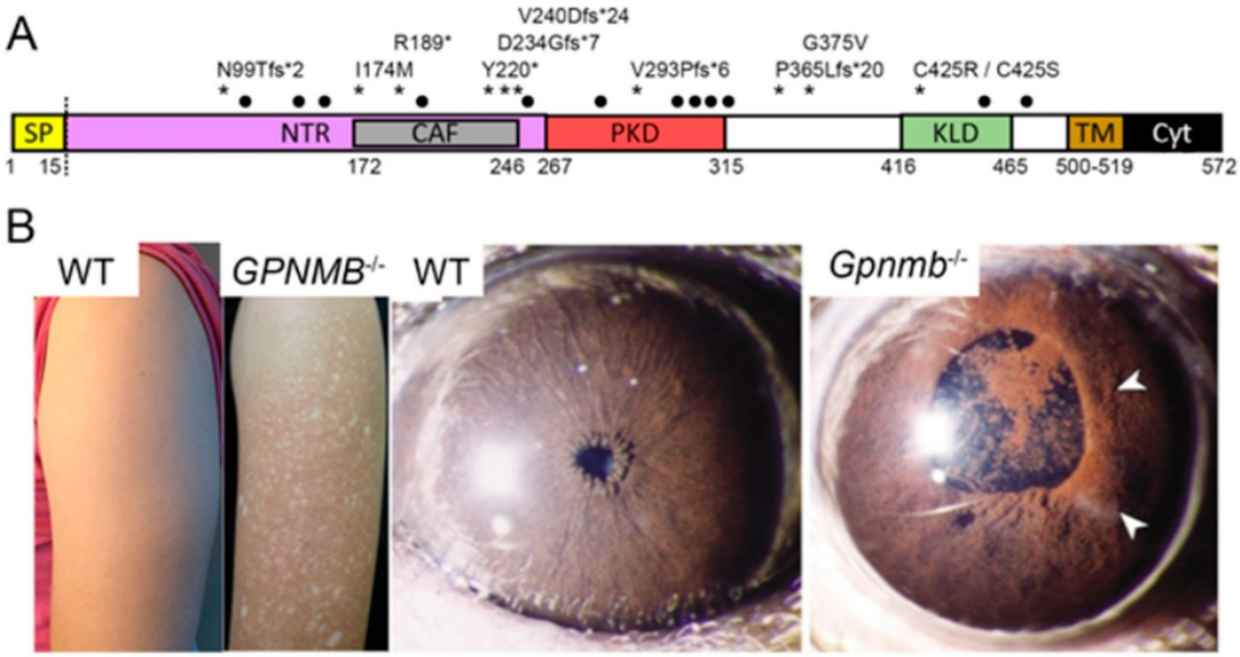

Figure 1-2. Human and animal mutations in GPNMB result in hypopigmented lesions, amyloidosis cutis dyschromica and ocular pathology.

(A) Schematic representation of human GPNMB (NP_001005340.1). Asterisks indicate the locations of variants that cause amyloidosis cutis dyschromica (ACD) [18,63–66]. Locations of N-linked glycosylation sites (black dots) and the cleavage site (dotted vertical line) are depicted. **(B)** ACD presents with hypopigmented lesions (right, from reference [18]). A wild-type murine iris compared to the iris pigment dispersion (arrowheads) of a Gpnmb-/- homozygote [8]. Images republished with permission.

Table 1-3. List of the human GPNMB variants associated with disease with the domain designation, inheritance pattern and reported phenotype[3].

Domain	HGVS cDNA	HGVS Protein	Inheritance	Phenotype	Notes	Reference
NTR/CAF	NM_001005340.2: c.296del, c.565C > T	NP_001005340.1: p.(Asn99ThrfsTer2) p.(Arg189Ter)	homozygous; putative recessive	ACD	Han Chinese	Yang 2018
CAF	NM_001005340.2: c.522C > G	NP_001005340.1: p.(Ile174Met)	homozygous; recessive	ACD	consanguineous; Pakistani	Rahman 2021
CAF	NM_001005340.2: c.565C > T	NP_001005340.1: p.(Arg189Ter)	homozygous; putative recessive	ACD	Han Chinese	Yang 2018
CAF	NM_001005340.2: c.565C > T	NP_001005340.1: p.(Arg189Ter)	homozygous; recessive	ACD	Chinese	Sha 2021
CAF/CAF	NM_001005340.2: c.565C > T, c.660T > G	NP_001005340.1: p.(Arg189Ter) p.(Tyr220Ter)	compound heterozygous; recessive	ACD, skin blisters	Han Chinese	Yang 2018
CAF/btw PKD + KLD	NM_001005340.2: c.565C > T, c.1092del	NP_001005340.1: p.(Arg189Ter) p.(Pro365LeufsTer20)	compound heterozygous; semi-dominant	ACD	Taiwanese; Han Chinese	Onoufriadis 2019; Yang 2018
CAF/KLD	NM_001005340.2: c565C > T, c.1273T > C	NP_001005340.1: p.(Arg189Ter) p.(Cys425Arg)	compound heterozygous; recessive	ACD	Thai	Chiu 2021
CAF	NM_001005340.2: c.700 + 5G > T	NP_001005340.1: p.(Asp234GlyfsTer7)	homo- / heterozygous; semi-dominant	ACD	consanguineous; Kuwaiti Bedouin	Onoufriadis 2019
CAF/PKD	NM_001005340.2: c.719_720del, c.877_880del	NP_001005340.1: p.(Val240AspfsTer24) p.(Val293ProfsTer6)	compound heterozygous; putative recessive	ACD	Han Chinese	Yang 2018
btw PKD + KLD	NM_001005340.2: c.1124G > T	NP_001005340.1: p.(Gly375Val)	homozygous; recessive	ACD	consanguineous; Pakistani	Rahman 2021
KLD	NM_001005340.2 c.1274G > C	NP_001005340.1: p.(Cys425Ser)	homo- / heterozygous; semi-dominant	ACD	Filipino	Onoufriadis 2019

[3] NTR = N-terminal region, CAF = core amyloid fragment, PKD = polycystic kidney disease domain, KLD = Kringle-like domain, Cyt = cytosomal portion and ACD = amyloidosis cutis dyschromica.

Table 1-4. List of published animal Gpnmb mutations with the domain designation, inheritance pattern and reported phenotype[4].

Domain	Animal	HGVS cDNA	HGVS Protein	Inheritance	Phenotype	Notes	Reference
NTR	Mouse	NM_053110.4: c.653C > T	NP_444340.3: p.(Arg150Ter)	recessive	PDS, PG	DBA/2J (D2)	Anderson 2002
btw CAF + PKD	Zebrafish	ENSDART00000090883.6: c.799C > T	ENSDARP00000085316.5 P.(Gln267Ter)	N/A	none reported	ZFIN ID: ZDB-ALT-130411-2760	Dooley 2019
PKD	Zebrafish	ENSDART00000090883.6: c.854G > A	ENSDARP00000085316.5 p.(Trp285Ter)	N/A	none reported	ZFIN ID: ZDB-ALT-130411-2835	Dooley 2019

[4] NTR = N-terminal region, CAF = core amyloid fragment, PKD = polycystic kidney disease, PDS = pigment dispersion syndrome and PG = pigmentary glaucoma.

- the following tables and figures are primarily the work of Dr. Paul Chrystal until next stated –

Table 1-5. Percentage sequence identity of human PTHR11861 members at the cDNA level.

PKAT *family cDNA alignment*			
	TMEM130	**GPNMB**	**PMEL**
TMEM130	100	-	-
GPNMB	32.476	100	-
PMEL	38.713	33.202	100

Table 1-6. Percentage sequence identity of human PTHR11861 members at the protein level.

PKAT *family protein alignment*			
	TMEM130	**GPNMB**	**PMEL**
TMEM130	100	-	-
GPNMB	17.327	100	-
PMEL	13.663	24.929	100

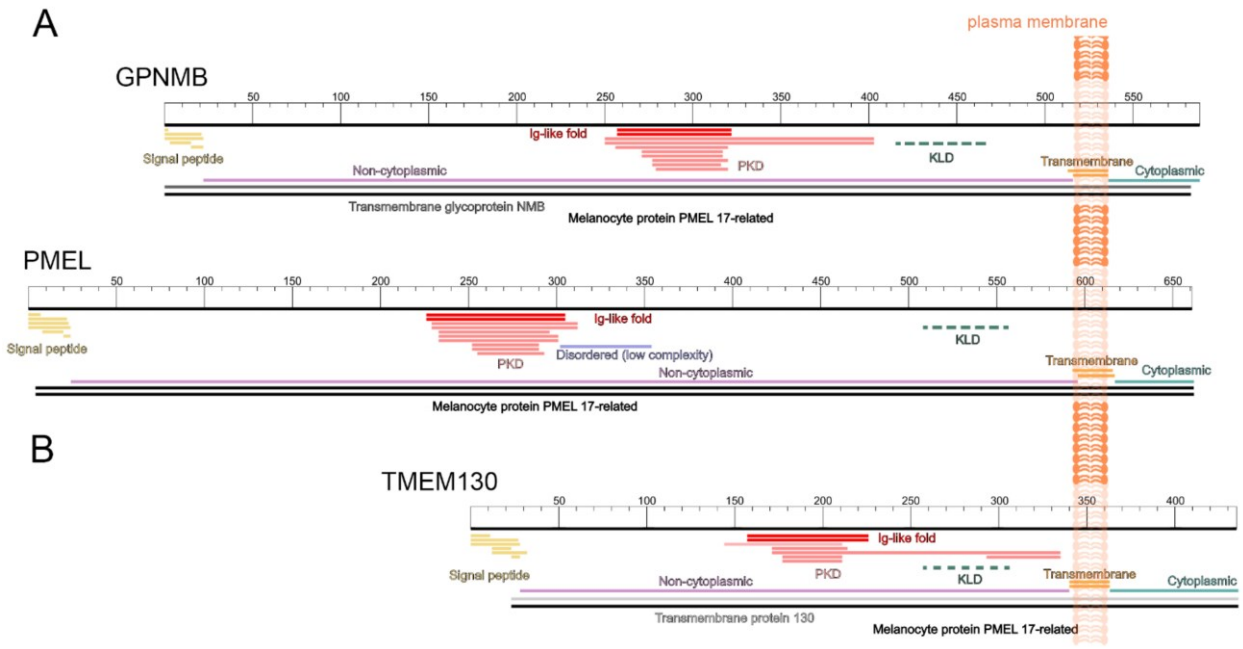

Figure 1-3. GPNMB, PMEL and TMEM130 form a family of related proteins with a homologous domain architecture.

Schematic representation of the human GPNMB (ENST00000647578.1) and PMEL (ENST00000548493.5) proteins **(A)**, and TMEM130 (ENST00000416379.6) **(B)** transmembrane proteins annotated with their predicted function domains. Each protein is represented by a segmented white box displaying the relative amino acid length: 588, 661 and 435 residues, respectively. Below the protein schematic, the InterPro Scan domain predictions are denoted by colored lines to represent the signal peptide (yellow), Ig-like fold (red), polycystic kidney disease domain (PKD, pink), non-cytoplasmic region (purple), transmembrane domain (orange) and cytoplasmic region (green). PMEL was predicted to possess a disordered (low complexity) region (blue). The homology of these sequences to GPNMB (dark grey), PMEL (black) and TMEM130 (light grey) was also flagged. The Kringle-like domain (KLD, dotted green line) was not detected by InterPro Scan but was identified by the sequence alignment. This order and arrangement of the functional domain is characteristic of the PKD and KLD-Associated Transmembrane (PKAT) family.

Table 1-7. Functional domains predicted in human TMEM130 (ENST00000416379.6), GPNMB (ENST00000647578.1) and PMEL (ENST00000548493.5) by InterPro server.

Human TMEM130 **TMEM130-203** **ENST00000416379.6**

Descriptor	Start	End	Length	Source	Ref no.
Signal Peptide	1	27	27	PHOBIUS entry	SIGNAL_PEPTIDE (1)
Signal peptide N-region	1	11	11	PHOBIUS entry	SIGNAL_PEPTIDE_N_REGION (6)
SignalP-noTM	1	28	28	SIGNALP_EUK entry	SignalP-noTM (8)
Signal peptide H-region	12	22	11	PHOBIUS entry	SIGNAL_PEPTIDE_H_REGION (2)
Tmhelix	12	31	20	TMHMM entry	Tmhelix (7)
Signal peptide C-region	23	27	5	PHOBIUS entry	SIGNAL_PEPTIDE_C_REGION(4)
PKD	144	210	67	CDD entry	cd00146
Ig-like_fold	157	225	69	InterPro homologous superfamily	IPR013783
Immunoglobulins	157	225	69	CATH-Gene3D	G3DSA:2.60.40.10
PKD domain	171	213	43	SUPERFAMILY	SSF49299
PKD_dom_sf	171	334	164	InterPro homologous superfamily	IPR035986
PKD_dom	177	210	34	InterPro domain	IPR000601
PKD_dom	177	210	34	PROSITE profiles	PS50093
PKD domain	293	334	42	SUPERFAMILY	SSF49299
Transmembrane region	340	362	23	PHOBIUS entry	TRANSMEMBRANE (5)
Tmhelix	340	362	23	TMHMM entry	Tmhelix (9)
Cytoplasmic domain	363	435	73	PHOBIUS entry	CYTOPLASMIC_DOMAIN (3)
Non cytoplasmic domain	28	339	312	PHOBIUS entry	NON_CYTOPLASMC_DOMAIN (10)
MELANOCYTE PROTEIN PMEL 17-related	23	435	413	PANTHER entry	PTHR11861
TRANSMEMBRANE PROTEIN 130	23	435	413	PANTHER entry	PTHR11861:SF10

Human GPNMB **GPNMB-215** **ENST00000647578.1**

Descriptor	Start	End	Length	Source	Ref no.
Signal peptide N-region	1	2	2	PHOBIUS entry	SIGNAL_PEPTIDE_N_REGION (2)
Signal Peptide	1	21	21	PHOBIUS entry	SIGNAL_PEPTIDE (6)
SignalP-noTM	1	22	22	SIGNALP_EUK entry	SignalP-noTM (4)
Signal peptide H-region	3	14	12	PHOBIUS entry	SIGNAL_PEPTIDE_H_REGION (5)
Signal peptide C-region	15	21	7	PHOBIUS entry	SIGNAL_PEPTIDE_C_REGION (9)
PKD/Chitinase_dom	250	402	153	InterPro domain	IPR022409
PKD_9	250	402	153	SMART	SM00089

PKD	256	319	64	CDD entry	cd00146
Ig-like_fold	257	321	65	InterPro homologous superfamily	IPR013783
Immunoglobulins	257	321	65	CATH-Gene3D	G3DSA:2.60.40.10
PKD_dom_sf	271	316	46	InterPro homologous superfamily	IPR035986
PKD domain	271	316	46	SUPERFAMILY	SSF49299
PKD_dom	277	319	43	InterPro domain	IPR000601
PKD	277	315	39	PROSITE profiles	PS50093
PKD	279	319	41	Pfam	PF00801
Tmhelix	513	535	23	TMHMM entry	Tmhelix (8)
Transmembrane region	516	535	20	PHOBIUS entry	TRANSMEMBRANE (7)
Cytoplasmic domain	536	588	53	PHOBIUS entry	CYTOPLASMIC_DOMAIN (3)
Non cytoplasmic domain	22	515	494	PHOBIUS entry	NON_CYTOPLASMIC_DOMAIN (1)
TRANSMEMBRANE GLYCOPROTEIN NMB	1	583	583	PANTHER entry	PTHR11861:SF11
MELANOCYTE PROTEIN PMEL 17-RELATED	1	583	583	PANTHER entry	PTHR11861

Human PMEL **PMEL-204** **ENST00000548493.5**

Descriptor	Start	End	Length	Source	Ref no.
Signal peptide N-region	1	7	7	PHOBIUS entry	SIGNAL_PEPTIDE_N_REGION
SignalP-TM	1	22	22	SIGNALP_GRAM_POSITIVE entry	SignalP-TM (10)
Signal Peptide	1	23	23	PHOBIUS entry	SIGNAL_PEPTIDE (8)
SIGNALP_EUK entry	1	24	24	SignalP_EUK entry	SignalP-noTM (4)
Signal peptide H-region	8	19	12	PHOBIUS entry	SIGNAL_PEPTIDE_H
Signal peptide C-region	20	23	4	PHOBIUS entry	SIGNAL_PEPTIDE_C_REGION (9)
Non cytoplasmic domain	24	595	572	PHOBIUS entry	NON_CYTOPLASM
Ig-like_fold	226	304	79	InterPro homologous superfamily	IPR013783
Immunoglobulins	226	304	79	CATH-Gene3D	G3DSA:2.60.40.10
PKD/Chitinase_dom	229	311	83	Interpro Domain	IPR022409
PKD_9	229	311	83	SMART	SM00089
PKD	233	295	63	CDD entry	cd00146
PKD_Dom	233	300	68	Interpro Domain	IPR000601
PKD	233	300	68	Pfam	PF00801
PKD_dom_sf	252	289	38	InterPro homologous superfamily	IPR035986

PKD domain	252	289	38	SUPERFAMILY	SSF49299
PKD	255	292	38	PROSITE profiles	PS50093
disorder_prediction	302	353	52	MOBIDB_LITE entry	mobidb-lite (3)
Tmhelix	593	615	23	TMHMM entry	Tmhelix (7)
Transmembrane region	596	616	21	PHOBIUS entry	TRANSMEMBRANE
Cytoplasmic domain	617	661	45	PHOBIUS entry	CYTOPLASMIC DOMAIN (11)
Melanocyte protein PMEL 17 -related	4	661	658	PANTHER entry	PTHR11861
Melanocyte protein PMEL	4	661	658	PANTHER entry	PTHR11861:SF1

Table 1-8. Clade-representative paralog sequences used.

	Tmem130	gpnmb	pmel
Human (Homo sapiens)	ENST00000416379.6	NP_001005340.1	ENST00000548493.5
Chicken (Gallus gallus)	ENSGALT00000041067.4	ENSGALT00000017821.6	ENSGALG00000035350
Common lizard (Zootoca vivipara)	XP_034987520.1	XP_034985369.1	XP_034959827.1
Tropical clawed frog (Xenopus tropicalis)	XP_012826896.2	NP_001124514.1	XP_002934561.3
Coelacanth (Latimeria chalumnae)	XP_006000848.2	XP_005997158.1	XP_005986276.1
Zebrafish (Danio rerio)	ENSDART00000169019.3	ENSDART00000090883.6	ENSDART00000123568.4 ENSDART00000046268.7
Thorny skate (Amblyraja radiata)	XP_032896444.1	XP_032902250.1	XP_032871492.1
Sea lamprey (Petromyzon marinus)		XP_032818521.1	XP_032813209.1
Sea lamprey (Petromyzon marinus)		XP_032807179.1	XP_032831262.1
European starfish (Asterias rubens)	XP_033631068.1		
Acorn worm (Saccoglossus kowalevskii)	XP_002739013.1		
Common Spider (Parasteatoda tepidariorum)	XP_015915338.1		
Cauliflower coral (Pocillopora damicornis)	RMX49586.1		
Trichoplax (Trichoplax adhaerens)	RDD42042.1		

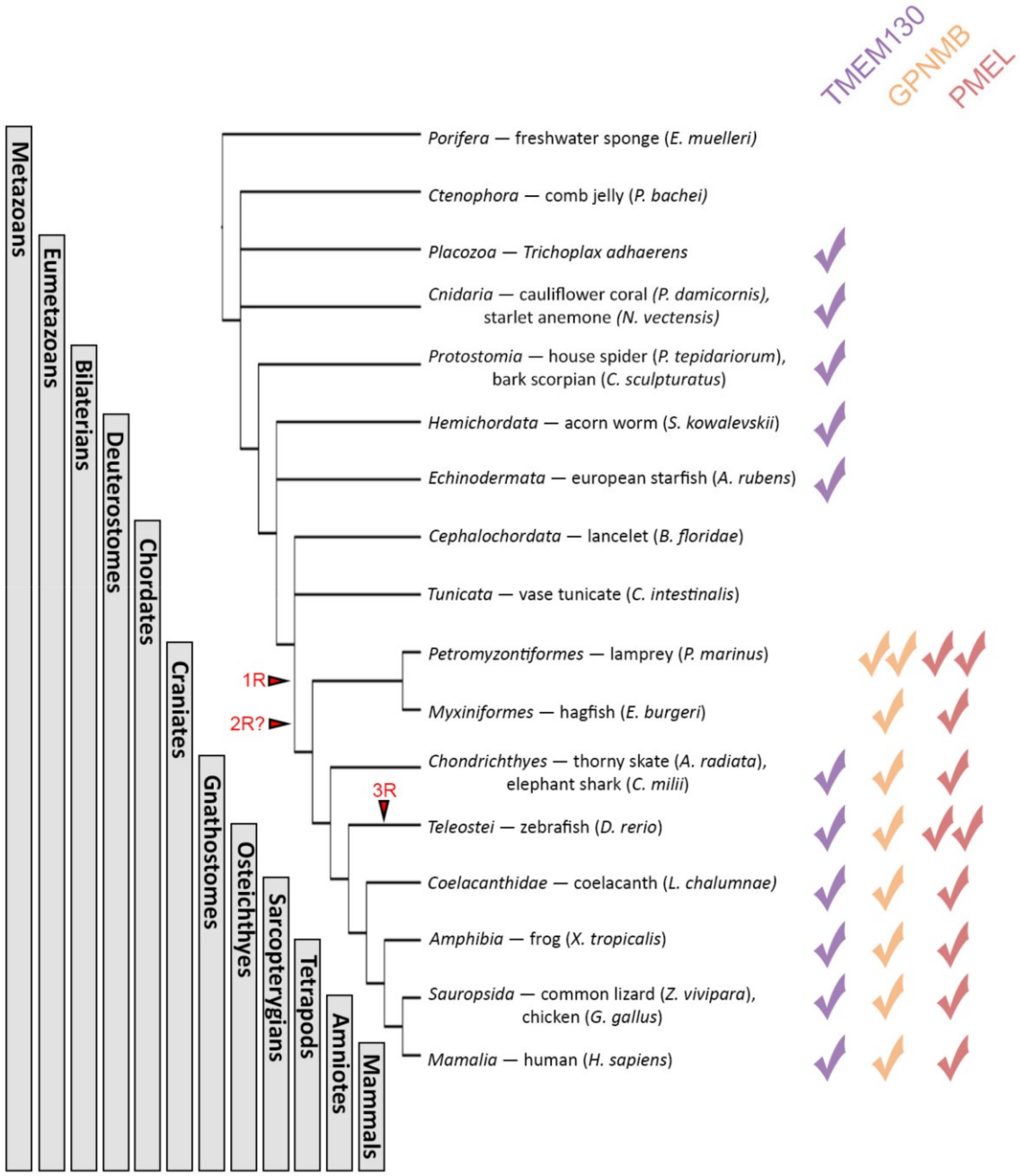

Figure 1-4. TMEM130 is the most ancient member of the PKAT family in the basal metazoa, with GPNMB and PMEL originating prior to the craniate radiation. Schematic representation of the major animal taxa and cladogram demonstrating their evolutionary relationship and where whole-genome duplication events occurred (1R, 2R and 3R). Check marks demonstrate which of the paralogous genes are found within the species inside these taxa. The presence of two check marks of the same colour indicates that two paralogs of that gene are found in that species.

Table 1-9 Paralogous genes from human, chicken or thorny skate that were found neighbouring lamprey gpnmb, pmel-like, pmel or gpnmb-like.

H. sapiens Ch 7 [GPNMB]		H. sapiens Ch 12 [PMEL]		G. gallus Ch 2 [gpnmb]		G. gallus Ch 33 [pmel]		A. radiata Ch2 [gpnmb]		A. radiata Ch 46 [pmel]	
Gene symbol	Accession	Gene symbol	Accession	Gene symbol	Accession	Gene symbol	Accession	Gene symbol	Accession	Gene symbol	Accession
RPA3	ENSG00000106399	RACGAP1P	ENSG00000257331	CHPF2	ENSGALG00000036477	TMBIM6	ENSGALG00000031426	dlec1	NC_045957.1	cd63	NC_046001.1
ICA1	ENSG00000003147	SLC48A1	ENSG00000211584	ASB10	ENSGALG00000032845	TFCP2	ENSGALG00000035530	gars1	NC_045957.1	tfcp2	NC_046001.1
AGMO	ENSG00000187546	ASB8	ENSG00000177981	FASTK	ENSGALG00000003058	SLC4A8	ENSGALG00000031274	itgb1	NC_045957.1	b4galnt1	NC_046001.1
SOSTDC1	ENSG00000171243	LMBR1L	ENSG00000139636	SLC4A2	ENSGALG00000034284	FAIM2	ENSGALG00000031615	pard3	NC_045957.1	racgap1	NC_046001.1
ANKMY2	ENSG00000106524	TUBA1A	ENSG00000167552	IBA57	ENSGALG00000005328	SPATS2	ENSGALG00000033957	pitrm1	NC_045957.1	pym1	NC_046001.1
BZW2	ENSG00000136261	SPATS2	ENSG00000123352	ARF1	ENSGALG00000005393	MCRS1	ENSGALG00000035203	sdhaf3	NC_045957.1	lmbr1l	NC_046001.1
AGR2	ENSG00000106541	MCRS1	ENSG00000187778	CCDC12	ENSGALG00000005487	CD63	ENSGALG00000055094	ppp1r9a	NC_045957.1	pa2g4	NC_046001.1
TMEM196	ENSG00000173452	TMBIM6	ENSG00000139644	SETD2	ENSGALG00000042051	GDF11	ENSGALG00000036806	bet1	NC_045957.1	cdk2	NC_046001.1
NUP42	ENSG00000136243	TFCP2	ENSG00000135457	KLHL18	ENSGALG00000005582	SARNP	ENSGALG00000030342	elp2	NC_045957.1	pmel	NC_046001.1
GPNMB	ENSG00000136235	SLC4A8	ENSG00000050438	DLEC1	ENSGALG00000005826	RACGAP1	ENSGALG00000033231	gabbr2	NC_045957.1	mcrs1	NC_046001.1
MALSU1	ENSG00000156928	MFSD5	ENSG00000182544	U6	ENSGALG00000025663	SLC48A1	ENSGALG00000036380	nfx1	NC_045957.1	spats2	NC_046001.1
IGF2BP3	ENSG00000136231	AAAS	ENSG00000094914	CRYGN	ENSGALG00000006189	ATP5F1B	ENSGALG00000038801	chmp5	NC_045957.1	slc4a8	NC_046001.1
CCDC126	ENSG00000169193	ATF7	ENSG00000170653	RHEB	ENSGALG00000039880	TIMELESS	ENSGALG00000034688	bag1	NC_045957.1	agap2	NC_046001.1
NPY	ENSG00000122585	COPZ1	ENSG00000111481	GALNT11	ENSGALG00000006233	CS	ENSGALG00000030466	mtrr	NC_045957.1	sarnp	NC_046001.1
SNX10	ENSG00000086300	CD63	ENSG00000135404	NOM1	ENSGALG00000006437	CDK2	ENSGALG00000032699	erp44	NC_045957.1	gdf11	NC_046001.1
HOXA1	ENSG00000105991	GDF11	ENSG00000135414	LARP4B	ENSGALG00000006672	PMEL	ENSGALG00000035350	stx17	NC_045957.1	dnajc14	NC_046001.1
HOXA4	ENSG00000197576	SARNP	ENSG00000205323	PITRM1	ENSGALG00000007036	PYM1	ENSGALG00000046169	sec61b	NC_045957.1	timeless	NC_046001.1
HOXA9	ENSG00000078399	DNAJC14	ENSG00000135392	PARD3	ENSGALG00000007125	TUBA1A	ENSGALG00000037953	iba57	NC_045957.1	trnas-cga	NC_046001.1
HOXA10	ENSG00000253293	PYM1	ENSG00000170473	ITGB1	ENSGALG00000007145	LMBR1L	ENSGALG00000037665	crygn	NC_045957.1		
HOXA11	ENSG00000005073	PMEL	ENSG00000185664	SVIL	ENSGALG00000007331	MFSD5	ENSGALG00000033927	rheb	NC_045957.1		
JAZF1	ENSG00000153814	CDK2	ENSG00000123374	ARMC4	ENSGALG00000007417	ASB8	ENSGALG00000037396	galnt11	NC_045957.1		

FKBP14	ENSG00000106080	PA2G4	ENSG00000170515	RAB18	ENSGALG00000007435	AAAS	ENSGALG00000032843	nom1	NC_045957.1		
GARS1	ENSG00000106105	CS	ENSG00000062485	YME1L1	ENSGALG00000007492	COPZ1	ENSGALG00000043336	larp4b	NC_045957.1		
LSM5	ENSG00000106355	CNPY2	ENSG00000257727	MASTL	ENSGALG00000007507			idi1	NC_045957.1		
AVL9	ENSG00000105778	TIMELESS	ENSG00000111602	ACBD5	ENSGALG00000007519			svil	NC_045957.1		
BBS9	ENSG00000122507	ATP5F1B	ENSG00000110955	ABI1	ENSGALG00000007547			bzw2	NC_045957.1		
BMPER	ENSG00000164619	NDUFA4L2	ENSG00000185633	PDSS1	ENSGALG00000007559			ankmy2	NC_045957.1		
VPS41	ENSG00000006715	MARS1	ENSG00000166986	ABCB1	ENSGALG00000008912			sostdc1	NC_045957.1		
RALA	ENSG00000006451	B4GALNT1	ENSG00000135454	SRI	ENSGALG00000008985			crppa	NC_045957.1		
SUGCT	ENSG00000175600	AGAP2	ENSG00000135439	AKAP9	ENSGALG00000040724			agmo	NC_045957.1		
INHBA	ENSG00000122641	OTOGL	ENSG00000165899	KRIT1	ENSGALG00000042651			ica1	NC_045957.1		
PSMA2	ENSG00000106588	APAF1	ENSG00000120868	PEX1	ENSGALG00000009410			rpa3	NC_045957.1		
MRPL32	ENSG00000106591			BET1	ENSGALG00000024485			tmem196	NC_045957.1		
ADCY1	ENSG00000164742			PPP1R9A	ENSGALG00000009686			trnad-guc	NC_045957.1		
UPP1	ENSG00000183696			RPA3	ENSGALG00000010700			nup42	NC_045957.1		
LANCL2	ENSG00000132434			ICA1	ENSGALG00000010708			gpnmb	NC_045957.1		
VOPP1	ENSG00000154978			AGMO	ENSGALG00000010792			malsu1	NC_045957.1		
ABCB1	ENSG00000085563			CRPPA	ENSGALG00000010795			igf2bp3	NC_045957.1		
SRI	ENSG00000075142			SOSTDC1	ENSGALG00000036836			ccdc126	NC_045957.1		
AKAP9	ENSG00000127914			ANKMY2	ENSGALG00000010804			npy	NC_045957.1		
KRIT1	ENSG00000001631			BZW2	ENSGALG00000010809			pex1	NC_045957.1		
PEX1	ENSG00000127980			AGR2	ENSGALG00000010825			thrb	NC_045957.1		
BET1	ENSG00000105829			TMEM196	ENSGALG00000010865			rarb	NC_045957.1		
PPP1R9A	ENSG00000158528			GPNMB	ENSGALG00000010949			ngly1	NC_045957.1		
SDHAF3	ENSG00000196636			MALSU1	ENSGALG00000010954			nek10	NC_045957.1		
MUC17	ENSG00000169876			IGF2BP3	ENSGALG00000010961			azi2	NC_045957.1		
TPK1	ENSG00000196511			CCDC126	ENSGALG00000010976			fkbp14	NC_045957.1		

SLC4A2	ENSG00000164889			NPY	ENSGALG00000010983			jazf1	NC_045957.1		
FASTK	ENSG00000164896			SNX10	ENSGALG00000011046			hoxa11	NC_045957.1		
ASB10	ENSG00000146926			HOXA1	ENSGALG00000028095			hoxa10	NC_045957.1		
CHPF2	ENSG00000033100			HOXA4	ENSGALG00000022622			hoxa9	NC_045957.1		
CRYGN	ENSG00000127377			HOXA9	ENSGALG00000028983			hoxa4	NC_045957.1		
RHEB	ENSG00000106615			HOXA10	ENSGALG00000026631			hoxa1	NC_045957.1		
GALNT11	ENSG00000178234			HOXA11	ENSGALG00000040021			snx10	NC_045957.1		
NOM1	ENSG00000146909			JAZF1	ENSGALG00000030455			ankh	NC_045957.1		
				FKBP14	ENSGALG00000011181			fyco1	NC_045957.1		
				HACL1	ENSGALG00000011211			glipr2	NC_045957.1		
				BTD	ENSGALG00000011216			tmem245	NC_045957.1		
				ANKRD28	ENSGALG00000011226			frrs1l	NC_045957.1		
				GALNT15	ENSGALG00000011235			adcy1	NC_045957.1		
				OXNAD1	ENSGALG00000011239			tpk1	NC_045957.1		
Syntanous w/ gpnmb				TBC1D5	ENSGALG00000011251			lancl2	NC_045957.1		
Syntanous w/ pmel				KCNH8	ENSGALG00000011262			vopp1	NC_045957.1		
				KAT2B	ENSGALG00000011278			hacl1	NC_045957.1		
				SGO1	ENSGALG00000011281			btd	NC_045957.1		
				THRB	ENSGALG00000011294			ankrd28	NC_045957.1		
				RARB	ENSGALG00000011298			galnt15	NC_045957.1		
				NGLY1	ENSGALG00000011304			oxnad1	NC_045957.1		
				NEK10	ENSGALG00000011322			tbc1d5	NC_045957.1		
				AZI2	ENSGALG00000011428			kcnh8	NC_045957.1		
				DNAJC13	ENSGALG00000035068			kat2b	NC_045957.1		
				ACKR4	ENSGALG00000041491			sgo1	NC_045957.1		
				TMEM108	ENSGALG00000036412			abitram	NC_045957.1		

				FYCO1	ENSGALG00000040212			krit1	NC_045957.1		
				LZTFL1	ENSGALG00000054523			akap9	NC_045957.1		
				CLASP2	ENSGALG00000032647			sri	NC_045957.1		
				ARPP21	ENSGALG00000043240			ackr4	NC_045957.1		
				BMPER	ENSGALG00000029811			dnajc13	NC_045957.1		
				BBS9	ENSGALG00000031650			lztfl1	NC_045957.1		
				AVL9	ENSGALG00000041568			myo10	NC_045957.1		
				LSM5	ENSGALG00000041625			znf622	NC_045957.1		
				VPS41	ENSGALG00000031635			tmem108	NC_045957.1		
				RALA	ENSGALG00000031893			fbxl7	NC_045957.1		
				SUGCT	ENSGALG00000031758			trnag-gcc	NC_045957.1		
				INHBA	ENSGALG00000034616			pdss1	NC_045957.1		
				PSMA2	ENSGALG00000039387			abi1	NC_045957.1		
				MRPL32	ENSGALG00000037258			acbd5	NC_045957.1		
				VOPP1	ENSGALG00000042773			mastl	NC_045957.1		
				LANCL2	ENSGALG00000032570			yme1l1	NC_045957.1		
				TPK1	ENSGALG00000040298			armc4	NC_045957.1		
				ADCY1	ENSGALG00000031170			psma2	NC_045957.1		
				NFX1	ENSGALG00000043724			mrpl32	NC_045957.1		
				RECK	ENSGALG00000036829						
				ZNF622	ENSGALG00000037171						
				FBXL7	ENSGALG00000031947						
				ANKH	ENSGALG00000012964						
				MTRR	ENSGALG00000039424						
				UPP1	ENSGALG00000013073						
				TMEM245	ENSGALG00000013138						

				FRRS1L	ENSGALG0 0000025792						
				BAG1	ENSGALG0 0000013157						
				CHMP5	ENSGALG0 0000013160						
				GABBR2	ENSGALG0 0000013200						
				ELP2	ENSGALG0 0000039034						
				ERP44	ENSGALG0 0000013452						
				STX17	ENSGALG0 0000013462						
				SEC61B	ENSGALG0 0000013569						
				GLIPR2	ENSGALG0 0000028821						
				MOS	ENSGALG0 0000042082						

Table 1-10. Additional PMEL paralog sequences used for RPT domain predictions.

Agassiz's desert tortoise (Gopherus agassizii)	ENSGAGT00000005719.1
Atlantic herring (Clupea harengus)	ENSCHAT00000043664.1
Barn Owl (Tyto alba)	AUD07748.1
Barred-Tailed Pigeon (Patagioenas fasciata monilis)	OPJ72592.1
Blind Cavefish (Astyanax fasciatus mexicanus)	A0A4W6F2T7
Blunt snouted clingfish (Gouania willdenowi)	ENSGWIT00000010238.1
Brown Trout (Salmo trutta)	ENSSTUT00000048284.1
Central Bearded Dragon (Pogona vitticeps)	XP_020638533.1
Cod (Gadus morhua)	ENSGMOT00000001759.1
Cow (Bos taurus)	NP_001073684.2
Dog (Canis lupus familiaris)	NP_001096686.1
Electric Eel (Electrophorus electricus)	XP_026888855.1
European Rabbit (Oryctolagus cuniculus)	CCA62427.1
Gaboon caecilian (Geotrypetes seraphini)	XP_033793418.1
Great blue-spotted mudskipper (Boleophthalmus pectinirostris)	XP_020792628.1
Greater Horseshoe Bat (Rhinolophus ferrumequinum)	XP_032972790.1
Horse (Equus caballus)	NP_001157361.1
Japanese quail (Coturnix japonica)	XP_032296948.1
Lesser hedgehog tenrec (Echinops telfairi)	XP_004700634.2
Mouse (Mus musculus)	NP_068682.2
Okarito brown kiwi (Apteryx rowi)	XP_025911704.1
Owl Parrot (Strigops habroptila)	XP_030366358.1
Pachon Cavefish (Astyanax Mexicanus Pachon)	ENSAMXT00005031725.1
Platypus (Ornithorhynchus anatinus)	XP_028928770.1
Sperm Whale (Physeter catodon)	XP_007129391.2
Tasmanian devil (Sarcophilus harrisii)	XP_031797073.1
Tongue Sole (Cynoglossus semilaevis)	XP_024915820.1
Tufted Duck (Aythya fuligula)	XP_032060670.1
Two-lined caecilian (Rhinatrema bivittatum)	XP_029450632.1

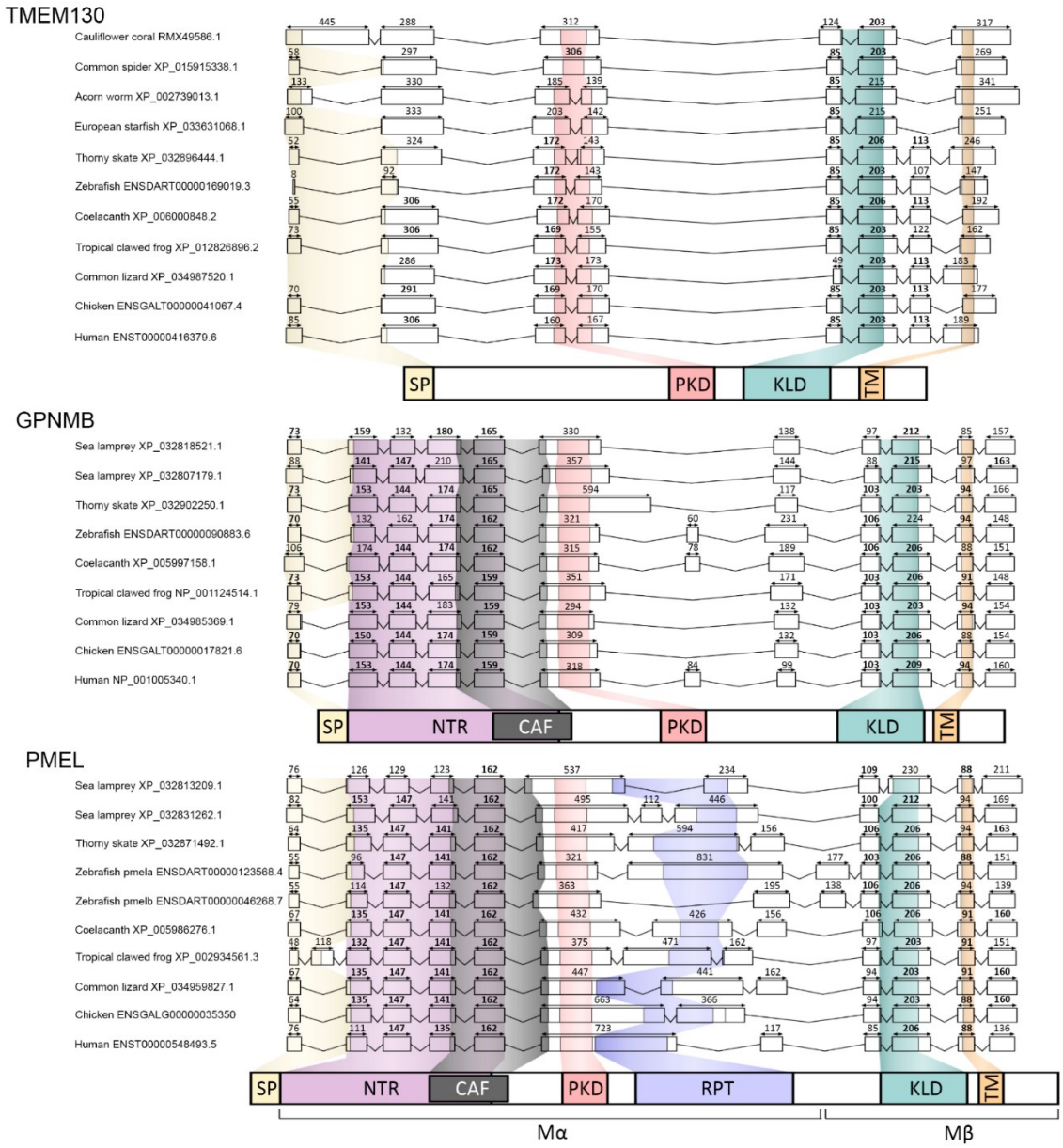

Figure 1-5. The intron-exon architecture supports a common ancestry for the PKAT family genes.

Schematic representation of gene family orthologs showing exons (boxes, to scale) and separated by introns (lines, not to scale). The nucleotides coding for different protein domains are colour coded: signal peptide (yellow), N-terminal region (NTR; purple), core amyloid fragment (CAF; black) polycystic kidney domain (PKD; red), repeat domain (RPT; blue), kringle-like domain (KLD; green), transmembrane domain (TM; orange). Numbers above the exons denote exon length in basepairs, bold donates when exon lengths are shared between >3 orthologs (_5%).

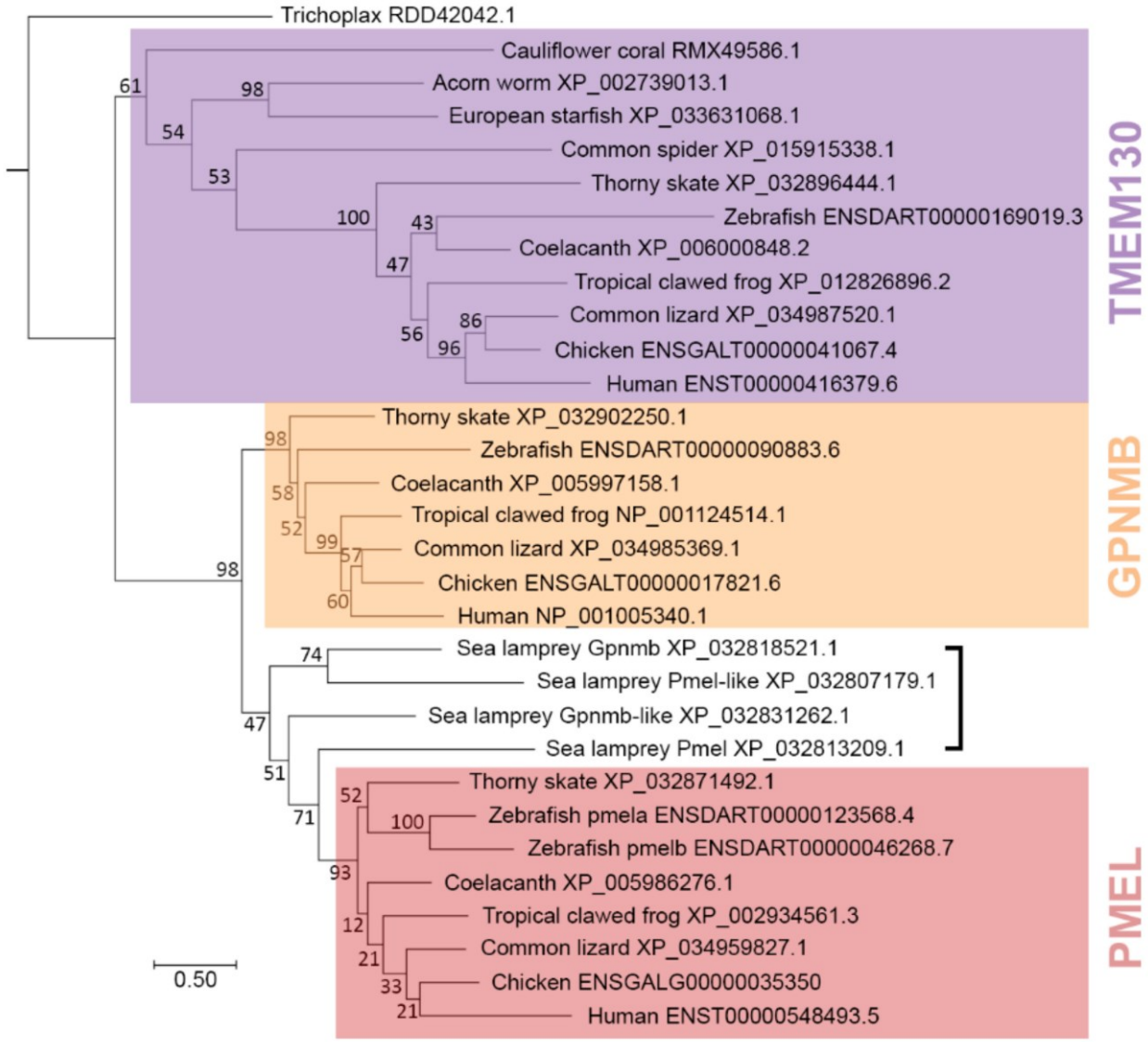

Figure 1-6. Phylogenetic tree representing the outparalog TMEM130, GPNMB and PMEL protein sequences separated by speciation events.

Phylogeny was inferred by the Maximum Likelihood method and Whelan and Goldman + Frequency model. The BS _1000 and percentage of trees in which the associated taxa clustered together are shown next to the branches. Branch lengths represent the substitutions per site.

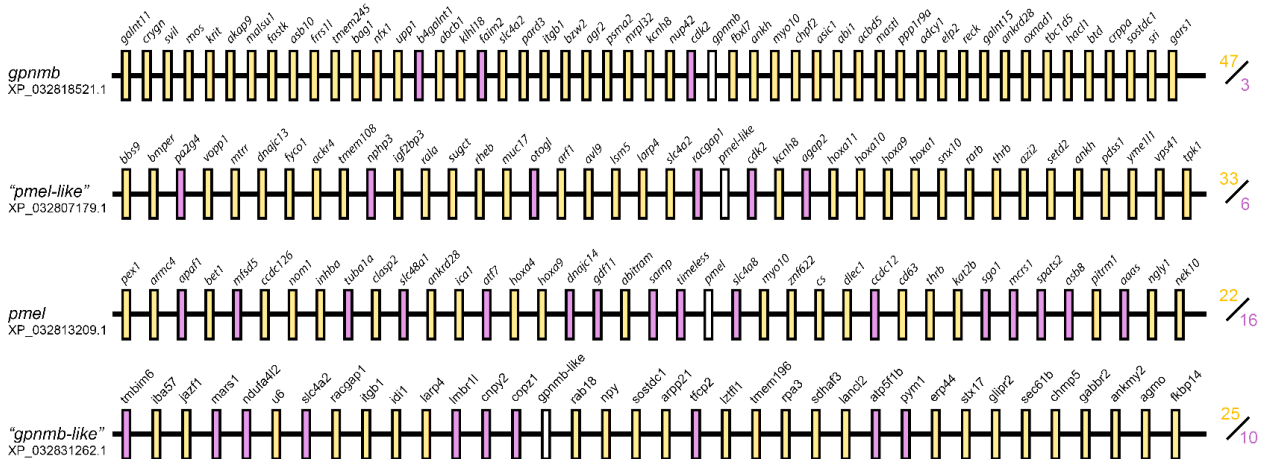

Figure 1-7. Gene synteny analysis of *pmel* and *gpnmb* inparalogs in lamprey.

Schematic representation of lamprey genes neighbouring pmel, pmel-like, gpnmb, and gpnmb-link that have a paralogous gene in human, chicken or thorny skate. Genes that are paralogous to GPNMB in human, chicken and thorny skate are in yellow. Genes that are paralogous to PMEL in human, chicken and thorny skate are in purple.

---- the following figures are primarily the work of Justin Jensen until next stated ----

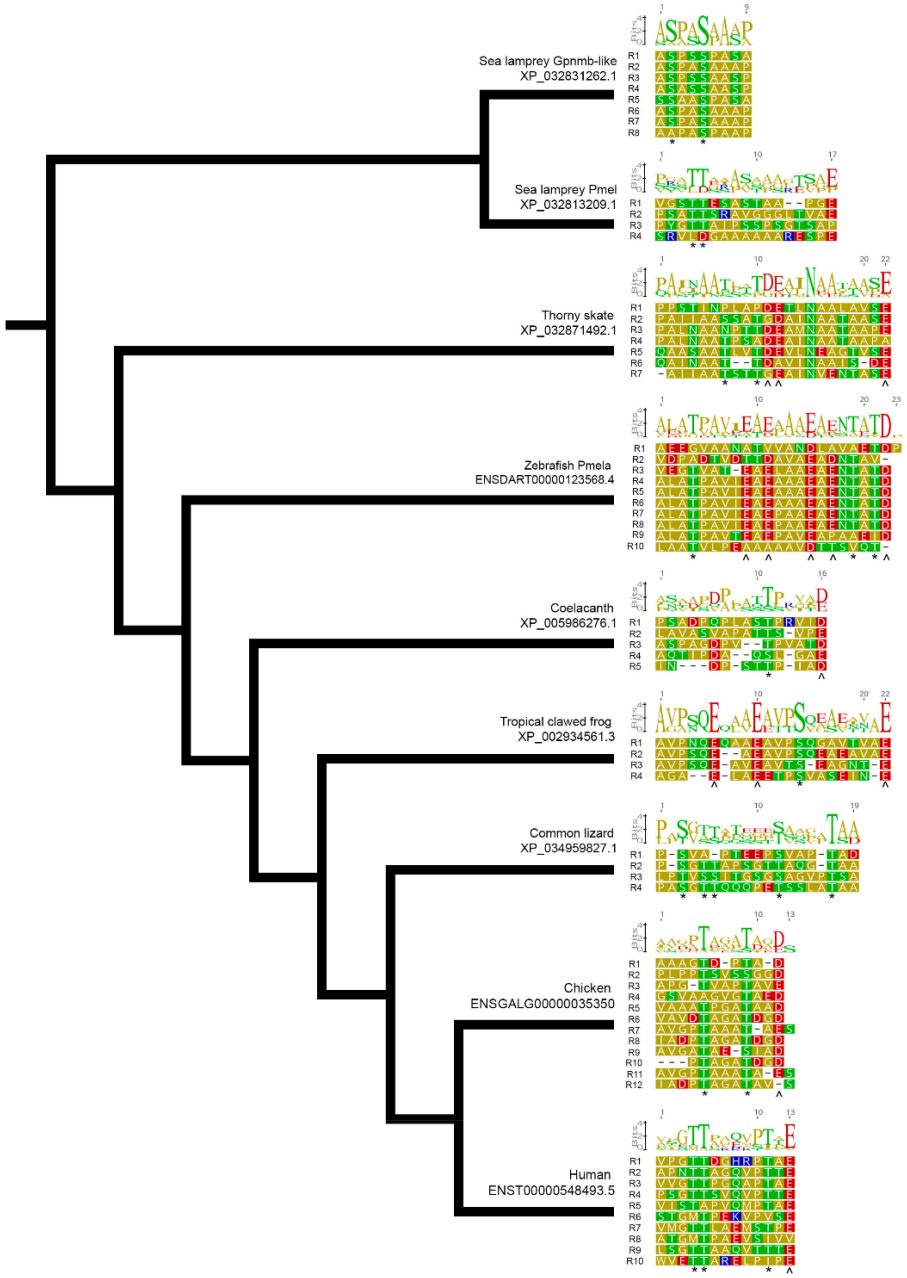

Figure 1-8. The PMEL repeat domain varies in size and amino acid composition, but T/S ladders and D/E ladders are a frequent feature.

Alignments of individual PMEL repeat units of clade-representative organisms displayed in a cladogram. Sequence logos above the raw sequence represent the degree of sequence identity within a species. Conserved T/S ladders * and conserved D/E ladders ˆ. Residues are color-coded for the polarity of their amino acid side chains (yellow, nonpolar; green, uncharged polar; red, acidic; blue, basic).

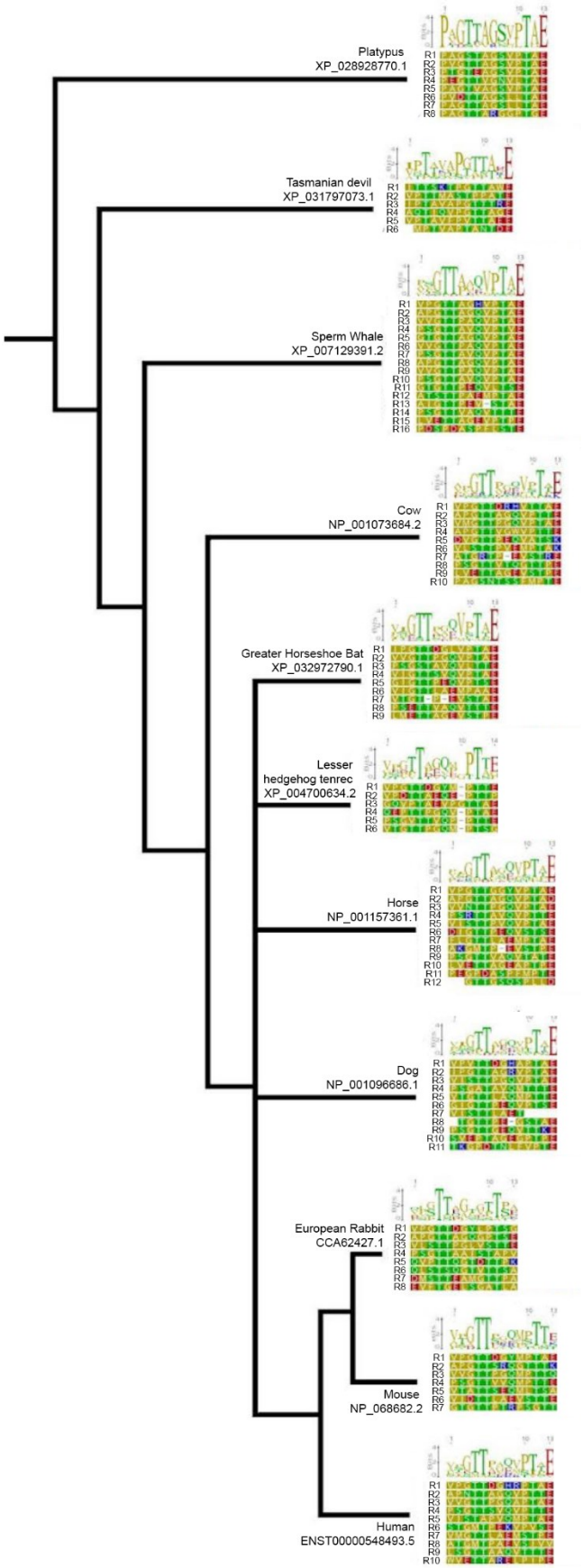

Figure 1-9. Cladogram of mammalian RPT domains.

Mammalian species were selected from the following orders Monotremata, Afrosoricida, Dasyuromorphia, Cetacea, Lagomorpha, Diprotodontia, Carnivora, Artiodactyla, Rodentia, and Primates. Amino acids are color-coded according to polarity (yellow, non-polar; green, uncharged polar; red, acidic; blue, basic). Accession numbers are listed in table 1-10.

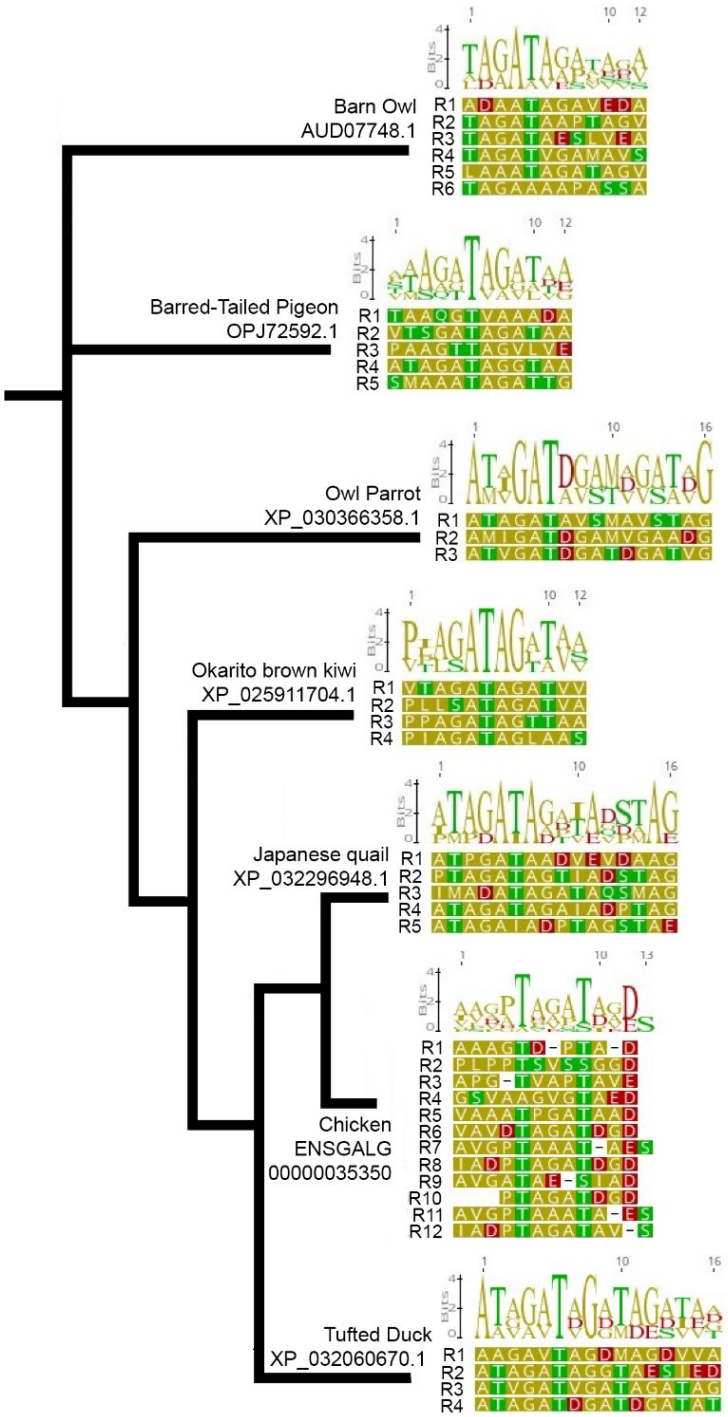

Figure 1-10. Cladogram showing Avian species Pmel RPT domains.

Avian species were selected from the following orders: Struthioniformes, Galliformes, Anseriformes, Psittaciformes, Strigiformes, and Columbiformes. Amino acids are color-coded according to polarity (yellow, non-polar; green, uncharged polar; red, acidic; blue, basic). Accession numbers are listed in table 1-10.

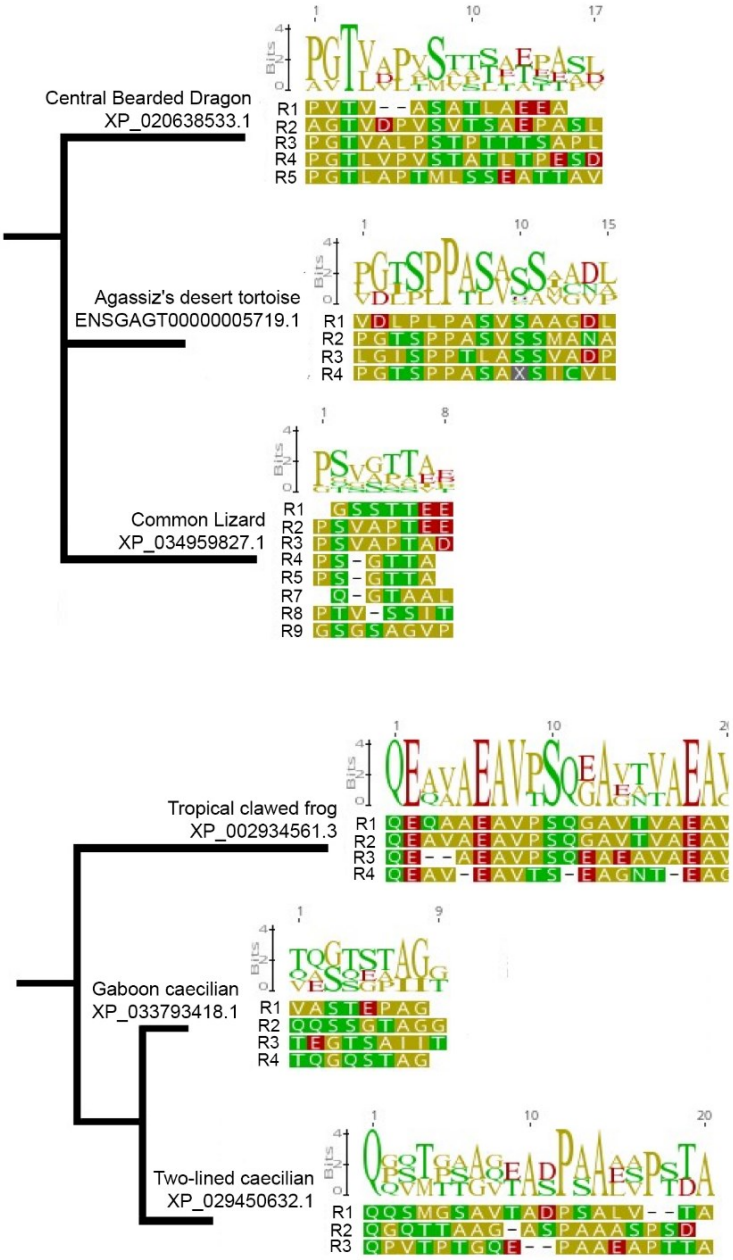

Figure 1-11. Cladogram showing the Amphibians and Reptiles Pmel RPT domains. **(A)** Reptiles were selected from the following orders Testudines, Squamata. **(B)** Amphibians were selected from the orders Anura and Gymnophiona. Amino acids are color-coded according to polarity (yellow, non-polar; green, uncharged polar; red, acidic; blue, basic). Accession numbers are listed in table 1-10.

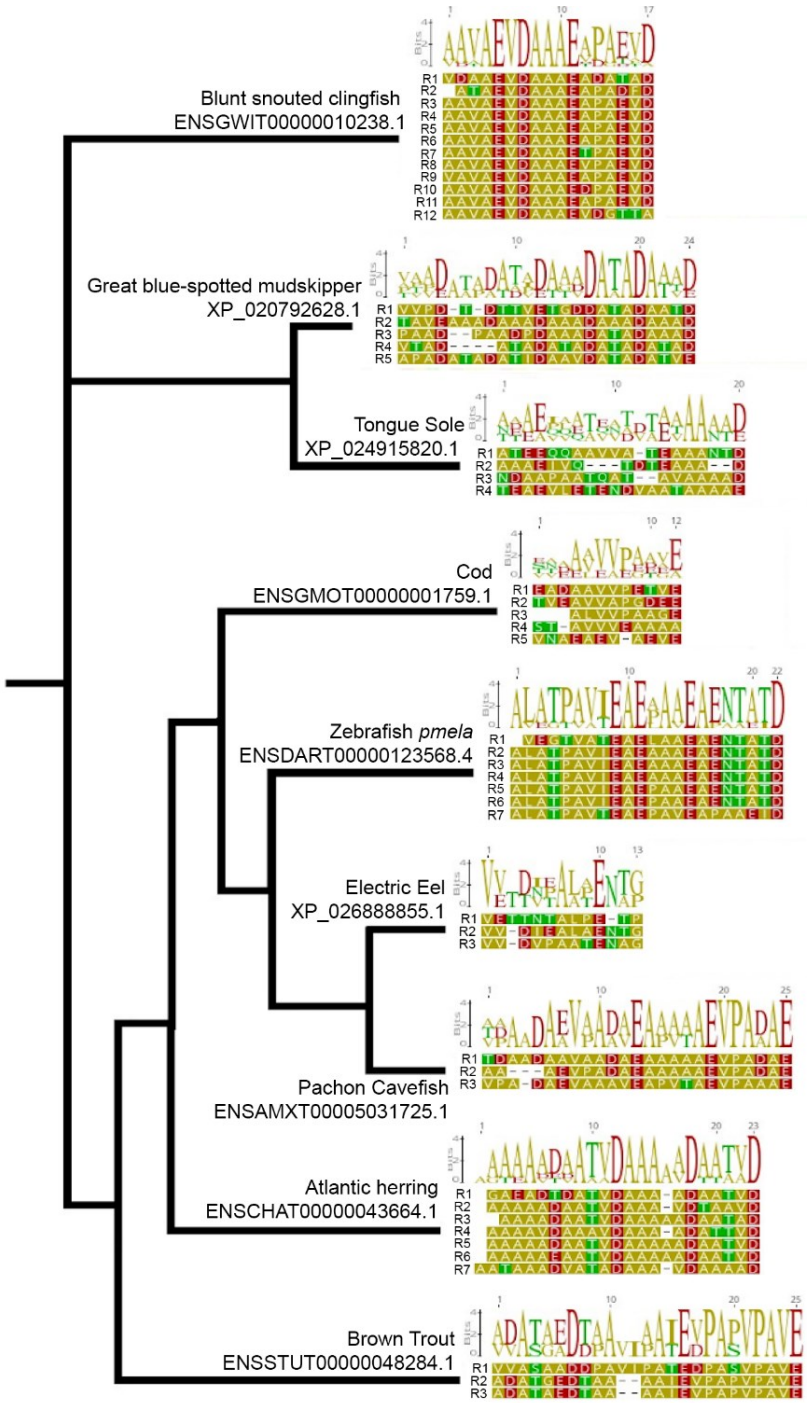

1-12. Cladogram showing the fishes Pmel RPT domain.

Within the Teleostei class species were selected from the following orders Salmoniformes, Clupeiformes, Characiformes, Gadiformes, Pleuronectiformes, Perciformes, Gymnotiformes, Cypriniformes. Amino acids are color-coded according to polarity (yellow, non-polar; green, uncharged polar; red, acidic; blue, basic). Accession numbers are listed in table 1-10.

---- The following is my own work unless otherwise stated ----

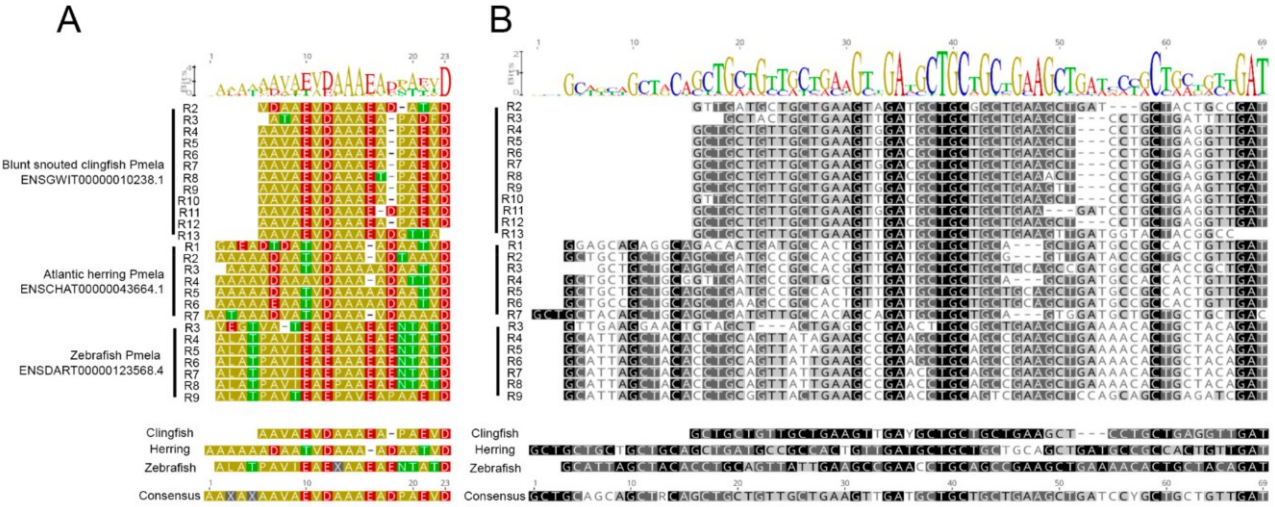

Figure 1-13. Conservation and divergence of PMEL RPT domains in fish.

Amino acid **(A)** and cDNA **(B)** sequences of three teleost fish Pmela repeat domains were aligned to accentuate the insertions or deletions that differentiate the repeat unit structures of these separate species. Common sequence logos are shown above the alignments, with individual species and combined consensus sequences below. An "X" represents less than 50% consensus. **(A)** Residues are color coded for the polarity of their amino acid side chains (yellow, nonpolar; green, uncharged polar; red, acidic; blue, basic). **(B)** The corresponding cDNA is color-coded by similarity (from darkest to lightest: 100%, >80%, >60% and <60%). An "R" represents a purine A/G, and a "Y" represents a pyrimidine C/T.

Chapter 2

Premelanosome protein (PMEL) repeat domain disturbance, reflective of pigmentary glaucoma patient mutations, is sufficient to disturb amyloid function

The figures and writing in this chapter are my own with the exception of parts of figure 2-1 which was modified from Chapter 1, figures 2-7 and 2-8 where the optical coherence tomography images were acquired by Dr. Nicole Noel, and figures 2-2 and 2-10 which were produced by Drs. Paul Chrystal and W. Ted Allison, respectively.

2.1 Abstract

Pigmentary glaucoma can be caused by dominantly inherited, non-synonymous point mutations in the repeat domain of the premelanosome protein (PMEL). Patient variants in PMEL led to altered fibril formation when assessed *in vitro.* This change in PMEL fibril structure contrasts previous observations from zebrafish, mouse, and quail models that are recessively inherited null mutations. Due to poor primary sequence conservation (despite functional conservation), these mutations are difficult to model in zebrafish. Lab members generated zebrafish with an in-frame deletion (12 base pair) within the repeat domain to reflect genetic changes being restricted to this one domain in pigmentary glaucoma patients. To test the hypothesis that the repeat domain is required for melanosome function, we compare this new repeat domain mutant with wildtype and a *pmela* null (or strong hypomorph) mutant.

Mutations in the zebrafish homolog of *PMEL* (*pmela*) were created via clustered regularly interspaced short palindromic repeats (CRISPR) Cas9 technology. The sequence encoding the repeat region of *pmela* was targeted, and a four amino acid deletion was engineered. Fish were monitored for pigmentation defects. Retinal health was assessed via transmission electron microscopy, and optical coherence tomography. Intraocular pressure was evaluated by rebound tonometry.

Disruption of the repeat region is sufficient to cause melanosomal and ocular phenotypes in homozygous zebrafish larvae. This new mutant contrasts the *pmela* null mutant zebrafish in that it is predicted to produce (modified) Pmela. The repeat domain mutant interestingly exhibits a heterozygote phenotype when evaluating the even distribution of melanin in the melanosome and developmental ocular size. The ocular phenotypes are not observed in adulthood when evaluated clinically with OCT and rebound tonometry, however, the dilute body pigmentation persists. Use of rebound tonometry in zebrafish is described, and provides an easy tool to assess intraocular pressure, a hallmark of glaucoma, in zebrafish models.

It is striking that this novel repeat domain mutant has a phenotype that is mostly consistent with the phenotypes of the other previously described mutations in zebrafish *pmela* that are predicted to have more devastating outcomes on protein domains or abundance. It is also distinct in having a clear heterozygous phenotype, which is consistent with previously described missense mutations producing more severe disease outcomes than null mutation in other species.

These data support the importance of the repeat domain generally, which is consistent with Pigmentary Glaucoma patient mutations being enriched in this domain. These data lead us to speculate that maintaining this register of the repeats is crucial for Pmela's ability to form amyloid scaffolding for melanin deposition in zebrafish.

2.2 Introduction

Pigmentary glaucoma is a heritable cause of blindness that lacked a genetic cause until a recent international collaboration identified mutations in the *PMEL* gene (encoding premelanosome protein (PMEL)) in multiple countries and patient lineages [9]. PMEL forms the fibrillar scaffold (a functional amyloid) for the deposition of eumelanin pigment and elongates the melanosome (the pigment-containing organelle) during its development [24, 25, 31-33]. The disease mechanism associated with these mutations is unknown, limiting successful medical management.

PMEL's repeat domain is thought to be integral in amyloid formation and a similar repetitive region is found in other amyloidogenic proteins [20, 22, 34, 127, 128, 129]. However, *in vitro* work on this region of human, mouse, and zebrafish PMEL has shown it to be both sufficient and dispensable for fibril formation [102-105] prompting our investigation of whether it is necessary *in vivo*. *In vivo* work has the advantage of not only assessing whole organism outcomes, but also in allowing for species appropriate post translational processing. The repeat region of PMEL is O-glycosylated and this could play an important role in tertiary and quaternary amyloid protein structures [23-30]. PMEL protein is highly conserved within people, however, the repeat domain sequence is poorly conserved between taxa making exact modelling of the disease-causing mutations difficult [40, chapter 1]. Mouse would be a natural model choice, and conserved residues could allow mutation of the same PMEL residues that are altered in pigmentary glaucoma patients. However, no ocular phenotypes have been reported for PMEL mouse mutants, whereas phenotypes are apparent in zebrafish [40, 130] (Figure 1-1, and Table 1-10). Zebrafish have an obvious repetitive domain in their homolog Pmela (Chapter 1). Although the sequence differs, the fact that it exists in a homologous location on the protein and with similar glutamic acid/aspartic acid ladders within serine/threonine rich areas (Figure 2-1b & c, Chapter 1), suggest its function is likely conserved.

Zebrafish with mutations in or reduced abundance of *pmela* gene products demonstrate that Pmela is required for normal pigmentation and melanosome biology due to their visibly paler colour [9, 41, 131, 132, 9]. To date, manipulations in zebrafish have decreased Pmela protein abundance and/or led to loss of the multiple Pmela protein domains (Figures 2-1a, 2-6). The *fading vision* zebrafish model is truncated within the repetitive region of Pmela and the *ua5022* mutation has dramatically reduced transcript abundance, presumably through nonsense mediated decay [41, 9, 131]. We sought to examine zebrafish with relatively small perturbations in the repeat domain. This is similar to the human disease associated mutations, speaks to the functionality of the repeat domain in zebrafish, and is distinct from any other previously described zebrafish *pmela* mutants (Figure 2-1a & b). Although an in-frame deletion mutant, along with the substitutions in human disease mutations, do not seem particularly dramatic when visualizing how they could derail the register of the repeats, one can imagine how this may affect protein structure and function if this area is integral in binding together adjacent repeats and/or repeats of neighboring Pmela proteins (Figure 2-1b & c).

An additional rationale for pursuing this manipulation of the repetitive region is to assess the validity of using zebrafish Pmela as a model for PMEL. Graham *et al.* manipulated human cells in culture to support their interpretation that the function of PMEL's repeat region is to establish appropriate spacing amongst the amyloid fibrils [22]. Interestingly, the repeat region from zebrafish Pmela was less effective compared to other species repeat regions when substituted into human and Xenopus PMEL proteins, thus questioning this region's equivalent functionality. They supported this potential decrease in functionality with the cavitations observed within wildtype zebrafish melanosomes [22, 132]. By looking at melanosomal anatomy in our mutants, we can address the amount of functionality lost from baseline/wildtype when the repeat region is mutated within the appropriate biological host (with appropriate post translation modifications).

The precise pathologic pathway resulting in pigmentary glaucoma remains unknown in humans. Pigmentary glaucoma is often, but not always, preceded by pigment dispersion syndrome (when pigment is sloughed from the posterior side of the iris and freely follows the flow of the aqueous humour) [133]. Hypotheses of why the pigment is released into the anterior chamber include either a cytotoxic effect of PMEL and/or anterior segment conformational abnormalities, causing mechanical damage to the iris through the zonular fibres rubbing [133].

The pigment could either increase eye pressure to result in glaucoma by physically blocking or by damaging the trabecular meshwork cells that control aqueous humour drainage out of the eye.

Either of these potential mechanisms would increase intraocular pressure and the risk for glaucoma/optic nerve death and, ultimately, vision loss. Additional hypothesis of a cytotoxic or developmental/anatomical effect not connected to ocular hypertension should also be considered, because not all pigmentary glaucoma patients have increased eye pressure and the full extent of the role of the PMEL protein in ocular development remains unknown [133]. However, elevated intraocular pressure does remain a prominent risk factor and symptom of glaucoma, in addition to being a common treatment target.

We report on this new zebrafish *pmela* mutant with an in frame twelve base pair deletion in the repeat domain (designated as the *ua5030* allele), with both biological assays in addition to testing that is more reflective of how patients would be evaluated clinically with use of optical coherence tomography and rebound tonometry.

2.3 Methods

Bioinformatics

Geneious Prime 2020.1.2., created by Biomatters (https://wwww.geneious.com) was used to create the protein repeat alignment figures. Refer to Chapter 1 for how repeats were originally located and defined.

Animal Care

Zebrafish were housed at the University of Alberta aquatics facility and used under the Animal Use Protocol 00000077 approved by the Biosciences Animal Care and Use Committee, which adheres to both the association for research in vision and ophthalmology (ARVO) guidelines for use of animals in ophthalmic and vision research as well as the Canadian Council for Animal Care guidelines.

Transmission Electron Microscopy

Whole five days post fertilization embryos were fixed in 2.5% Glutaraldehyde and 2% Paraformaldehyde in 0.1M Phosphate Buffer (pH 7.2 – 7.4). The day of processing, they were

washed three times for 10-15 minutes in 0.1M phosphate buffer. They were left for 1 hour in 1% osmium tetroxide in 0.1M phosphate buffer. The initial three washes were repeated. The samples were dehydrated using increasing concentrations of ethanol every 15 minutes (50%, 70%, 90%, 100%, 100%, 100%). They were placed in 1:1 Ethanol:Spurr for 1-3 hours and then pure Spurr resin overnight. The next day the Spurr resin was changed twice prior to embedding the sample in flat molds with fresh Spurr resin and curing at 70°C overnight. A Reichert-Jung Ultracut E Ultramicrotome was used to cut sections to 70-90nm thickness prior to staining them with uranyl acetate followed by lead citrate on a grid. A Philips FEI Margagni 268 transmission electron microscope operating at 80kV was used with a Gatan Orius CCD camera to visualize the samples.

One representative image was taken from the limits of the retinal pigmented epithelium and two from the mid retinal area for each fish. Fiji win 64 was used to evaluate the images. Set scale for measurement by manually measuring scale bar included at the time of image capture. Set threshold by visually minimizing melanosome touching while not losing the melanosome shape, this was variable but never exceeded 0-150. Used the analyze particles manager to select particles that were greater than 0.02μm^2 in size, and to exclude those touching edges. Holes within the particles were included. Each image was reevaluated and measurements from multiple touching melanosomes were manually discarded. The measurements were all average to a singular value for each fish prior to conducting ANOVA's with post hoc Tukey tests using Graph Pad Prism 9.3.1.

Optical Coherence Tomography

Conducted as per [134]. Fish were anaesthetized and positioned for imaging and retinal images were captured at the location of the optic nerve. A measure of the full thickness of the retina and the proportion of it that each layer occupied was taken from both sides of the optic nerve as soon as the layers were clearly identifiable using Fiji. A Mann Whitney test was performed comparing each genotype with an age matched control.

Intraocular Pressure

Individual zebrafish were anaesthetized by immersion in MS222 and facility water until operculation was slowed/irregular. They were propped up to be in anatomical position at the

edge of the counter (see Chapter 3). The Icare Tonovet plus (TV011, © 2016 Icare Finland Oy, Vantaa, Finland) needs to stay upright during use and this allows space for it below the height of the counter. The Tonovet plus was kept level and pointed at the middle of the globe prior to propelling the probe. The Tonovet plus requires 6 measurements, discards the highest and the lowest prior to averaging the remaining 4. It assigns a colour score for variance. It discards any measurements where the probe is too far or too near and gives correction to the user. Only green (the most consistent) measurements were accepted, and two to three (averaged) measurements were averaged for each eye. The right eye was always measured first unless otherwise stated. If the eyes were becoming dry (probe sticking as opposed to rebounding) a drip of the anaesthetic/water was put over the head. The two eyes were then averaged, and a Kruskal-Wallace test was used to compare between genotypes using Graph Pad Prism 9.3.1. For further validation please see chapter 3.

2.4 Results

Zebrafish pmela mutant made to reflect human patient variations in PMEL

A new zebrafish *pmela* mutant (*ua5030*) was created (through Allison lab efforts led by Dr. Paul Chrystal), which possesses a twelve-base pair (four amino acid), in frame, deletion in the repeat domain of the protein. The repeat domain is homologous to the domain in human PMEL where two thirds of the human patient mutations cluster (Figure 2-1a). Due to this deletion being in frame, the protein should still be produced, albeit in an altered form. Comparing the rigidity of the protein repeats to one another in humans and zebrafish and taking into consideration the similarly subtle protein changes (point mutations) that cause pigmentary glaucoma in humans, we think it is reasonable to suppose that the molecular function of the repeat domain will be relatably altered between *ua5030* Pmel and human PMEL repeat domain variants (Figure 2-1b). Moreover, *ua5030* Pmel, is undoubtedly more similar to the human patient variants than any other previously described zebrafish mutants or morphants as they are all nulls or hypomorphs (from greatly decreased abundance of gene products or due to lack of entire protein domains) [9, 131, and 41, respectively].

Zebrafish larval pmela mutants have pigmentary defects

The zebrafish *pmela* mutants from both of our alleles are grossly hypopigmented when bred to homozygosity (Figures 2-2a & b, and 2-9). This was expected for the previously published null allele (*ua5022*) given that body colouration is diluted in previously described *PMEL* mutants across several taxa (see Chapter 1, Figure 1-1 and Table 1-1). However, that this phenotype was recapitulated when only the repeat domain was affected in the *ua5030* mutant is a new finding (Figures 2-2a & b, & 2-9). Pigment defects were obvious upon gross examination of both larval and adult fish, so we focused on the (melanosome rich) retinal pigmented epithelium, at five days post fertilization to characterize the melanosomes in detail. The morphology of melanosomes in the repeat domain mutant (*ua5030)* retinal pigmented epithelium were consistent with melanosomes described in other loss of function mutations as they were smaller and rounder (40, 41, Figures 2-3, 2-4, 2-5, & 2-6). Both the *ua5022* and *ua5030* melanosomes fail to elongate, shown by the Feret's diameter/caliper length being roughly one fifth shorter than wildtype suggesting that Pmela is not creating normal fibrils (Figure 2-4b). Melanosomes from both mutants also have more variable electron density (calculated as the standard deviation of each melanosome's grayscale values (assigned to each pixel)), suggesting that mutant Pmela amyloid no longer provides an efficacious scaffold for consistent, even, melanin deposition and leaves it clumped irregularly within the melanosome (Figure 2-5b). These results are shown by averaging the outputs from individually measured melanosomes of each fish. Data at the melanosome level is provided to allow for visualization of the variability within individuals (Figures 2-4a & 2-5a).

The ua5030 heterozygote larvae has an intermediate phenotype for both pigmentation and ocular size, contrasting the ua5022 mutant phenotypes

Melanosomes from heterozygous *pmela*$^{+/ua5030}$ larvae exhibited starkly variable electron density (Figure 2-5), whereas other heterozygous mutants such as *pmela*$^{+/ua5022}$ larvae did not. Additionally, *ua5030* has an intermediate micropthalmia between homozygote *pmela* mutants and wildtype larvae (Figure 2-2c). Although the average melanosomal length (Feret's diameter) was not significantly different between heterozygote mutants and wildtype fish, we noted some longer outlier melanosomes in both heterozygote mutants which were not observed in any wildtype fish sections (Figure 2-4a).

Zebrafish larval pmela mutants have a prominent ocular phenotype

The hypothesis that *PMEL* causes pigmentary glaucoma via anatomical changes in the anterior segment (see Introduction) is somewhat supported by both zebrafish homozygous phenotypes and the *ua5030* heterozygote mutant phenotypes. All three genotypes showed decreased eye size starting at 3 dpf and persisting until 7 dpf (Figure 2-2) in addition to the previously described changes in shape of the anterior segment of *ua5022* homozygous larvae suggestive of increase intraocular pressure [9].

The retinal pigmented epithelium is rich in melanosomes and provides a supporting role to the photoreceptors it surrounds. A suboptimally functioning retinal pigmented epithelium presumably explains why photoreceptor abnormalities have been reported previously in zebrafish with altered Pmela expression [132, 41]. Ocular sections of 5dpf zebrafish retinas, evaluated by transmission electron microscopy, showed delayed or perturbed photoreceptor development from different *pmela* mutations. *Ua5022* homozygous fish had no to very few photoreceptors (Figures 2-3c, & 2-6). This was also the case in two thirds of the *ua5030* homozygotes, with the remaining individual having photoreceptors with abnormal outer segments (Figures 2-3c, & 2-6). The homozygote mutant retinal pigmented epithelium had variable "pigment clots" (aggregations of abnormal pigmented organelles in the retinal pigmented epithelium), vacuoles, and melanosome numbers between individuals and across each retina. The heterozygote mutants all had normal photoreceptors suggesting that only one working copy of *pmela* is required for sufficient retinal pigmented epithelial support of photoreceptor development and/or maintenance.

The overall pattern of photoreceptor and retinal pigmented epithelium phenotypes are summarized for each genotype in Figure 2-6.

Adult zebrafish pmela mutants did not have a grossly apparent ocular phenotype

No marked ocular changes were observed in the mature *ua5022* and *ua5030 pmela* homozygous mutant fish (Figures 2-7 through 2-9). Optical coherence tomography (OCT) was performed by Dr. Nicole Noel and used to measure the relative depth of the retinal layers adjacent to the optic nerve and detected no difference between age matched wildtype (AB) individuals.

Intraocular pressure measurement (detailed and validated in Chapter 3) also showed no detectable difference between the different genotypes (Figure 2-9a). This is a new, more accessible method of determining intraocular pressure in zebrafish that seems to produce similar results in wildtype zebrafish compared to the previously described servonull methods (135).

2.5 Discussion

The ua5030 phenotype highlights the importance of the repeat region of Pmela

The pronounced phenotype I observed, resulting from the small in frame mutation (*ua5030*) in the repeat region of Pmela, caused similar changes in the homozygous individuals to those described in previously published null mutations (*ua5022*, *fading vision*), which supports the importance of this repeat region (figures 2-6). Zebrafish and humans are the only animals known to have phenotypes from mutations in this domain (Chapter 1, Figure 1-1, & Tables 1-1 & 1-2). Considering the presumed role of the repetitive region in fibril formation, fibril derangement underpinning Pmela's altered functioning is a natural prediction (Figure 2-10) [22, 102-105]. The mutation could impact not only the conformation and function of the individual Pmela protein molecules but also how they interact with the other molecules of Pmela protein. Fibril structure could potentially be resolved by assessing mutated fibrils within depigmented melanosomes of cells and/or fish to determine variation between *pmela* mutations. The factors responsible for the change in the functionality of the repetitive region could help explain the variable disease course in humans with *PMEL* mutations in addition to contributing to our general understanding of the role of repetitive regions in amyloidogenic proteins. Some ideas include O-glycosylation not only affecting tertiary and quaternary protein structure but also shielding the cell membranes from toxic PMEL amyloid, and/or facilitating increased binding of toxic intermediates from pigment production that could otherwise cause cell stress [22]. Furthering the knowledge of amyloid biology concerning mechanisms that perturb protein aggregation, or cause amyloid related toxicity, have the possibility of eventually aiding to ameliorate the courses of prion-like diseases.

Phenotypic variation reflective of incomplete penetrance and variable progression of human pigmentary glaucoma

The *ua5030* allele presented with an increased severity of a heterozygous phenotype compared to the *ua5022* allele consistent with having abnormal protein, as opposed to decreased abundance of abnormal protein (respectively). A unique heterozygote phenotype with changes only made to the repeat region suggests a potentially different or toxic function of mutant Pmela (as opposed to the strict loss of function mutation suggested by the melanosome morphology) (Figures 2-2 and 2-5). Amongst various species it appears that missense mutations are more likely to cause dominant phenotypes with more severe outcomes compared to only the dilution of body pigmentation observed with null mutations (Chapter 1, Figure 1-1, & Table 1-1). The hypothesis of *PMEL* mutations being toxic has previously been explored and supported through comparison of different *Pmel* genotypes in chickens [16, 45]. An insertion mutation in the transmembrane domain causes a dominant white plumage. When a second mutation is introduced onto this allele the phenotype is modified to an intermediate "smoky" colour (akin to typical null phenotypes). Remarkably, in a separate lineage, a different mutation in *Pmel* also makes a dilute "dun" colouration.

An alternative explanation for phenotypes in heterozygotes is haploinsufficiency, but this would logically present even more clearly in the null mutations (*ua5022*) rather than those still producing protein (*ua5030*). Quantification of gene products (qPCR, Western blot) would likely ease in the interpretation of null vs. toxic mutations.

Other factors (genetic background, effects on developmental rate, chance) may affect this phenotype, as there was phenotypic variation within, in addition to between, genotypes. For example, the dominant white phenotype in chickens has decreased penetrance in males (sex is not something we were able to evaluate in larval zebrafish) [16]. The trend towards longer melanosomes in both the *ua5030* and *ua5022* heterozygotes existed only in certain individuals (Figure 2-4a). Similarly, photoreceptors were only in one of the *ua5022* mutants and only one of the *ua5030* mutants had sufficient photoreceptors to view consistent abnormalities in outer segments. Phagocytosis and blunting of photoreceptors were only observed in *fading vision* fish (Figure 2-6) [41]. This could be explained by a partial loss of function or a partial compensation mechanism that causes variability in homozygous zebrafish *pmela* mutants (or alternatively other

unexpected genetic anomalies). Larger sample sizes would be required to rule out any technical artefacts.

Use of larval and adult zebrafish as models of pigmentary glaucoma

It is important to be able to assess disease symptoms in a way that is relevant to what is done in human patients, to be able to best provide translational results. In diseases that variably progress, like pigmentary glaucoma, non-invasive, easily repeatable and longitudinal measurements are of great utility in tracking disease progression within individual research subjects. Intraocular pressure is part of the minimum database assessed routinely in ophthalmic patients and is an important risk factor and treatment target for glaucoma [135].

Rebound tonometry provides a relatively "tank-side" diagnostic tool to measure intraocular pressure in zebrafish glaucoma models in a minimally invasive way. Previously described methods in zebrafish, although considered the gold standard for accuracy, are not easily adopted or amenable to repeated measures [135, 136, 137].

Rebound tonometry did not show a difference in intraocular pressure between zebrafish genotypes, which could mean that PMEL disruption is not the direct molecular cause of this glaucoma symptom. However, the data should be interpreted with caution as the lack of clear difference could be due to variability and/or later onset/recovery of phenotypes in fish (Figure 2-9). To fully assess our new *ua5030* mutant, it would be ideal to serially measure it (and other genetic causes of heightened intraocular pressure in zebrafish), in concert with OCT until senescence. That approach might determine a timeline and elucidate further details of the pathobiological relationship between intraocular pressure and ganglion cell death beyond pigmentary glaucoma progression. However, we must also consider the limitations of a zebrafish model. The ocular anatomy of humans and zebrafish is sufficiently different that conformational/developmental changes that predispose to pigmentary glaucoma may not be fully represented in the zebrafish anatomy. In humans, the aqueous humour of the anterior segment is drained through the trabecular meshwork cells, this can be blocked, heightening intraocular pressure, through either clogging of the meshwork with debris or through damaging these specialized cells [138]. Zebrafish have an analogous drainage structure, the ventral canalicular network, but it is distinct from the trabecular meshwork of humans [138]. Additionally, retinal regeneration is common in zebrafish and this apparent resolution of the ocular phenotype could

reflect their resilience and redundancy outshining the human ability to overcome ocular damage [139, 140, 141, 142]. Our model is likely most relevant to the hypothetical cytotoxic mechanistic cause of pigmentary glaucoma. However, the human mutations could have a unique toxic aspect to them resulting in pigment sloughing to the trabecular meshwork, or other unique pathologies within the eye.

The differences between the larval and adult phenotypes could simply be reflective of ontogeny. However, I think it worth mentioning that I noticed a much lower survival rate among homozygous mutant larvae compared to wildtype, which could be suggestive of only the mildly affected individuals surviving to adulthood. Larvae with better vision would undoubtedly be more successful at feeding and surviving. Secondly, as we were originally interested in the repetitive domain, Pmela was the natural choice as a functional homolog to PMEL, as zebrafish Pmelb lacks an obvious repetitive domain and homologous trafficking cues (Figure 1-5) [124]. However, it is possible that *pmelb* could compensate for other functions of *pmela* in adult fish.

Regardless, it is exciting to have developed a mutant that more closely mimics the genetic cause of pigmentary glaucoma and displays a relevant pigmentary phenotype, in addition to describing a noninvasive tool for zebrafish glaucoma/ocular hypertension research.

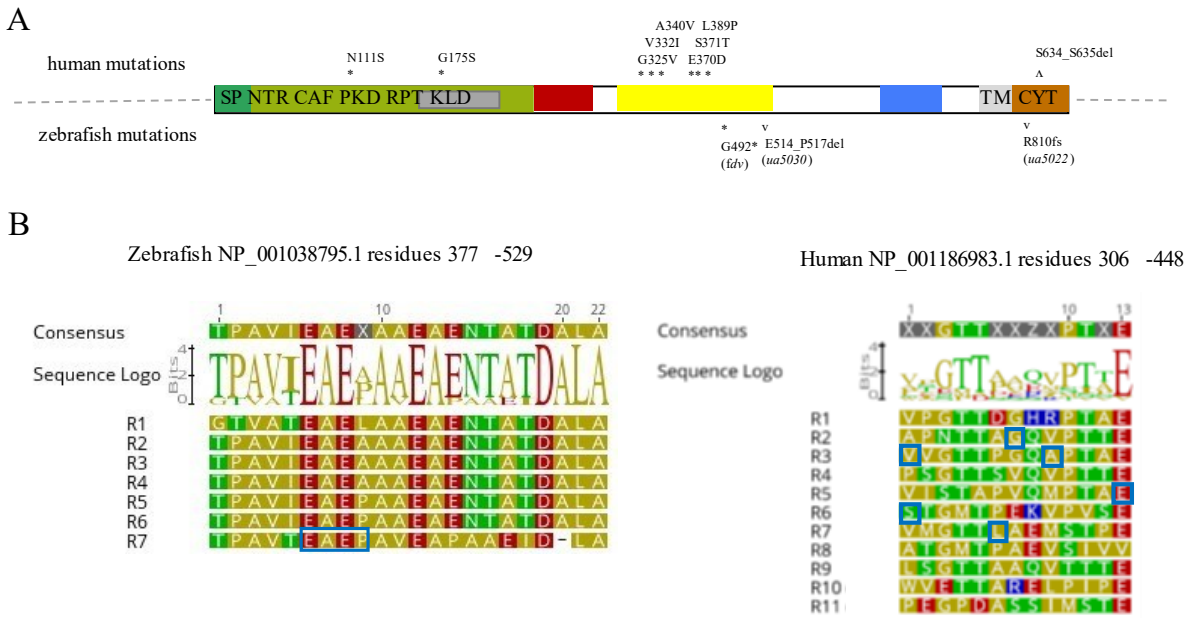

Figure 2-1. Zebrafish *pmela* mutant alleles.

(A) Schematic representation of PMEL protein showing the functional domains (SP = signal peptide; NTR = N-terminal region; CAF = core amyloid fragment; PKD = polycystic kidney domain; RPT = repeat domain; KLD = kringle-like domain; TM = transmembrane domain; Cyt = cytoplasmic domain), site of pathogenic human variants above and zebrafish mutations below (asterisks; (modified from Chapter 1). Human mutations are enriched in the repeat domain. **(B)** Zebrafish and human repeat domain repeats stacked upon themselves to illustrate the functionally conserved aspects of this region as well as the *ua5030* deletion (left) and the human point mutations (right; both shown by boxed amino acids). All of these relatively small changes result in gross phenotypes likely due to the importance of the repetitive nature of this area to its function.

---- the following figure is the work of Dr. Paul Chrystal ----

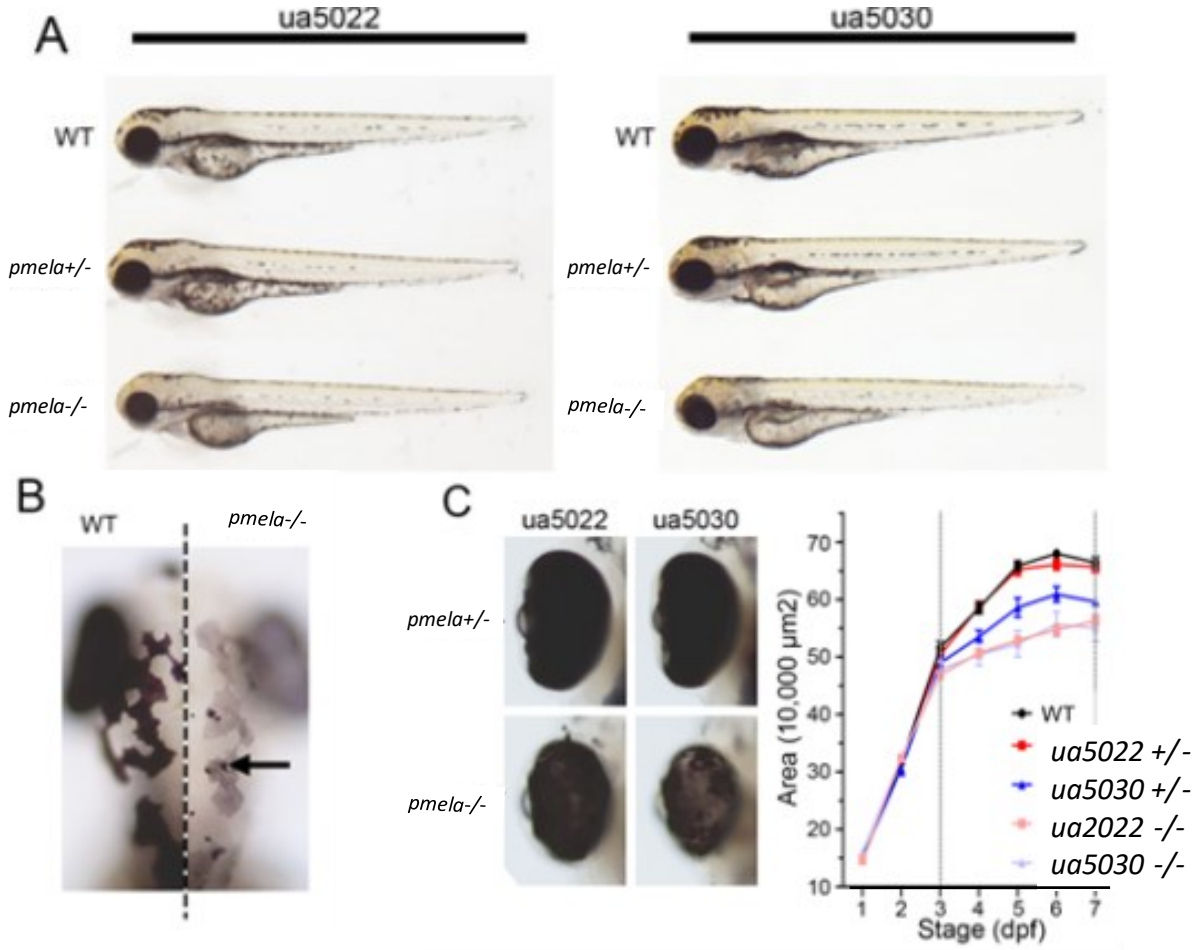

Figure 2-2. *pmela* mutants display systemic hypopigmentation and decreased ocular area **(A)** Both *pmela* mutant lines (*ua5022* and *ua5030*) cause systemic hypopigmentation in homozygotes at 3 days post fertilization (dpf). **(B)** In addition to lighter, "washed-out" pigmented epidermal tissues, some melanocytes are abnormally constricted to fine puncta (arrow). **(C)** From 3dpf to 7dpf homozygotes from both alleles had decreased ocular area compared to wildtype larvae. The in-frame (*ua5030*) heterozygote mutation exhibited an intermediate eye size.

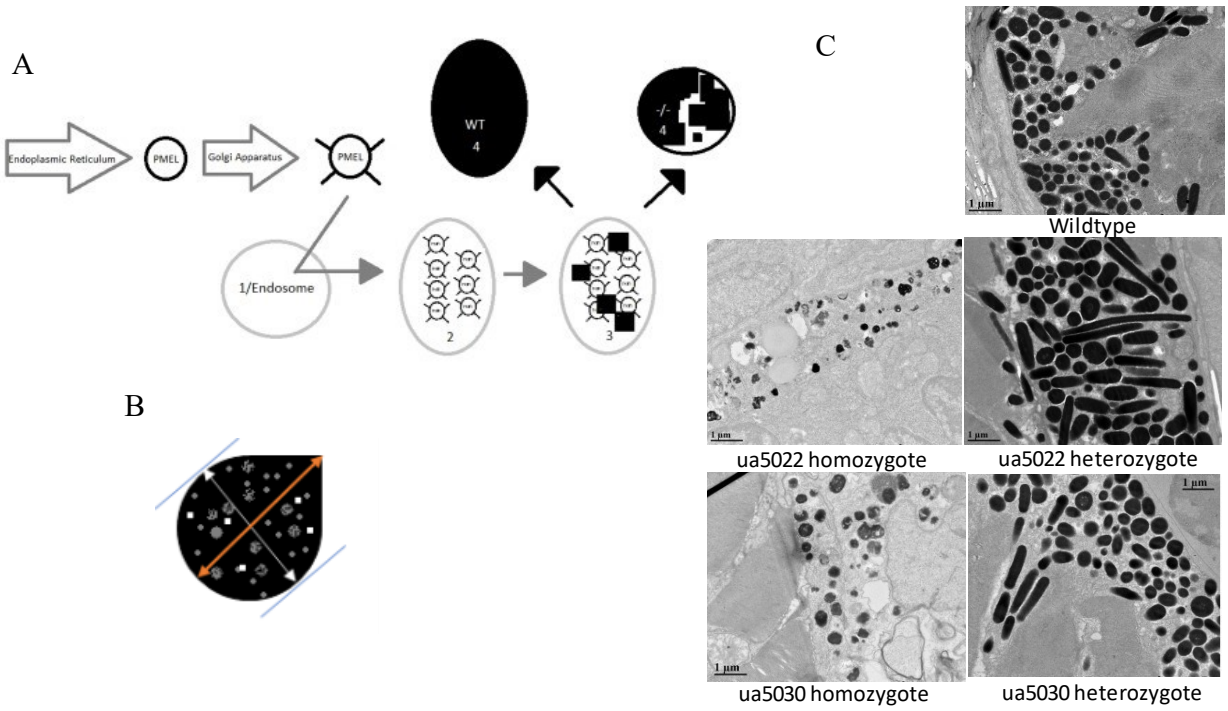

Figure 2-3. Melanosome development, measurement, and imaging.

(A) Schematic of the maturation of premelanosome protein (PMEL) and the melanosome. PMEL is synthesized in the endoplasmic reticulum and modified in the Golgi apparatus before entering an endosome. The endosome goes through four stages (1>4) of maturation before becoming a fully formed (WT) melanosome. Stage 1: fibril free endosome, Stage 2: fibrils begin forming, Stage 3: melanin starts to be deposited on the fibrils, Stage 4: melanin is evenly distributed, obscuring the fibrils. Melanosomes are oblong in shape (WT). In *Pmel* knockout mice (-/-) the mature melanosome has irregularly distributed melanin and is round analagous to stage 1 [40]. **(B)** A pictographic melanosome to show Feret's diameter (orange arrow) is the longest distance that could be measured in a straight line within the confines of the melanosome. The average grayscale value is measured by pixels within single melanosomes and the grayscale standard deviation calculated on individual melanosomes. This standard deviation was used as a metric for general variation within all the melanosomes of an individual (Figures 3 and 4). Wildtype melanosomes are homogenous with low standard deviation, in contrast, mutants had variable electron density due to unequal distribution (clumping) within the melanosomes. **(C)** Sample transmission electron microscopy images of retinas from 5 days post fertilization zebrafish of various genotypes: wildtype, *ua5022* homozygous and heterozygous, and *ua5030* homozygous and heterozygous.

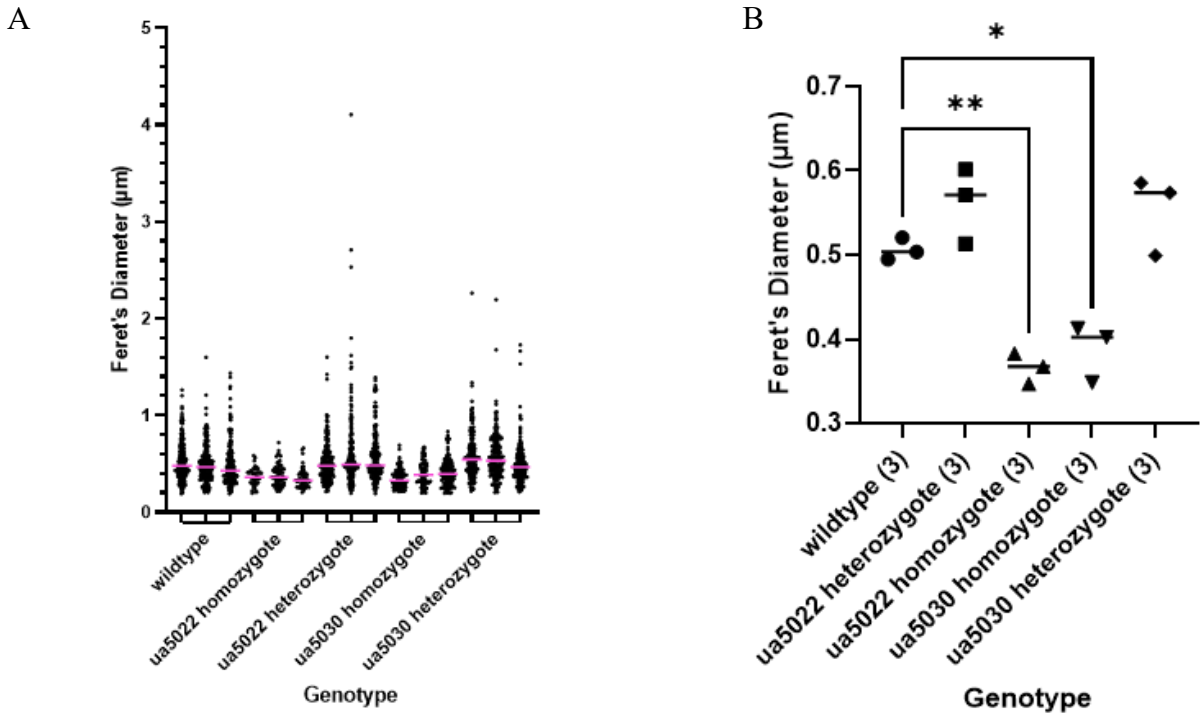

Figure 2-4. The repeat region of Pmela is required for elongation of melanosomes. **(A)** The Feret's diameter (maximum length of straight line within a shape) of each individual melanosome is plotted for each fish and the average measurement for each fish is shown with a pink line (which is also plotted in panel B). **(B)** An ANOVA with Tukey's post hoc test shows the average Feret's diameter of melanosomes is shorter in the two homozygote mutants, *ua5022* and *ua5030* when compared to wildtype. Both the *ua5022* and *ua5030* melanosomes fail to elongate, shown by the Feret's diameter/caliper length being roughly one fifth shorter than wildtype suggesting that Pmela is not creating normal fibrils.

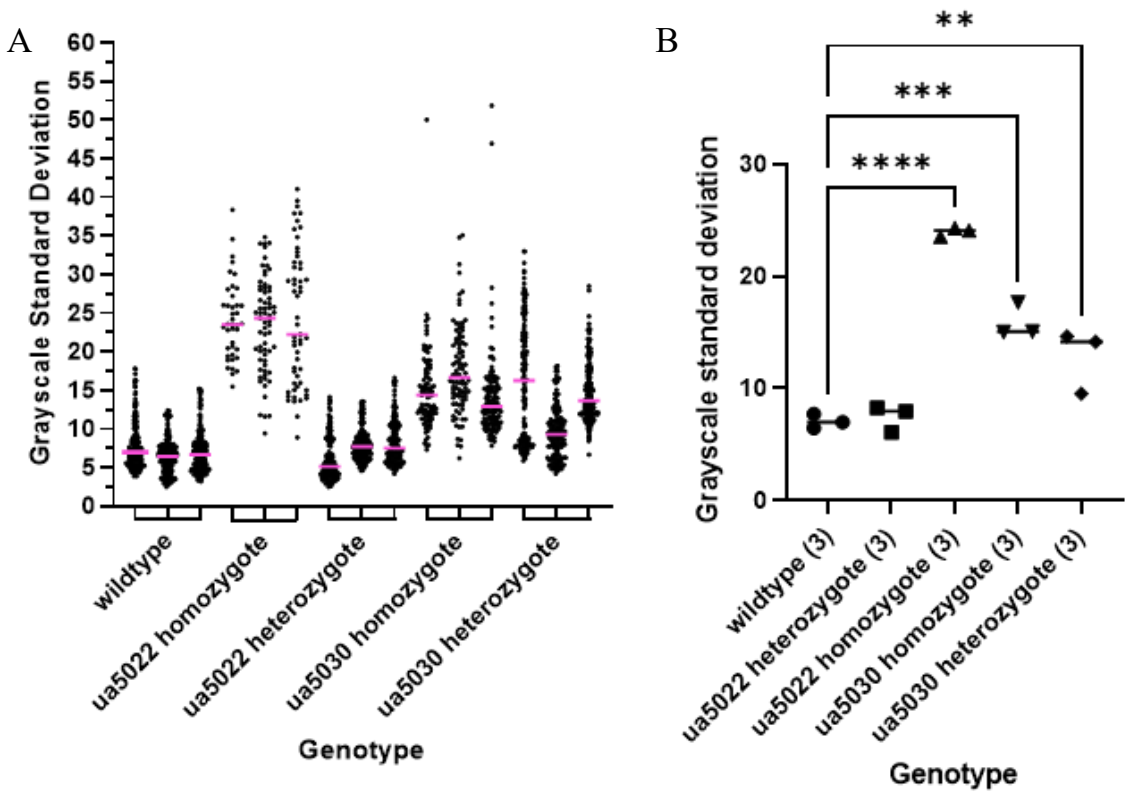

Figure 2-5. The repeat region of Pmela is required for even distribution of melanin within melanosomes.

(A) The grayscale standard deviation between pixels of individual melanosome is plotted for each biological replicate with the mean delineated in pink. **(B)** An ANOVA with Tukey's post hoc test shows the average grayscale standard deviation is more variable in *ua5022* homozygotes, and *ua5030* homozygotes and heterozygotes compared to wildtype. The inconsistent electron density suggest that melanin is clumped within the melanosomes of the *ua5022* homozygotes, and *ua5030* homozygotes and heterozygotes as opposed to evenly distributed across the Pmela amyloid framework of wildtype melanosomes.

Protein Schematic							
Genotype	wildtype	Ua5022 homozygote *pmela* -/-	Ua5022 heterozygote *pmela* +/-	Ua5030 homozygote *pmela* -/-	Ua5030 heterozygote *pmela* +/-	Fading vision (*fdv*) *pmela* -/- [41]	*pmela* morpholino injected [132]
Photoreceptors		Generally absent		Abnormal outer segments. 2/3 had a reduced number.		Blunted photoreceptors	Missing or disrupted photoreceptor outer segments.
Retinal pigmented epithelium		Smaller melanosomes with greater variability in electron density. Qualitatively fewer melanosomes with pigment clots and vacuoles.	Sporadic longer melanosomes	Shorter melanosomes with greater variability in electron density.	Intermediate variability in electron density of melanosomes. Longer melanosomes?	Decreased density of melanosomes. Melanosomes were "fuzzy" in appearance and the retinal pigmented epithelium had pigment clots and vacuoles.	Fewer elongated melanosomes. Decreased melanin in the apical processes for the retinal pigmented epithelium.

Legend
> Oblong, round, small/mottled melanosomes
> Normal, blunted, and disrupted photoreceptor outer segments
> Vacuole

Figure 2-6. Phenotype of the retinal pigmented epithelium varies with different genetic disruptions.

Protein schematic illustrates the different phenotypes using grey colouration for hypomorphs or null mutations, a lightning bolt for mutations, and truncations as shorter. The legend shows the various changes to the photoreceptors and retinal pigmented epithelium (also described in their respective sections with text from previously and presently published works [9, 41, 131, 132]).

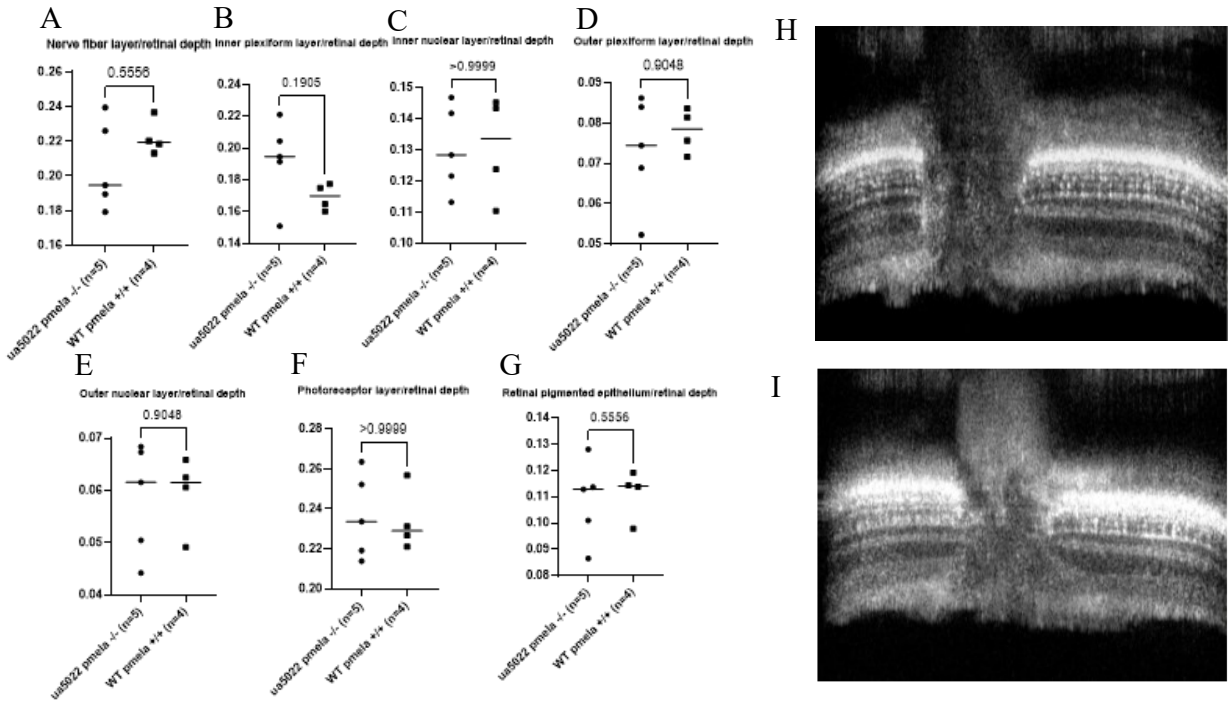

Figure 2-7. *ua5022 pmela* -/- mutants and wildtype zebrafish retinal layers show no statistical difference in thickness when evaluated by optical coherence tomography (OCT). OCTs were obtained from 1.5 year old *ua5022 pmela* -/- **(H)** and age matched wildtype **(I)** zebrafish and the ratio of each of the retinal layers to retinal depth was compared using a Kruskal Wallace statistical tests **(A-G)**.

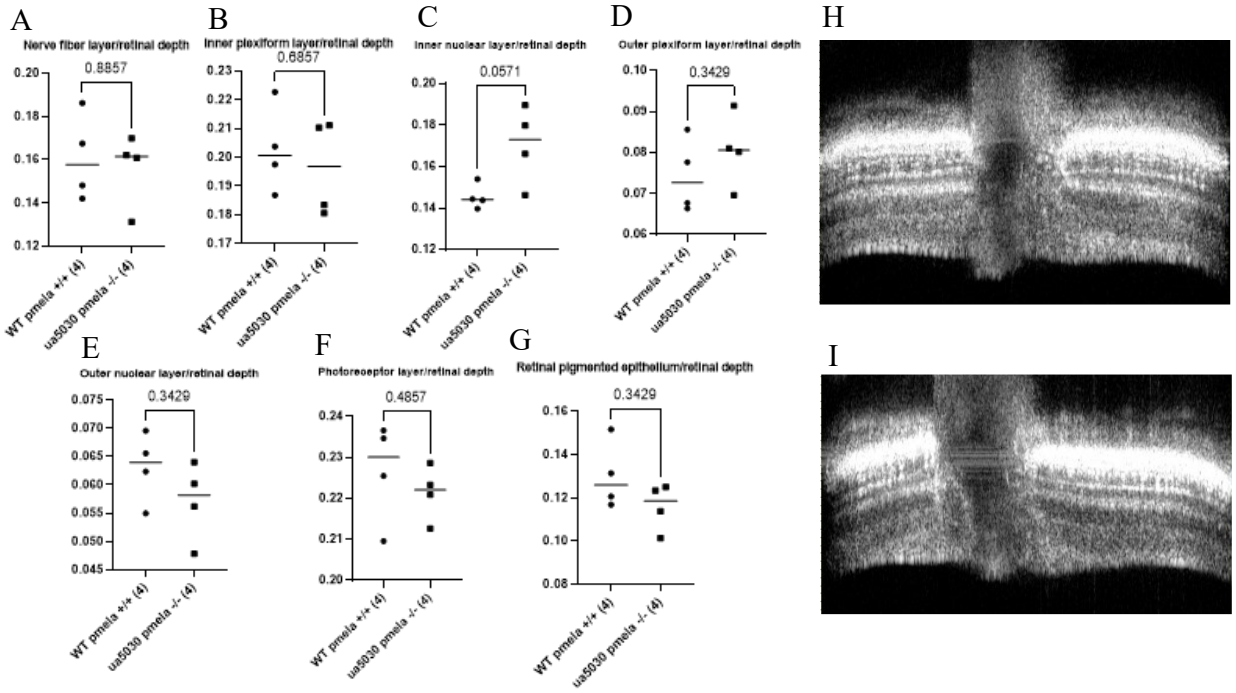

Figure 2-8. *ua5030 pmela* -/- mutants and wildtype zebrafish retinal layers show no statistical difference when evaluated by optical coherence tomography (OCT).

OCTs were obtained from 1 year old *ua5030 pmela* -/- **(H)** and age matched **(I)** zebrafish and the ratio of each retinal layer to retinal depth was compared using a Kruskal Wallace statistical tests **(A-G)**.

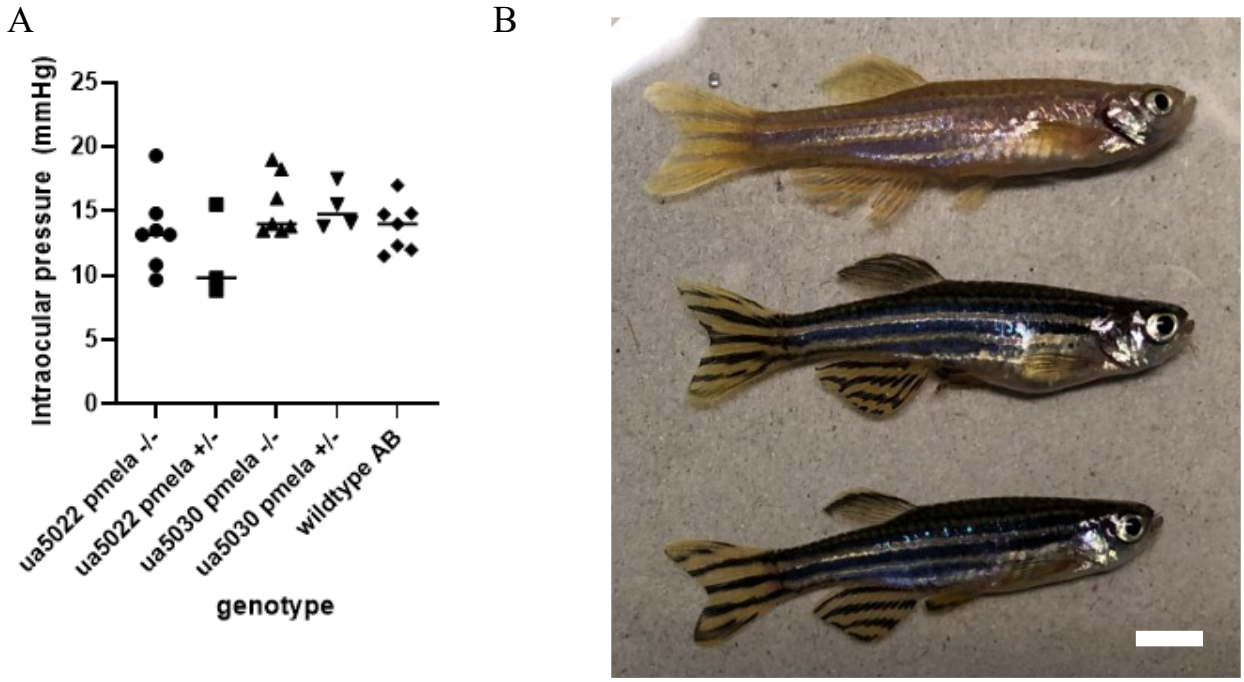

Figure 2-9. Adult zebrafish mutants did not have measurably different intraocular pressure despite retaining dilute colouration.

(A) Intraocular pressure (mmHg) was measured on adult zebrafish using a Tonovet plus. Average readings for each fish were plotted. A Kruskal-Wallace statistical test showed no significant differences between means. **(B)** From top to bottom: ua5030 homozygote with dilute colouration compared to ua5030 heterozygous, and wildtype adult zebrafish. 5mm scale bar.

---- the following figure is the work of Dr. W. Ted Allison ----

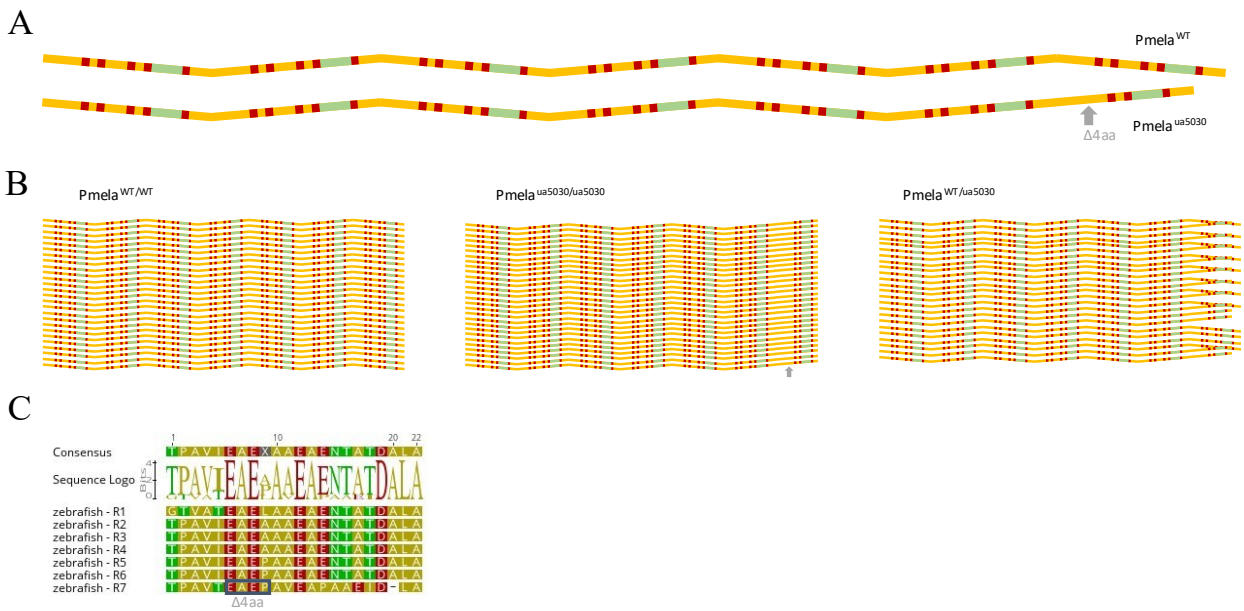

Figure 2-10. Hypothetical schematic of altered fibril formation with premelanosome protein mutation.

(A) The ua5030 mutation is hypothesized to cause a change in conformation of the protein compared to WT Pmela. **(B)** This change affects its ability to create fibrils with wildtype Pmela that is only apparent in heterozygote individuals that have two different proteins. This could underpin the dominant inheritance of pigment dispersion/pigmentary glaucoma in people through altered fibril function. This figure is not meant to represent the structure of Pmela protein with any fidelity, but it instead assumes a simple structure to assist in visualizing how having two variants of Pmela (heterozygote state) might be more disruptive than the homozygous state. **(C)** Zebrafish repeat sequence from figure 2-1, colour coding relates to the linear representation of this region in parts A and B with the ua5030 four amino acid deletion outlined in part C shown as an irregular bend in parts A and B.

Chapter 3

Zebrafish Intraocular Pressure Measurement using a portable, and accessible rebound tonometer, the Tonovet Plus (Icare, Vantaa, Finland)

The figures and writing in this Chapter are my own.

3.1 Abstract

Due to the strong ties between glaucoma and ocular hypertension, the use of a handheld, portable tonometer to measure intraocular pressure furthers the use of zebrafish for glaucoma research. We present a novel method for the measurement of zebrafish intraocular pressure and initial validation comparing intraocular pressure to fish size, to age, between eyes, and in response to two different topical eye drops that are labelled to reduce eye pressure: dorzolamide and latanoprost. Once fully validated, this straight forward method could be used to screen for phenotypes and serially test subjects for research purposes, or for the care of chronic ocular diseases.

3.2 Introduction

Zebrafish are a powerful ophthalmological model and are already used in glaucoma research [143, 140]. Most zebrafish glaucoma models are created from mimicking genetic causes of glaucoma in people (ex: *FOXC1, PITX2, LRP2, PMEL*), although using chemicals or oxidative stress has also been used to cause damage to the retinal ganglion cells [140, 144, 145, 9].

Zebrafish are particularly useful for genetic research as there are numerous genetic and behavioural tools available. Zebrafish have fast, visible, external development with a short generation time and a high number of offspring which greatly facilitates screening for phenotypes in comparison to mammals [140, 143,139]. Their small size makes them amenable to medium throughput drug screening, and behavioural testing. For ophthalmological research, they have distinct advantages over most rodents as they are diurnal with cone dominated retinas, with superior colour vision and visual acuity [140].

Although the small size of zebrafish gives them many advantages (less space, cost, and time spent evaluating), it does limit easy translation of clinical assays used with other animals such as humans [135]. Another limitation in their use for glaucoma research is their robust ability to regenerate retinal ganglion cells (the nervous tissue affected in glaucoma) [140, 141, 142].

Intraocular pressure is an important risk factor in developing glaucoma and thus it is important to measure in animal models. Glaucoma is a progressive disease and serial intraocular

pressure measurements are required to determine the relationship between ocular hypertension and optic nerve degeneration. Intraocular pressure was first measured invasively in zebrafish [135]. Many fish were successfully assessed and recovered from the electrode/cannula intraocular insertion required for the servo null/electrophysiological measurement. This method was extensively validated by creating a standard curve of different experimentally produced intraocular pressures *in vivo*. The servonull system also convincingly distinguished two different zebrafish strains and a mutant with elevated intraocular pressure (*brass* and *lrp2* (bugeye) [135, 145]. Similarly, pressure transduction has been used in fish with larger eyes (Rainbow trout and Lake trout) to measure intraocular pressure [146]. Despite great accuracy, the method requires breaching the cornea, introducing not only the risk for infection and inflammation in the eye but also a variable that is likely to alter the future health and intraocular pressure of the eye (especially when many repeated measures are needed) [135, 147].

Two minimally invasive types of measuring intraocular pressure in fish have also been reported: applanation and rebound tonometry. Both have been used to measure intraocular pressure in both research and clinical cases. Applanation tonometry is a method that infers intraocular pressure indirectly, calculated through deformation of the cornea, and has been previously applied to measure intraocular pressure in koi, red drum fish, red pacu, and zebrafish [148, 149, 136]. We attempted this in mature zebrafish and found their eyes were too small for Tonopen (Icare) use and did not have a pneumotonometer available. Rebound tonometry indirectly calculates intraocular pressure by the speed and length of impact of a probe with the cornea and has been reported in brook trout, koi carp, zebrafish, and goldfish [150, 151, 152, 137, 153).

To date, with adult zebrafish, two minimally invasive means have been reported: pneumotonometry, and rebound tonometry [136, 137]. Pneumotonometry distinguished between mutants with elevated intraocular pressure but was only published as a meeting abstract. Rebound tonometry has many advantages including a relatively lower cost, higher portability, and increased subject comfort (no topical anaesthetic is needed) [154]. Quint et al. recently published use of rebound tonometry as one element in a diagnostic pipeline for zebrafish ocular mutants, and it successfully distinguished between two mutants with increasingly elevating intraocular pressure compared to wildtype at various ages [127]. We present an additional method of rebound tonometry that requires less infrastructure (is more accessible). To provide

initial validation of the method, we assess intraocular pressure alongside a variety of different variables, within individuals and amongst populations: pharmaceuticals, standard length, time, age, right vs. left eye.

3.3 Methods

Animal Ethics

Zebrafish were maintained and bred using typical husbandry methods and with the approval of the Animal Care and Use Committee at the University of Alberta (protocol AUP00000077).

Measuring zebrafish intraocular pressure

Individual zebrafish were anaesthetized by immersion in MS222 and facility water until operculation was slowed/irregular. They were propped up to be in anatomical position at the edge of the lab bench (Figure 3-1). It was important to have the head right against the petridish used for this purpose as the probe had enough momentum to move the head otherwise. The Icare Tonovet plus (TV011, © 2016 Icare, Vantaa, Finland) was used. Similar to the majority of clinical rebound tonometers, this tonometer model needs to stay upright during use; and the positioning of the zebrafish described above allows space for the tonometer below the height of the counter. The Tonovet plus was kept level and pointed at the middle of the globe prior to triggering/propelling its probe (Figure 3-1). The Tonovet plus acquires 6 measurements, discards the highest and the lowest prior to averaging them and assigning the result a colour score for variance. It discards any measurements where the probe is too far or too near the subject and gives correction to the user. Only green (the most consistent) measurements were accepted, and generally two to three measurements were averaged for each eye. Unless otherwise indicated, the right eye was always measured first. If the eyes were becoming dry (probe sticking as opposed to rebounding) a drip of the anaesthetic/water was applied to the head.

Topical drug application

Following anaesthetic induction, the fish were place in anatomical position and the right eye pressure was taken (as described above). Immediately following, a single drop of drug was

administered to the right eye taking care to not drip into the gills or to the other side of the head. Intraocular pressure was immediately taken on the left side, then repeated on the right side again prior to recovering the fish in facility water. The fish were kept individually, and the right and left eye pressures were repeated following the initial assessment in the same order.
The two drugs used were 2% dorzolamide (Trusopt ®, Purdue Pharma, Pickering, Ontario (drug identification number (DIN) 02216205) and 50mcg/mL latanoprost (APOTEX Inc., Toronto, Ontario (drug identification number (DIN) 02296527)).

Statistics

Graph Pad Prism 9.3.1 was used to create graphs and perform all statistical tests -these are specified in each figure.

3.4 Results and Discussion

The intraocular pressure measurements obtained through using the Tonovet plus were generally within the range of 5-25 mmHg (Figures 3-2 through 3-4). This is consistent with the measurements using the gold standard servonull electrophysiology technique [135].

Neither the fish's size (standard length) or age contributed substantially on intraocular pressure (Figure 3-2a & 3-2b). In the absence of any other pre-existing issues, we assumed that the right and left eyes would have somewhat similar intraocular pressures within an individual. Many individuals met this expectation, somewhat validating the methods with three quarters of the fish having intraocular pressure within 5mmHg of each other (Figure 3-3a). However, when plotted against each other there was a noticeable deviation in the line of best fit favouring higher measurements in the right compared to the left eye (Figure 3-3a). This could be a procedural artifact as the right eye was always measured first, and potentially the fish were not at the same state throughout all the measurements (ex: differing anaesthetic depth could potentially affect both blood pressure and muscle tone). To address this, we reassessed the identical individual fish and compared their readings six weeks later but in the opposite order (left eyes assessed first). Qualitatively, it did not make a difference with some readings going up and some going down for both the right and the left eyes (Figure 3-3c and Figure 3-3d). There was a noticeable reduction in the spread of the readings at the second time point potentially reflecting an improvement in user skill over that period (Figures 3-3e & 3-3b). However, the right eye still had

qualitatively higher pressures than the left eye, with the left eyes even showing a significant decrease in their mean intraocular pressure between the two time points (Figures 3-3b & c). This puzzling difference between right and left eyes could be due to the small sample size, inherent biological variation, some sort of ergonomic factor, or husbandry factor that affects the sides differentially. This could potentially be improved through trying everything in a somewhat backwards setup or using methods similar to how Quint et al. described their set up by mounting the fish in a more consistent holder infused with anaesthetic (sculpted sponge?) and potentially even mounting the Tonovet plus as well [137]. This second idea would decrease some of the appeal of having a handheld portable device with minimal set up but could likely improve consistency. Variation is not unexpected between two time points as intraocular pressure is a physiological output that is affected by many variables. Across many species, the following affect intraocular pressure measurement: circadian rhythm, contraction of the retractor bulbi muscles, coughing/Valsalva maneuver, blood pressure changes, pulse, struggling/handling, electroshock, changes in head/body position, pharmacological agents, acidosis, aging, race/breed, hormones, obesity, myopia, gender, and season [155]. In a healthy dog, a variation of 4mmHg over a day is standard (without any other contributing factors like an anaesthetic). Typically, most species have an upper end intraocular pressure value that is considered painful and at risk of causing damage to the optic nerve/decreased vision.

We attempted to measure a decrease in intraocular pressure using two different medications labelled for the treatment of glaucoma in people: latanoprost and dorzolamide. Neither latanoprost, a prostaglandin analogue, that increases drainage of the aqueous humour, or dorzolamide, a carbonic anhydrase inhibitor, that decreases aqueous humour production, had measurable effects on the mean intraocular pressure when measured within 5 minutes of application and then again one to two hours later (Figure 3-4a & b). Dorzolamide has been used clinically in other fish species, however, not a lot of information exists about the efficacy of topical application for either drug [149, 146].

Future work could continue to validate this method by assessing fish with forced ocular hypertension. Experimental manipulation characterizing a mutant with ocular hypertension has been used to validate other means of measuring pressure [135, 136, 137]. We did not have access to those fish (bugeye mutants, *lrp2-/-*) due to a zebrafish importation ban imposed by the Canadian Food Inspection Agency (CFIA) [156]. We attempted to generate such mutants via

CRISPR, though the efficacy of the mutagenesis was unclear and no elevated IOP was evident. Ongoing attempts to repeat this approach with improved CRISPR methods may help to clarify the validity of our approach. Additional validation methods could include creating a standard curve through injecting known volumes of liquid into the eye post-mortem or continuing to try other pharmacological agents or drug delivery methods.

3.5 Conclusions

We have presented additional species-specific information for zebrafish and rebound tonometry and introduced a user-friendly method of measuring intraocular pressure using standard veterinary equipment. This technique is similar to those used clinically in specialty veterinary practice, so the information is relevant to both experimental and clinical use [153; diagnosis of glaucoma followed by successful enucleation (eye removal) in a goldfish]. An accessible means of evaluating intraocular pressure allows for straightforward screening for phenotypes as was demonstrated in Chapter 2 (Figure 2-9 did not find a phenotype in the *pmel* mutants) as well as a minimally invasive way that can be used repeatedly. Serial measurement is so important when investigating complex, progressive, diseases with multiple contributing factors like glaucoma. Not only would rebound tonometry let us track disease progression in zebrafish models of glaucoma but it could also potentially help untangle the relationship of ocular hypertension with optic nerve degeneration.

Figure 3-1. Using a Tonovet plus to measure intraocular pressure in zebrafish.
The zebrafish is supported in anatomical position using a petri dish behind the head and lying on a moistened towelette. The probe of the tonometer (white piece touching the eye in photo) is held close to the eye and is aimed at the middle of the cornea. Distance is corrected for by the Tonovet plus. The Tonovet Plus requires six measurements and uses the middle four to give an average reading.

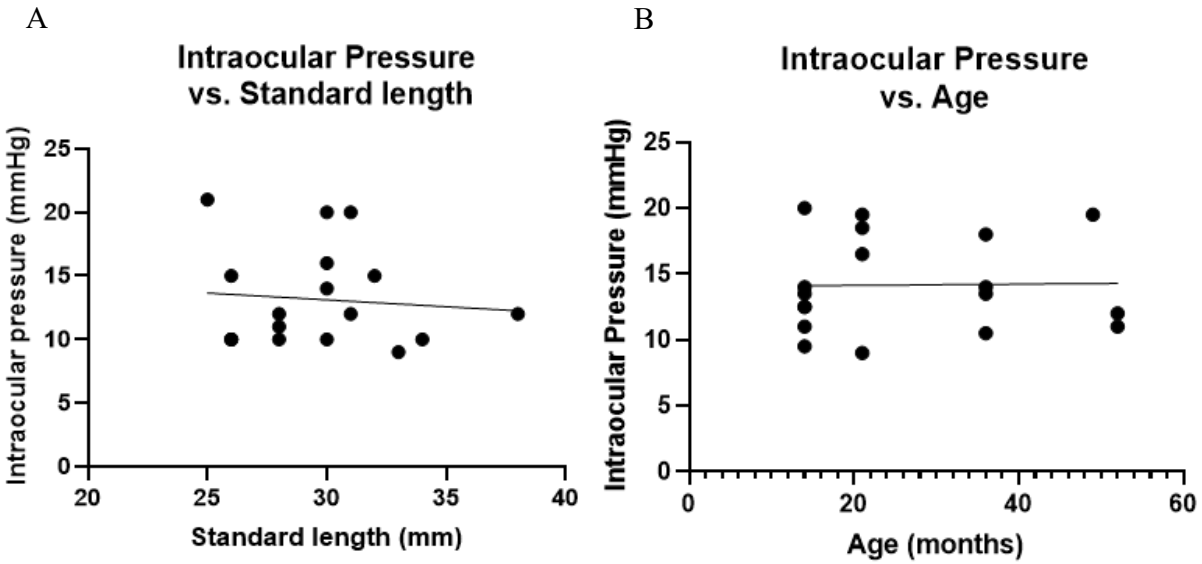

Figure 3-2. Assessing factors that could influence intraocular pressure (IOP) in zebrafish. Intraocular pressure did not seem to be affected by body length of zebrafish **(A)** or by age **(B)**. Each dot represents the average measurements for an individual fish and the lines of best fit were produced using a simple linear regression, neither of which had significantly non-zero slopes.

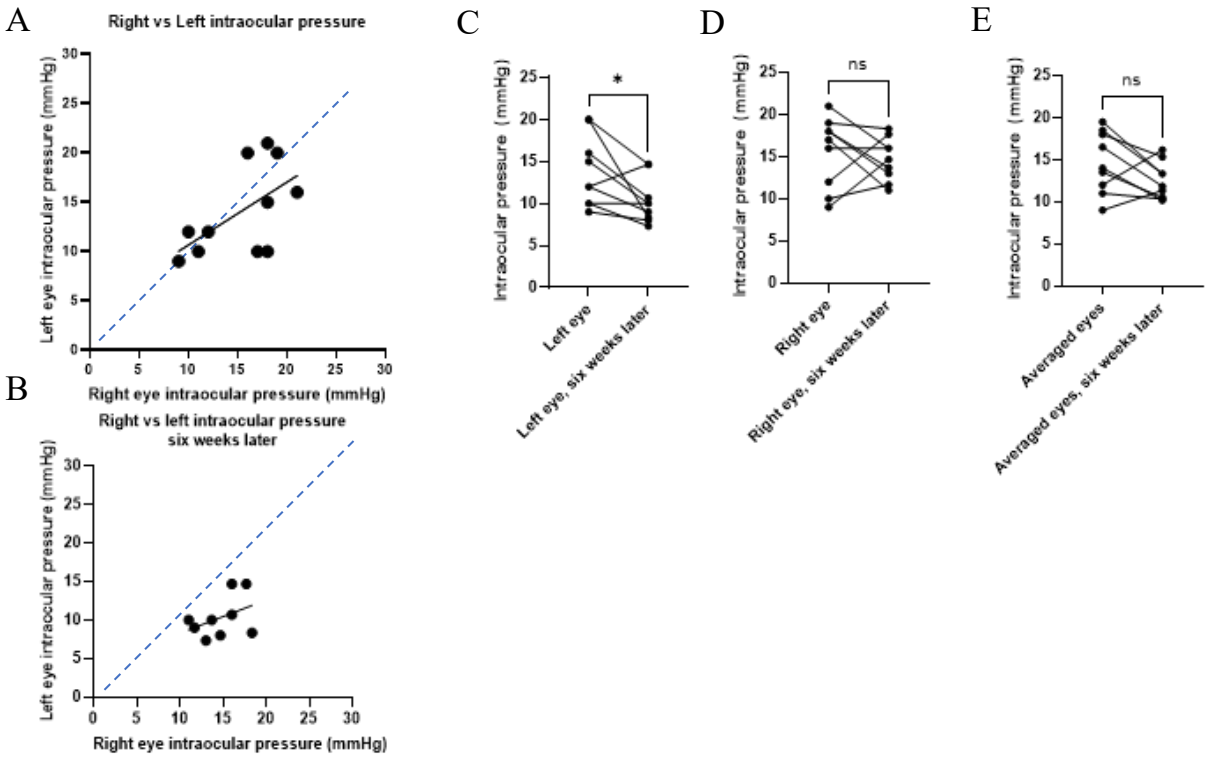

Figure 3-3. Assessing intraocular pressure (IOP) within an individual fish.
(A) Comparing intraocular pressure between the right and the left eye of an individual revealed some variability. The expected result, assuming both eyes have identical IOP, is presented as blue dashed line. Each dot represents the average measurements for an individual's eyes and the black line of best fit was produced using a simple linear regression, which lacked a significantly non-zero slope. **(B)** This was repeated in six weeks. The values collected from these two days of measuring were plotted in various, additional, ways, by matching the identical eyes **(C** (left) and **D** (right)**)** as well as averaging the results between the eyes for each individual fish **(D)**. A line is shown on graphs C-E to tie together measurements from specific eyeballs.

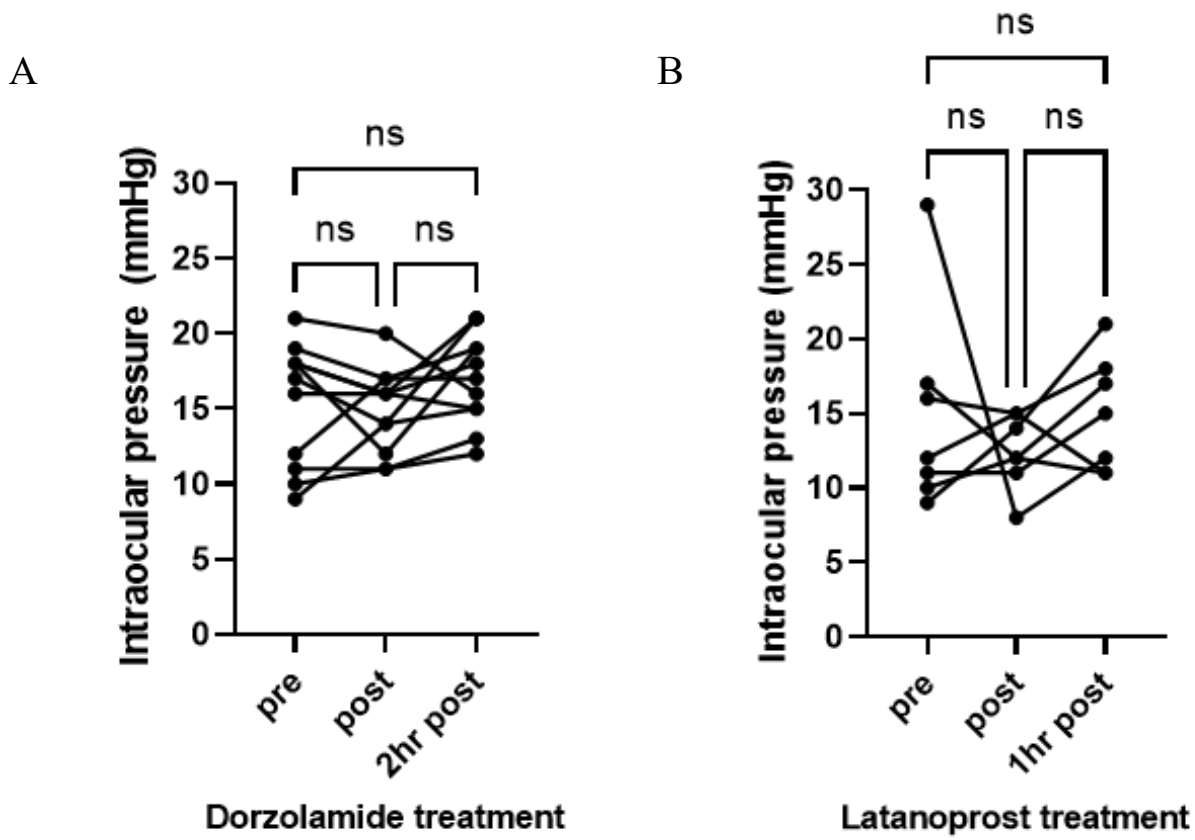

Figure 3-4. Attempted pharmacological reduction of zebrafish intraocular pressure. Intraocular pressures were measured prior to and following application of one drop of dorzolamide or latanoprost onto the right eye. Following application, measurement occurred within 5 minutes and 2, or 1 hours later for dorzolamide and latanoprost, respectively. A line is drawn between points to signify measurements from the same eyeball. An ANOVA with a Friedman test was performed for each figure and showed that the groups were not significantly (ns) different from each other.

4.0 Future Directions

Our in vivo work demonstrates that the repetitive region of the premelanosome protein (PMEL) is critical from the organelle to organ level (Chapter 2). This region warrants further investigation from multiple fields: evolutionary genetics, human and veterinary medicine, and amyloid biology.

The genetic material of the repeat region of PMEL is puzzling when compared across taxa. It defies the concept that important areas are conserved *between* species and rather demonstrates a strong selection for repeats to have a conserved sequence and length *within* species. It is stunning how many different ways this protein has evolved to serve presumably similar functions. A shortcoming of my and Justin Jensen's work on these domains across taxa is that we were looking for obvious repeats. I think an analysis of the species where RADAR detected repeats that were not as clear would be interesting to determine the shared basic features when the sequence is not so easily identified as repetitive. Teleosts are a group that warrants further investigation, as they often have two copies of Pmel, and I have already observed within cyprinids an abundance of variation. An even more difficult conundrum would be determining how to critically assess what about these regions makes them so susceptible to mutation. Potentially comparing between different proteins with repetitive regions could provide clues as to whether this was involving (not limited to) gene conversion, duplication, deletions, unequal crossing over, or recombination.

It is obvious that increasing our knowledge of PMEL biology and disease mechanisms increases our likelihood of providing therapeutic options – or even a cure or preventative strategy for pigmentary glaucoma and the various veterinary pathologies. However, the hidden contribution this work makes to both human and veterinary medicine is providing a demonstration of how important it is to study animal diseases! So much was already known about *PMEL* from the various spontaneously occurring animal mutations, it really enhanced the tools and knowledge that could be used from the moment *PMEL* was shown to cause pigmentary glaucoma. I think following the care of genetic issues in veterinary medicine could greatly enhance knowledge through both comparative biology and medicine. I see potential for creating more connections with veterinary ophthalmologists and pathologists to facilitate future work

with canine and equine developmental ocular issues relating to the anatomical differences reported in humans with pigmentary glaucoma.

Amyloid is often considered pathogenic, so it is exciting that PMEL provides an avenue to investigate under which conditions, and through which mechanisms, healthy amyloid becomes toxic to cells [127]. Continued targeted mutagenesis in zebrafish and/or fibril assessment in cell culture could help determine whether toxicity was from aberrant folding, glycosylation, or fibrilization causing cell stress through PMEL itself, an abundance of soluble melanin byproducts, or through membrane damage.

In addition to the dominant mutations discussed in chapter 1, *ua5030* did suggest that having a single copy of Pmela with an aberrant repeat region could affect fibril formation (as it had a heterozygous change in grayscale variation compared to the null mutant, *ua5022*) and ocular developmental anatomy (microphthalmia). Having a described, genetically relevant mutant for pigmentary glaucoma will provide a valued *in vivo* component to further research on PMEL pathomechanisms. It is also particularly useful to have a practical, minimally invasive tool kit that can be used to evaluate zebrafish over the time course of glaucomatous disease, and I think my contribution of using rebound tonometry is valuable to the field beyond this particular research aim.

Works Cited

1. Theos, A.C.; Truschel, S.T.; Raposo, G.; Marks, M.S. The Silver locus product Pmel17/gp100/Silv/ME20: Controversial in name and in function. *Pigment Cell Res.* **2005**, 18, 322–336.

2. Weterman, M.A.J.; Ajubi, N.; Vandinter, I.M.R.; Degen,W.G.J.; Vanmuijen, G.N.P.; Ruiter, D.J.; Bloemers, H.P.J. NMB, a novel gene, is expressed in low-metastatic human-melanoma cell-lines and xenografts. *Int. J. Cancer* **1995**, 60, 73–81.

3. Onaga, M.; Ido, A.; Hasuike, S.; Uto, H.; Moriuchi, A.; Nagata, K.; Hori, T.; Hayash, K.; Tsubouchi, H. Osteoactivin expressed during cirrhosis development in rats fed a choline-deficient, L-amino acid-defined diet, accelerates motility of hepatoma cells. *J. Hepatol.* **2003**, 39, 779–785.

4. Rose, A.A.N.; Pepin, F.; Russo, C.; Abou Khalil, J.E.; Hallett, M.; Siegell, P.M. Osteoactivin promotes breast cancer metastasis to bone. *Mol. Cancer Res.* **2007**, 5, 1001–1014.

5. Wagner, S.N.; Wagner, C.; Schultewolter, T.; Goos, M. Analysis of Pmel17/gp100 expression in primary human tissue specimens: Implications for melanoma and gene-therapy. *Cancer Immunol. Immunother.* **1997**, 44, 239–247.

6. Nawrath, M.; Pavlovic, J.; Dummet, R.; Schultz, J.; Strack, B.; Heinrich, J.; Moelling, K. Reduced melanoma tumor formation in mice immunized with DNA expressing the melanoma-specific antigen gp100/pmel17. *Leukemia* **1999**, 13, S48–S51.

7. John, S.W.M.; Smith, R.S.; Savinova, O.V.; Hawes, N.L.; Chang, B.; Turnbull, D.; Davisson, M.; Roderick, T.H.; Heckenlively, J.R. Essential iris atrophy, pigment dispersion, and glaucoma in DBA/2J mice. *Investig. Ophthalmol. Vis. Sci.* **1998**, 39, 951–962.

8. Anderson, M.G.; Smith, R.S.; Hawes, N.L.; Zabaleta, A.; Chang, B.; Wiggs, J.L.; John, S.W.M. Mutations in genes encoding melanosomal proteins cause pigmentary glaucoma in DBA/2J mice. *Nat. Genet.* **2002**, 30, 81–85.

9. Lahola-Chomiak, A.A.; Footz, T.; Nguyen-Phuoc, K.; Neil, G.J.; Fan, B.J.; Allen, K.F.; Greenfield, D.S.; Parrish, R.K.; Linkroum, K.; Pasquale, L.R.; et al. Non-Synonymous variants in premelanosome protein (PMEL) cause ocular pigment dispersion and pigmentary glaucoma. *Hum. Mol. Genet.* **2019**, 28, 1298–1311.

10. Zhu, S.C.; Wuolikainen, A.; Wu, J.F.; Ohman, A.; Wingsle, G.; Moritz, T.; Andersen, P.M.; Forsgren, L.; Trupp, M. Targeted Multiple Reaction Monitoring Analysis of CSF Identifies UCHL1 and GPNMB as Candidate Biomarkers for ALS. *J. Mol. Neurosci.* **2019**, 69, 643–657.

11. Deckl, P.; Weydt, P.; Thal, D.R.; Weishaupt, J.H.; Ludolph, A.C.; Otto, M. Proteomics in cerebrospinal fluid and spinal cord suggests UCHL1, MAP2 and GPNMB as biomarkers and underpins importance of transcriptional pathways in amyotrophic lateral sclerosis. *Acta Neuropathol.* **2020**, 139, 119–134.

12. Pihlstrom, L.; Axelsson, G.; Bjornara, K.A.; Dizdar, N.; Fardell, C.; Forsgren, L.; Holmberg, B.; Larsen, J.P.; Linder, J.; Nissbrandt, H.; et al. Supportive evidence for 11 loci from genome-wide association studies in Parkinson's disease. *Neurobiol. Aging* **2013**, 34, 1708.e7–1708.e13.

13. Dean, D.N.; Lee, J.C. Defining an amyloid link Between Parkinson's disease and melanoma. *Proc. Natl. Acad. Sci. USA* **2020**, 117, 22671–22673.

14. Haraszti, T.; Trantow, C.M.; Hedberg-Buenz, A.; Grunze, M.; Anderson, M.G. Spectral analysis by XANES reveals that GPNMB influences the chemical composition of intact melanosomes. *Pigment Cell Melanoma Res*. **2011**, 24, 187–196.

15. Kwon, B.S.; Chintamaneni, C.; Kozak, C.A.; Copeland, N.G.; Gilbert, D.J.; Jenkins, N.; Barton, D.; Francke, U.; Kobayashi, Y.; Kim, K.K. A Melanocyte-Specific Gene, Pmel-17, Maps

Near The Silver Coat Color Locus On Mouse Chromosome-10 And Is In A Syntenic Region On Human Chromosome-12. *Proc. Natl. Acad. Sci. USA* **1991**, 88, 9228–9232.

16. Kerje, S.; Sharma, P.; Gunnarsson, U.; Kim, H.; Bagchi, S.; Fredriksson, R.; Schutz, K.; Jensen, P.; von Heijne, G.; Okimoto, R.; et al. The Dominant white, Dun and Smoky color variants in chicken are associated with insertion/deletion polymorphisms in the PMEL17 gene. *Genetics* **2004**, 168, 1507–1518.

17. Brunberg, E.; Andersson, L.; Cothran, G.; Sandberg, K.; Mikko, S.; Lindgren, G. A missense mutation in PMEL17 is associated with the Silver coat color in the horse. *BMC Genet.* **2006**, 7, 46.

18. Yang, C.F.; Lin, S.P.; Chiang, C.P.; Wu, Y.H.; H'ng, W.S.; Chang, C.P.; Chen, Y.T.; Wu, J.Y. Loss of GPNMB Causes Autosomal-Recessive Amyloidosis Cutis Dyschromica in Humans. *Am. J. Hum. Genet.* **2018**, 102, 219–232.

19. Biswas, K.B.; Takahashi, A.; Mizutani, Y.; Takayama, S.; Ishitsuka, A.; Yang, L.L.; Yang, F.; Iddamalgoda, A.; Katayama, I.; Inoue, S. GPNMB is expressed in human epidermal keratinocytes but disappears in the vitiligo lesional skin. *Sci. Rep.* **2020**, 10, 4930.

20. Fowler, D.M.; Koulov, A.V.; Alory-Jost, C.; Marks, M.S.; Balch, W.E.; Kelly, J.W. Functional amyloid formation within mammalian tissue. *PLoS Biol.* **2006**, 4, e6.

21. McGlinchey, R.P.; Shewmaker, F.; McPhie, P.; Monterroso, B.; Thurber, K.;Wickner, R.B. The repeat domain of the melanosome fibril protein Pmel17 forms the amyloid core promoting melanin synthesis. *Proc. Natl. Acad. Sci. USA* **2009**, 106, 13731–13736.

22. Graham, M.; Tzika, A.C.; Mitchell, S.M.; Liu, X.R.; Leonhardt, R.M. Repeat domain-associated O-glycans govern PMEL fibrillar sheet architecture. *Sci. Rep.* **2019**, 9, 6101.

23. Valencia, J.C.; Rouzaud, F.; Julien, S.; Chen, K.G.; Passeron, T.; Yamaguchi, Y.; Abu-Asab, M.; Tsokos, M.; Costin, G.E.; Yamaguchi, H.; et al. Sialylated core 1 O-glycans influence the sorting of Pmel17/gp100 and determine its capacity to form fibrils. *J. Biol. Chem.* **2007**, 282, 11266–11280.

24. Harper, D.C.; Theos, A.C.; Herman, K.E.; Tenza, D.; Raposo, G.; Marks, M.S. Premelanosome amyloid-like fibrils are composed of only Golgi-processed forms of Pmel17 that have been proteolytically processed in Endosomes. *J. Biol. Chem*. **2008**, 283, 2307–2322.

25. Berson, J.F.; Harper, D.C.; Tenza, D.; Raposo, G.; Marks, M.S. Pmel17 initiates premelanosome morphogenesis within multivesicular bodies. *Mol. Biol. Cell* **2001**, 12, 3451–3464.

26. Kummer, M.P.; Maruyama, H.; Huelsmann, C.; Baches, S.;Weggen, S.; Koo, E.H. Formation of Pmel17 Amyloid Is Regulated by Juxtamembrane Metalloproteinase Cleavage, and the Resulting C-terminal Fragment Is a Substrate for gamma-Secretase. *J. Biol. Chem.* **2009**, 284, 2296–2306.

27. Kawaguchi, M.; Hozumi, Y.; Suzuki, T. ADAM protease inhibitors reduce melanogenesis by regulating PMEL17 processing in human melanocytes. *J. Dermatol. Sci.* **2015**, 78, 133–142.

28. Rochin, L.; Hurbain, I.; Serneels, L.; Fort, C.;Watt, B.; Leblanc, P.; Marks, M.S.; De Strooper, B.; Raposo, G.; van Niel, G. BACE2 processes PMEL to form the melanosome amyloid matrix in pigment cells. *Proc. Natl. Acad. Sci. USA* **2013**, 110, 10658–10663.

29. Shimshek, D.R.; Jacobson, L.H.; Kolly, C.; Zamurovic, N.; Balavenkatraman, K.K.; Morawiec, L.; Kreutzer, R.; Schelle, J.; Jucker, M.; Bertschi, B.; et al. Pharmacological BACE1 and BACE2 inhibition induces hair depigmentation by inhibiting PMEL17 processing in mice. *Sci. Rep.* **2016**, 6, 21917.

30. Berson, J.F.; Theos, A.C.; Harper, D.C.; Tenza, D.; Raposo, G.; Marks, M.S. Proprotein convertase cleavage liberates a fibrillogenic fragment of a resident glycoprotein to initiate melanosome biogenesis. *J. Cell Biol.* **2003**, 161, 521–533.

31. Kobayashi, T.; Urabe, K.; Orlow, S.J.; Higashi, K.; Imokawa, G.; Kwon, B.S.; Potterf, B.; Hearing, V.J. The Pmel-17 Silver Locus Protein—Characterization And Investigation Of Its Melanogenic Function. *J. Biol. Chem.* **1994**, 269, 29198–29205.

32. Lee, Z.H.; Hou, L.; Moellmann, G.; Kuklinska, E.; Antol, K.; Fraser, M.; Halaban, R.; Kwon, B.S. Characterization and subcellular localization of human Pmel 17 silver, a 100-kDa (pre)melanosomal membrane protein associated with 5,6,-dihydroxyindole-2-carboxylic acid (DHICA) converting activity. *J. Investig. Dermatol.* **1996**, 106, 605–610.

33. Hurbain, I.; Geerts, W.J.C.; Boudier, T.; Marco, S.; Verkleij, A.J.; Marks, M.S.; Raposo, G. Electron tomography of early melanosomes: Implications for melanogenesis and the generation of fibrillar amyloid sheets. *Proc. Natl. Acad. Sci. USA* **2008**, 105, 19726–19731.

34. Watt, B.; van Niel, G.; Raposo, G.; Marks, M.S. PMEL: A pigment cell-specific model for functional amyloid formation. *Pigment Cell Melanoma Res*. **2013**, 26, 300–315.

35. Bissig, C.; Rochin, L.; van Niel, G. PMEL Amyloid Fibril Formation: The Bright Steps of Pigmentation. *Int. J. Mol. Sci.* **2016**, 17, 1438.

36. Silvers, W.K. The Coat Colors of Mice: A Model. For Mammalian Gene Action and Interaction; Springer: New York, NY, USA, 1979.

37. Kwon, B.S.; Kim, K.K.; Halaban, R.; Pickard, R.T. Characterization of mouse PMEL-17 gene and silver locus. *Pigment Cell Res.* **1994**, 7, 394–397.

38. Kwon, B.S.; Halaban, R.; Ponnazhagan, S.; Kim, K.; Chintamaneni, C.; Bennett, D.; Pickard, R.T. Mouse Silver Mutation Is Caused By A Single-Base Insertion In The Putative Cytoplasmic Domain Of Pmel-17. *Nucleic Acids Res.* **1995**, 23, 154–158.

39. Theos, A.C.; Berson, J.F.; Theos, S.C.; Herman, K.E.; Harper, D.C.; Tenza, D.; Sviderskaya, E.V.; Lamoreux, M.L.; Bennett, D.C.; Raposo, G.; et al. Dual loss of ER export and endocytic signals with altered melanosome morphology in the silver mutation of Pmel17. *Mol. Biol. Cell* **2006**, 17, 3598–3612.

40. Hellstrom, A.R.; Watt, B.; Fard, S.S.; Tenza, D.; Mannstrom, P.; Narfstrom, K.; Ekesten, B.; Ito, S.; Wakamatsu, K.; Larsson, J.; et al. Inactivation of Pmel Alters Melanosome Shape But Has Only a Subtle Effect on Visible Pigmentation. *PLoS Genet.* **2011**, 7, e1002285.

41. Schonthaler, H.B.; Lampert, J.M.; von Lintig, J.; Schwarz, H.; Geisler, R.; Neuhauss, S.C.F. A mutation in the silver gene leads to defects in melanosome biogenesis and alterations in the visual system in the zebrafish mutant fading vision. *Dev. Biol*. **2005**, 284, 421–436.

42. Ishishita, S.; Takahashi, M.; Yamaguchi, K.; Kinoshita, K.; Nakano, M.; Nunome, M.; Kitahara, S.; Tatsumoto, S.; Go, Y.; Shigenobu, S.; et al. Nonsense mutation in PMEL is associated with yellowish plumage colour phenotype in Japanese quail. *Sci. Rep*. **2018**, 8, 16732.

43. Karlsson, A.C.; Kerje, S.; Hallbook, F.; Jensen, P. The Dominant white mutation in the PMEL17 gene does not cause visual impairment in chickens. *Vet. Ophthalmol*. **2009**, 12, 292–298.

44. Kuliawat, R.; Santambrogio, L. A mutation within the transmembrane domain of melanosomal protein Silver (Pmel17) changes 85akista fragment interactions. *Eur. J. Cell Biol.* **2009**, 88, 653–667.

45. Watt, B.; Tenza, D.; Lemmon, M.A.; Kerje, S.; Raposo, G.; Andersson, L.; Marks, M.S. Mutations in or near the Transmembrane Domain Alter PMEL Amyloid Formation from Functional to Pathogenic. *PLoS Genet*. **2011**, 7, e1002286.

46. Komaromy, A.M.; Rowlan, J.S.; La Croix, N.C.; Mangan, B.G. Equine Multiple Congenital Ocular Anomalies (MCOA) syndrome in PMEL17 (Silver) mutant ponies: Five cases. *Vet. Ophthalmol.* **2011**, 14, 313–320.

47. Andersson, L.S.; Wilbe, M.; Viluma, A.; Cothran, G.; Ekesten, B.; Ewart, S.; Lindgren, G. Equine Multiple Congenital Ocular Anomalies and Silver Coat Colour Result from the Pleiotropic Effects of Mutant PMEL. *PLoS ONE* **2013**, 8, e75639.

48. Segard, E.M.; Depecker, M.C.; Lang, J.; Gemperli, A.; Cadore, J.L. Ultrasonographic features of PMEL17 (Silver) mutant gene associated multiple congenital ocular anomalies (MCOA) in Comtois and Rocky Mountain horses. *Vet. Ophthalmol*. **2013**, 16, 429–435.

49. Clark, L.A.; Wahl, J.M.; Rees, C.A.; Murphy, K.E. Retrotransposon insertion in SILV is responsible for merle patterning of the domestic dog. *Proc. Natl. Acad. Sci. USA* **2006**, 103, 1376–1381.

50. Ballif, B.C.; Ramirez, C.J.; Carl, C.R.; Sundin, K.; Krug, M.; Zahand, A.; Shaffer, L.G.; Flores-Smith, H. The PMEL Gene and Merle in the Domestic Dog: A Continuum of Insertion Lengths Leads to a Spectrum of Coat Color Variations in Australian Shepherds and Related Breeds. *Cytogenet. Genome Res*. **2018**, 156, 22–34.

51. Murphy, S.C.; Evans, J.M.; Tsai, K.L.; Clarke, L.A. Length variations within the Merle retrotransposon of canine PMEL: Correlating genotype with phenotype. *Mob. DNA* **2018**, 9, 26.

52. Kawahara, K.; Hirata, H.; Ohbuchi, K.; Nishi, K.; Maeda, A.; Kuniyasu, A.; Yamada, D.; Maeda, T.; Tsuji, A.; Sawada, M.; et al. The Novel Monoclonal Antibody 9F5 Reveals Expression of a Fragment of GPNMB/Osteoactivin Processed by Furin-like Protease(s)

in a Subpopulation of Microglia in Neonatal Rat Brain. *Glia* **2016**, 64, 1938–1961.

53. Abdelmagid, S.M.; Barbe, M.F.; Rico, M.C.; Salihoglu, S.; Arango-Hisijara, I.; Selim, A.H.; Anderson, M.G.; Owen, T.A.; Popoff, S.N.; Safadi, F.F. Osteoactivin, an anabolic factor that regulates osteoblast differentiation and function. *Exp. Cell Res*. **2008**, 314, 2334–2351.

54. Hoashi, T.; Sato, S.; Yamaguchi, Y.; Passeron, T.; Tamaki, K.; Hearing, V.J. Glycoprotein nonmetastatic melanoma protein b, a melanocytic cell marker, is a melanosome-specific and proteolytically released protein. *Faseb J.* **2010**, 24, 1616–1629.

55. Rose, A.A.N.; Annis, M.G.; Dong, Z.F.; Pepin, F.; Hallett, M.; Park, M.; Siegel, P.M. ADAM10 Releases a Soluble Form of the GPNMB/Osteoactivin Extracellular Domain with Angiogenic Properties. *PLoS ONE* **2010**, 5, e12093.

56. Chi, A.; Valencia, J.C.; Hu, Z.Z.;Watabe, H.; Yamaguchi, H.; Mangini, N.J.; Huang, H.Z.; Canfield, V.A.; Cheng, K.C.; Yang, F.; et al. Proteomic and bioinformatic characterization of the biogenesis and function of melanosomes. *J. Proteome Res.* **2006**, 5, 3135–3144.

57. Tomihari, M.; Hwang, S.H.; Chung, J.S.; Cruz, P.D.; Ariizumi, K. Gpnmb is a melanosome-associated glycoprotein that contributes to melanocyte/keratinocyte adhesion in a RGD-dependent fashion. *Exp. Dermatol*. **2009**, 18, 586–595.

58. Ripoll, V.M.; Meadows, N.A.; Raggatt, L.J.; Chang, M.K.; Pettit, A.R.; Cassady, A.I.; Hume, D.A. Microphthalmia transcription factor regulates the expression of the novel osteoclast factor GPNMB. *Gene* **2008**, 413, 32–41.

59. Loftus, S.K.; Antonellis, A.; Matera, I.; Renaud, G.; Baxter, L.L.; Reid, D.; Wolfsberg, T.G.; Chen, Y.D.; Wang, C.W.; Prasad, M.K.; et al. Gpnmb is a melanoblast-expressed, MITF-dependent gene. *Pigment Cell Melanoma Res*. **2009**, 22, 99–110.

60. Zhang, P.; Liu, W.; Yuan, X.Y.; Li, D.G.; Gu, W.J.; Gao, T.W. Endothelin-1 enhances the melanogenesis via MITF-GPNMB pathway. *Bmb Rep*. **2013**, 46, 364–369.

61. Gutknecht, M.; Geiger, J.; Joas, S.; Dorfel, D.; Salih, H.R.; Muller, M.R.; Grunebach, F.; Rittig, S.M. The transcription factor MITF is a critical regulator of GPNMB expression in dendritic cells. *Cell Commun. Signal.* **2015**, 13, 19.

62. Theos, A.C.;Watt, B.; Harper, D.C.; Janczura, K.J.; Theos, S.C.; Herman, K.E.; Marks, M.S. The PKD domain distinguishes the trafficking and amyloidogenic properties of the pigment cell protein PMEL and its homologue GPNMB. *Pigment Cell Melanoma Res*. **2013**, 26, 470–486.

63. Rahman, O.U.; Kim, J.; Mahon, C.; Jelani, M.; Kang, C. Two missense mutations in GPNMB cause autosomal recessive amyloidosis cutis dyschromica in the consanguineous Pakistani families. *Genes Genom.* **2021**, 43, 471–478.

64. Onoufriadis, A.; Hsu, C.K.; Eide, C.R.; Nanda, A.; Orchard, G.E.; Tomita, K.; Sheriff, A.; Scott,W.; Tierney, C.; Lee, J.Y.W.; et al. Semidominant GPNMB Mutations in Amyloidosis Cutis Dyschromica. *J. Investig. Dermatol.* **2019**, 139, 2550.

65. Chiu, F.P.C.;Wessagowit, V.; Cakmak, M.F.; Doolan, B.J.; Kootiratrakarn, T.; Chaowalit, P.; Bunnag, T.; Simpson, M.A.; McGrath, J.A.; Onoufriadis, A. Molecular basis and inheritance patterns of amyloidosis cutis dyschromica. *Clin. Exp. Dermatol*. **2020**, 45, 650–653.

66. Sha, Y.; Li, L. Amyloidosis cutis dyschromica due to homozygous variants of the GPNMB gene in a Chinese pedigree. Chin. *J. Med. Genet.* **2021**, 38, 123–126.

67. Owen, T.A.; Smock, S.L.; Prakash, P.; Pinder, L.; Brees, D.; Krull, D.; Castleberry, T.A.; Clancy, Y.C.; Marks, S.C.; Safadi, F.F.; et al. Identification and characterization of the genes encoding human and mouse osteoactivin. *Crit. Rev. Eukaryot. Gene Expr*. **2003**, 13, 205–220.

68. Huang, J.J.; Ma, W.J.; Yokoyama, S. Expression and immunolocalization of Gpnmb, a glioma-associated glycoprotein, in normal and inflamed central nervous systems of adult rats. *Brain Behav.* **2012**, 2, 85–96.

69. Shi, F.Y.; Duan, S.Y.; Cui, J.H.; Yan, X.R.; Li, H.M.; Wang, Y.J.; Chen, F.L.; Zhang, L.H.; Liu, J.; Xie, X. Induction of Matrix Metalloproteinase-3 (MMP-3) Expression in the Microglia by Lipopolysaccharide (LPS) via Upregulation of Glycoprotein Nonmetastatic Melanoma B (GPNMB) Expression. *J. Mol. Neurosci*. **2014**, 54, 234–242.

70. Murata, K.; Yoshino, Y.; Tsuruma, K.; Moriguchi, S.; Oyagi, A.; Tanaka, H.; Ishisaka, M.; Shimazawa, M.; Fukunaga, K.; Hara, H. The extracellular fragment of GPNMB (Glycoprotein nonmelanosoma protein B, osteoactivin) improves memory and increases hippocampal GluA1 levels in mice. *J. Neurochem*. **2015**, 132, 583–594.

71. Ripoll, V.M.; Irvine, K.M.; Ravasi, T.; Sweet, M.J.; Hume, D.A. Gpnmb is induced in macrophages by IFN-gamma and lipopolysaccharide and acts as a feedback regulator of proinflammatory responses. *J. Immunol*. **2007**, 178, 6557–6566.

72. Zhou, L.T.; Zhuo, H.; Ouyang, H.Y.; Liu, Y.X.; Yuan, F.; Sun, L.; Liu, F.Y.; Liu, H. Glycoprotein non-metastatic melanoma protein b (Gpnmb) is highly expressed in macrophages of acute injured kidney and promotes M2 macrophages polarization. Cell. *Immunol*. **2017**, 316, 53–60.

73. Mo, J.S.; Anderson, M.G.; Gregory, M.; Smith, R.S.; Savinova, O.V.; Serreze, D.V.; Ksander, B.R.; Streilein, J.W.; John, S.W.M. By altering ocular immune privilege, bone marrow-derived cells pathogenically contribute to DBA/2J pigmentary glaucoma. *J. Exp. Med*. **2003**, 197, 1335–1344.

74. Anderson, M.G.; Nair, K.S.; Amonoo, L.A.; Mehalow, A.; Trantow, C.M.; Masli, S.; John, S.W.M. Gpnmb(R150X) allele must be present in bone marrow derived cells to mediate DBA/2J glaucoma. *BMC Genet.* **2008**, 9, 30.

75. Safadi, F.F.; Xu, J.; Smock, S.L.; Rico, M.C.; Owen, T.A.; Popoff, S.N. Cloning and characterization of osteoactivin, a novel cDNA expressed in osteoblasts. J. Cell. *Biochem.* **2002**, 84, 12–26.

76. Sheng, M.H.C.; Wergedal, J.E.; Mohan, S.; Lau, K.H.W. Osteoactivin is a novel osteoclastic protein and plays a key role in osteoclast differentiation and activity. *FEBS Lett*. **2008**, 582, 1451–1458.

77. Selim, A.A.; Abdelmagid, S.M.; Kanaan, R.A.; Smock, S.L.; Owen, T.A.; Popoff, S.N.; Safadi, F.F. Anti-osteoactivin antibody inhibits osteoblast differentiation and function in vitro. *Crit. Rev. Eukaryot. Gene Expr*. **2003**, 13, 265–275.

78. Abdelmagid, S.M.; Barbe, M.F.; Arango-Hisijara, I.; Owen, T.A.; Popoff, S.N.; Safadi, F.F. Osteoactivin acts as downstream mediator of BMP-2 effects on osteoblast function. *J. Cell. Physiol.* **2007**, 210, 26–37.

79. Selim, A.A.; Castaneda, J.L.; Owen, T.A.; Popoff, S.N.; Safadi, F.F. The role of osteoactivin-derived peptides in osteoblast differentiation. *Med. Sci. Monit*. **2007**, 13, BR259–BR270.

80. Arosarena, O.A.; Del Carpio-Cano, F.E.; Dela Cadena, R.A.; Rico, M.C.; Nwodim, E.; Safadi, F.F. Comparison of Bone Morphogenetic Protein-2 and Osteoactivin for Mesenchymal Cell Differentiation: Effects of Bolus and Continuous Administration. *J. Cell. Physiol*. **2011**, 226, 2943–2952.

81. Ogawa, T.; Nikawa, T.; Furochi, H.; Kosyoji, M.; Hirasaka, K.; Suzue, N.; Sairyo, K.; Nakano, S.; Yamaoka, T.; Itakura, M.; et al. Osteoactivin upregulates expression of MMP-3 and MMP-9 in fibroblasts infiltrated into denervated skeletal muscle in mice. *Am. J. Physiol. Cell Physiol.* **2005**, 289, C697–C707.

82. Abe, H.; Uto, H.; Takami, Y.; Takahama, Y.; Hasuike, S.; Kodama, M.; Nagata, K.; Moriuchi, A.; Numata, M.; Ido, A.; et al. Transgenic expression of osteoactivin in the liver attenuates hepatic fibrosis in rats. *Biochem. Biophys. Res. Commun*. **2007**, 356, 610–615.

83. Sheng, M.H.C.; Wergedal, J.E.; Mohan, S.; Amoui, M.; Baylink, D.J.; Lau, K.H.W. Targeted Overexpression of Osteoactivin in Cells of Osteoclastic Lineage Promotes Osteoclastic Resorption and Bone Loss in Mice. *PLoS ONE* **2012**, 7, e35280.

84. Tonogai, I.; Takahashi, M.; Yukata, K.; Sato, R.; Nikawa, T.; Yasui, N.; Sairyo, K. Osteoactivin attenuates skeletal muscle fibrosis after distraction osteogenesis by promoting extracellular matrix degradation/remodeling. *J. Pediatr. Orthop. Part B* **2015**, 24, 162–169.

85. Arosarena, O.A.; Barr, E.W.; Thorpe, R.; Yankey, H.; Tarr, J.T.; Safadi, F.F. Osteoactivin regulates head and neck squamous cell carcinoma invasion by modulating matrix metalloproteases. *J. Cell. Physiol*. **2018**, 233, 409–421.

86. Utsunomiya, K.; Owaki, K.; Okumura, Y.; Yano, M.; Oto, T.; Suzuki, E.; Tamura, S.; Abe, T.; Kohno, S.; Ohno, A.; et al. An Intracellular Fragment of Osteoactivin Formed by Ectodomain Shedding Trans located to the Nucleoplasm and Bound to RNA Binding Proteins. B*iosci. Biotechnol. Biochem.* **2012**, 76, 2225–2229.

87. Furochi, H.; Tamura, S.; Mameoka, M.; Yamada, C.; Ogawa, T.; Hirasaka, K.; Okumura, Y.; Imagawa, T.; Oguri, S.; Ishidoh, K.; et al. Osteoactivin fragments produced by ectodomain shedding induce MMP-3 expression via ERK pathway in mouse NIH-3T3 fibroblasts. *FEBS Lett.* **2007**, 581, 5743–5750.

88. Moussa, F.M.; Hisijara, I.A.; Sondag, G.R.; Scott, E.M.; Frara, N.; Abdelmagid, S.M.; Safadi, F.F. Osteoactivin Promotes Osteoblast Adhesion Through HSPG and alpha v beta 1 Integrin. *J. Cell. Biochem.* **2014**, 115, 1243–1253.

89. Murthy, M.N.; Blauwendraat, C.; Guelfi, S.; Hardy, J.; Lewis, P.A.; Trabzuni, D.; UKBEC. Increased brain expression of GPNMB is associated with genome wide significant risk for Parkinson's disease on chromosome 7p15.3. *Neurogenetics* **2017**, 18, 121–133.

90. Moloney, E.B.; Moskites, A.; Ferrari, E.J.; Isacson, O.; Hallett, P.J. The glycoprotein GPNMB is selectively elevated in the substantia nigra of Parkinson's disease patients and increases after lysosomal stress. *Neurobiol. Dis.* **2018**, 120, 1–11.

91. Huttenrauch, M.; Ogorek, I.; Klafki, H.; Otto, M.; Stadelmann, C.; Weggen, S.; Wiltfang, J.; Wirths, O. Glycoprotein NMB: A novel Alzheimer's disease associated marker expressed in a subset of activated microglia. *Acta Neuropathol. Commun.* **2018**, 6, 108.

92. Budge, K.M.; Neal, M.L.; Richardson, J.R.; Safadi, F.F. Transgenic Overexpression of GPNMB Protects Against MPTP-Induced Neurodegeneration. *Mol. Neurobiol.* **2020**, 57, 2920–2933.

93. Tanaka, H.; Shimazawa, M.; Kimura, M.; Takata, M.; Tsuruma, K.; Yamada, M.; Takahashi, H.; Hozumi, I.; Niwa, J.; Iguchi, Y.; et al. The potential of GPNMB as novel neuroprotective factor in amyotrophic lateral sclerosis. *Sci. Rep.* **2012**, 2, 573.

94. Nagahara, Y.; Shimazawa, M.; Ohuchi, K.; Ito, J.; Takahashi, H.; Tsuruma, K.; Kakita, A.; Hara, H. GPNMB ameliorates mutant TDP-43-induced motor neuron cell death. *J. Neurosci. Res.* **2017**, 95, 1647–1665.

95. Mitchell, A.L.; Attwood, T.K.; Babbitt, P.C.; Blum, M.; Bork, P.; Bridge, A.; Brown, S.D.; Chang, H.Y.; El-Gebali, S.; Fraser, M.I.; et al. InterPro in 2019: Improving coverage, classification and access to protein sequence annotations. *Nucleic Acids Res.* **2019**, 47, D351–D360.

96. Altschul, S.F.; Gish,W.; Miller,W.; Myers, E.W.; Lipman, D.J. Basic local alignment search tool. *J. Mol. Biol.* **1990**, 215, 403–410.

97. Heger, A.; Holm, L. Rapid automatic detection and alignment of repeats in protein sequences. *Proteins-Struct. Funct. Genet.* **2000**, 41, 224–237.

98. Madeira, F.; Park, Y.M.; Lee, J.; Buso, N.; Gur, T.; Madhusoodanan, N.; Basutkar, P.; Tivey, A.R.N.; Potter, S.C.; Finn, R.D.; et al. The EMBL-EBI search and sequence analysis tools APIs in 2019. *Nucleic Acids Res.* **2019**, 47, W636–W641.

99. Koonin, E.V. Orthologs, paralogs, and evolutionary genomics. *Annu. Rev. Genet*. **2005**, 39, 309–338.

100. Ho, T.; Watt, B.; Spruce, L.A.; Seeholzer, S.H.; Marks, M.S. The Kringle-like Domain Facilitates Post-endoplasmic Reticulum Changes to Premelanosome Protein (PMEL) Oligomerization and Disulfide Bond Configuration and Promotes Amyloid Formation. *J. Biol. Chem.* **2016**, 291, 3595–3612.

101. Xie, R.; Okita, Y.; Ichikawa, Y.; Fikry, M.A.; Dam, K.T.H.; Tran, S.T.P.; Kato, M. Role of the kringle-like domain in glycoprotein NMB for its tumorigenic potential. *Cancer Sci.* **2019**, 110, 2237–2246.

102. McGlinchey, R.P.; Shewmaker, F.; Hu, K.N.; McPhie, P.; Tycko, R.; Wickner, R.B. Repeat Domains of Melanosome Matrix Protein Pmel17 Orthologs Form Amyloid Fibrils at the Acidic Melanosomal pH. *J. Biol. Chem.* **2011**, 286, 8385–8393.

103. Hoashi, T.; Muller, J.; Vieira, W.D.; Rouzaud, F.; Kikuchi, K.; Tamaki, K.; Hearing, V.J. The repeat domain of the melanosomal matrix protein PMEL17/GP100 is required for the formation of organellar fibers. *J. Biol. Chem*. **2006**, 281, 21198–21208.

104. Watt, B.; van Niel, G.; Fowler, D.M.; Hurbain, I.; Luk, K.C.; Stayrook, S.E.; Lemmon, M.A.; Raposo, G.; Shorter, J.; Kelly, J.W.; et al. N-terminal Domains Elicit Formation of Functional Pmel17 Amyloid Fibrils. *J. Biol. Chem*. **2009**, 284, 35543–35555.

105. Leonhardt, R.M.; Vigneron, N.; Hee, J.S.; Graham, M.; Cresswella, P. Critical residues in the PMEL/Pmel17 N-terminus direct the hierarchical assembly of melanosomal fibrils. *Mol. Biol. Cell* **2013**, 24, 964–981.

106. Kenny, N.J.; Francis, W.R.; Rivera-Vicens, R.E.; Juravel, K.; de Mendoza, A.; Diez-Vives, C.; Lister, R.; Bezares-Calderon, L.A.; Grombacher, L.; Roller, M.; et al. Tracing animal genomic evolution with the chromosomal-level assembly of the freshwater sponge Ephydatia muelleri. *Nat. Commun*. **2020**, 11, 3676.

107. Moroz, L.L.; Kocot, K.M.; Citarella, M.R.; Dosung, S.; Norekian, T.P.; Povolotskaya, I.S.; Grigorenko, A.P.; Dailey, C.; Berezikov, E.; Buckley, K.M.; et al. The ctenophore genome and the evolutionary origins of neural systems. *Nature* **2014**, 510, 109.

108. He, X.L.; Zhang, J.Z. Rapid subfunctionalization accompanied by prolonged and substantial neofunctionalization in duplicate gene evolution. *Genetics* **2005**, 169, 1157–1164.

109. Lynch, M.; Force, A. The probability of duplicate gene preservation by subfunctionalization. *Genetics* **2000**, 154, 459–473.

110. Holland, P.W.H.; Garciafernandez, J.; Williams, N.A.; Sidow, A. Gene Duplications And The Origins Of Vertebrate Development. *Development* **1994**, 1994, 125–133.

111. Dehal, P.; Boore, J.L. Two rounds of whole genome duplication in the ancestral vertebrate. *PLoS Biol.* **2005**, 3, e314.

112. Ohno, S. Evolution by Gene Duplication; Springer: Berlin, Germany, 1970.

113. Putnam, N.H.; Butts, T.; Ferrier, D.E.K.; Furlong, R.F.; Hellsten, U.; Kawashima, T.; Robinson-Rechavi, M.; Shoguchi, E.; Terry, A.; Yu, J.K.; et al. The amphioxus genome and the evolution of the chordate karyotype. *Nature* **2008**, 453, 1064–1071.

114. Smith, J.J.; Keinath, M.C. The sea lamprey meiotic map improves resolution of ancient vertebrate genome duplications. *Genome Res*. **2015**, 25, 1081–1090.

115. Sacerdot, C.; Louis, A.; Bon, C.; Berthelot, C.; Crollius, H.R. Chromosome evolution at the origin of the ancestral vertebrate genome. *Genome Biol*. **2018**, 19, 166.

116. Simakov, O.; Marletaz, F.; Yue, J.X.; O'Connell, B.; Jenkins, J.; Brandt, A.; Calef, R.; Tung, C.H.; Huang, T.K.; Schmutz, J.; et al. Deeply conserved synteny resolves early events in vertebrate evolution. *Nat. Ecol. Evol.* **2020**, 4, 820.

117. Smith, J.J.; Kuraku, S.; Holt, C.; Sauka-Spengler, T.; Jiang, N.; Campbell, M.S.; Yandell, M.D.; Manousaki, T.; Meyer, A.; Bloom, O.E.; et al. Sequencing of the sea lamprey (Petromyzon marinus) genome provides insights into vertebrate evolution. *Nat. Genet*. **2013**, 45, 415–421.

118. Albalat, R.; Canestro, C. Evolution by gene loss. *Nat. Rev. Genet*. **2016**, 17, 379–391.

119. Mehta, T.K.; Ravi, V.; Yamasaki, S.; Lee, A.P.; Lian, M.M.; Tay, B.H.; Tohari, S.; Yanai, S.; Tay, A.; Brenner, S.; et al. Evidence for at least six Hox clusters in the Japanese lamprey (Lethenteron japonicum). *Proc. Natl. Acad. Sci. USA* **2013**, 110, 16044–16049.

120. Jaillon, O.; Aury, J.M.; Brunet, F.; Petit, J.L.; Stange-Thomann, N.; Mauceli, E.; Bouneau, L.; Fischer, C.; Ozouf-Costaz, C.; Bernot, A.; et al. Genome duplication in the teleost fish Tetraodon nigroviridis reveals the early vertebrate proto-karyotype. *Nature* **2004**, 431, 946–957.

121. Meyer, A.; Van de Peer, Y. From 2R to 3R: Evidence for a fish-specific genome duplication (FSGD). *Bioessays* **2005**, 27, 937–945.

122. Inoue, J.; Sato, Y.; Sinclair, R.; Tsukamoto, K.; Nishida, M. Rapid genome reshaping by multiple-gene loss after whole-genome duplication in teleost fish suggested by mathematical modeling. *Proc. Natl. Acad. Sci. USA* **2015**, 112, 14918–14923.

123. Pasquier, J.; Braasch, I.; Batzel, P.; Cabau, C.; Montfort, J.; Nguyen, T.; Jouanno, E.; Berthelot, C.; Klopp, C.; Journot, L.; et al. Evolution of gene expression after whole-genome duplication: New insights from the spotted gar genome. *J. Exp. Zool. Part. B Mol. Dev. Evol.* **2017**, 328, 709–721.

124. Chrystal, P.W.; Footz, T.; Hodges, E.D.; Jensen, J.A.; Walter, M.A.; Allison, W.T. Functional Domains and Evolutionary History of the PMEL and GPNMB Family Proteins. *Molecules* **2021**. 26, 3529.

125. Hoashi, T.; Muller, J.; Tamaki, K.; Ohara, K.; Hearing, V.J. The internal repeat domain of the melanosomal matrix protein PMEL17/GP100 is required for fibrillogenesis but not for intracellular trafficking. *Pigment Cell Melanoma Res.* **2008**, 21, 303.

126. Goujon, M.; McWilliam, H.; Li,W.Z.; Valentin, F.; Squizzato, S.; Paern, J.; Lopez, R. A new bioinformatics analysis tools framework at EMBL-EBI. *Nucleic Acids Res.* **2010**, 38, W695–W699.

127. Allison, W.T.; DuVal, M.G.; Nguyen-Phuoc, K.; Leighton, P.L.A. Reduced abundance and subverted functions of proteins in prion-like diseases: gained functions fascinated but lost functions affect aetiology. *Int J Mol Sci* **2017**. 18, 10, 2223.

128. Fleish, V.C.; Leighton, P.A.; Wang, H.; Pillay, L.M.; Ritzel, R.G.; Roy, B.; Tierney, K.B.; Ali, D.W.; Waskiekicz, A.J.; Allison, W.T. Targeted mutation of the gene encoding prion protein in zebrafish reveals a conserved role in neuron excitability. *Neurobiology of Disease* **2013**. 55, 11-25.

129. Louros, N.N.; Baltoumas, F.A.; Homodrakas, S.J; Iconomidou, V.A. A B-solenoid model of th ePmel17 repeat domain: insights to the formation of functional amyloid fibrils. *J Comput Aided Mol Des* **2016**. 30, 153-164.

130. Martinez-Esparza, M.; Jimenez-Cervantes, C.; Bennett, D.C.; Lozano, J.A.; Solano, F.; Garcia-Borron, J.C. The monuse silver locus encodes a signle transcript truncated by the silver mutation. *Mamm Genome* **1999**. 10, 12, 1168-1171.

131. Nguyen-Phuoc, T.-K. Using a Zebrafish Animal Model to Identify the First Candidate Gener for Pigmentary Glaucoma. University of Alberta MSc Thesis. **2018**.

132. Burgoyne, T.; O'Connor, M.N.; Seabra, M.C.; Cutler, D.F.; Futter, C.E. Regulation of melanosome number, shape, and movement in the zebrafish retinal pigment epithelium b OA1 and PMEL. *Journal of Cell Science* 2015. 128, 1400-1407.

133. Lahola Chomiak, A.A.; Walter, M.A. Molecular Genetics of Pigment Dispersion Sndrome and Pigmentary Glaucoma; New Insights into Mechanisms. *Hindawi Journal of Ophthalmology* **2018**. 2018, 5926906.

134. Noel, N.C.L.; Nadolski, N.J.; Hocking, J.C.; MacDonald, I.M.; Allison, W.T. Progressive Photoreceptor Dysfunction and Age-Related Macular Degeneration-Like Features in *rp1l1* Mutant Zebrafish. *Cells* **2020**, *9*, 2214.

135. Link, B.A.; Gray, M.P.; Smith, R.S.; John, S. W. M. Intraocular pressure in zebrafish: comparison of inbred strains and identification of a reduced melanin mutant with raised IOP. *Investigative Ophthalmology & Visual Science*. **2004**, 45 (12), 4415-4422.

136. Cameron, D.J.; Davey, P. Non-invasive intraocular pressure measurements zebrafish. *Investigative Ophthalmology and Visual Science*. **2013**, 54 (15). 1973.

137. Quint, W.M.; Tadema, K.C.D.; Crins, J.H.C.; Kokke, N.C.C.J.; Meester-Smoor, M.A.; Willemsen, R.; Klaver, C.C.W.; Iglesias, A.I. Zebrafish: an in vivo screening model to study ocular phenotypes. *Translational Vision Science & Technology*. **2022**, 11 (3), 17.

138. Gray, M.P.; Smith, R.S.; Soules, K.A.; John, S.W.M.; Link, B.A. The Aqueous Humour Outflow Pathway in Zebrafish. *IOVS* **2009**. 50, 4, 1515-1521.

139. Stella, S.L.; Geathers, J.S.; Weber, S.R.; Grillo, M.A.; Barber, A.J.; Sundstrom, J.M.; Grillo, S.L. Neurodegeneration, Neuroprotection and Regeneration in the Zebrafish Retina. *Cells* **2021**, 10, 633.

140. Hong, Y.; Luo, Y. Zebrafish Model in Ophthalmology to Study Disease Mechanism and Drug Discovery. *Pharmaceuticals* **2021**, 14, 716.

141. Giannaccini, M.; Chiellini, M.; Usai, A.; Chiellini, F.; Guadagni, V.; Andreazzoli, M.; Ori, M.; Pasqualetti, M.; Dente, L.; Raffa, V. Neurotrophin conjugated nanoparticles prevent retina damage induced by oxidative stress. *Cell. Mol. Life Sci*. **2018**, 75, 1255–1267.

142. Sherpa, T.; Fimbel, S.M.; Mallory, D.E.; Maaswinkel, H.; Spritzer, S.D.; Sand, J.A.; Li, L.; Hyde, D.R.; Stenkamp, D.L. Ganglion cell regeneration following whole-retina destruction in zebrafish. *Dev. Neurobiol.* **2007**, 68, 166–181.

143. McMahon, C.; Semina, E.V.; Link, B.A. Using Zebrafish to study the complex genetics of glaucoma. *Comparative Biochemistry and Physiology, Part C*. **2004**, 138, 343-350.

144. French, C.R. Mechanistic Insights into Axenfeld-Rieger syndrome from Zebrafish foxc1 and pitx2 Mutants. *Int. J. Mol. Sci.* **2021**, *22*, 10001.

145. Veth, K.N.; Willer, J.R.; Collery, M.P.; Willer, G.B.; Wagner, D.S.; Mullins, M.C.; Udvadia, A.J.; Smith, R.S.; John, S.W.M.; Gregg, R.G.; Link, B.A. Mutations in zebrafish lro2

result in adult-onset ocular pathogenesis that models myopia and other risk factors for glaucoma. *PLoS Genetics.* **2011**, 7 (2), e1001310.

146. Hoffert, J.R. Observations on ocular fluid dynamicsand carbonic anhydrase in tissues of lake trout (Salvelinus fontinalis). *Comparative Biochemistry and Physiology Part A.* **1966**, 17 (1), 107-114.

147. Hu, Y.; Danias, J. Non-invasive intraocular pressure measurement in animal models of glaucoma. *Methods Molecular Biology.* **2018**, 1695, 49-61.

148. Mohoric, P.J.; Stengard, M. Ophthalmic examination and findings in adult red drum fish (Sciaenops ocellatus). *Veterinary Ophthalmology.* **2008**, 11 (6), 415-416.

149. Tehve-Swallow, K; Harms, C.A. Intraocular pressure, exophthalmia, and effect of an ophthalmic carbonic anhydrase inhibitor in fish eye. *Proceedings IAAAM Conference* **2002**, 1-2.

150. Hepps Keeney, C.; Vorbach, B.; Clayton, L.; Seeley, K. Intraocular pressure in clinically normal brook trout (Salvelinus fontinalis) by means of rebound tonometry. *Journal of Zoo and Wildlife Medicine.* **2019**, 50 (1), 107-110.

151. Lamglait, B.; Jalenques, M.; Summa, N.; Youcef, W.A.; Vargneau-Grosset, C. A preliminary study of intrinsic and extrinsic factors influencing intraocular pressure in brook trout (Salvelinus fontinalis). *Journal of Zoo and Wildlife Medicine.* **2020**, 51 (4), 1012-1016.

152. Lynch, G.L.; Hoffman, A.; Blocker, T. Central corneal thickness in koi fish: effects of age, sex, body length and corneal diameter. *Veterinary Ophthalmology*. **2007**, 10 (4), 211-215.

153. Cleymaet, A.M.; Henriksen, M.dL.; Pederson, S.L., Sadar, M.J.; Johnston, M.; Tovar-Lopez, G.; Daniels. J.; Sharley, L.; Teixeira, L.B.C. Pathology in Practice. *Journal of the American Veterinary Medical Association* **2022**. 259, S2.

154. Cervino, A. Rebound tonometry: new opportunities and limitations of non-invasive determination of intraocular pressure. *British Journal of Ophthalmology*. **2006**, 90 (12), 1444-1446.

155. Gelatt, K. N.; Gilger, B.C.; Kern, T. J. Veterinary Ophthalmology 5th edition. John Wiley and Sons Incorporated. 2013.

156. Hanwell, D.;Hutchinson, S.A.; Collymore, C.; Bruce, A. E.; Louis, R.; Ghalami, A.; Allison, W. T.; Ekker, M.; Eames, B. F.; Childs, S.; Kurrasch, D. M.; Gerlai, R.; Thiele, T.; Scott, I.; Ciruna, B.; Dowling, J.J.; McFarlane, S.; Huang, P.; Wen, X.-Y.; Akimenko, M.-A.; Waskiewicz, A.J.; Drapeau, P.; BAbiuk, L.A.; Dragon, D.; Smida, A.; Buret, A. (G.); O'Grady, E.; Wilson, J.; Sowden-Plunkett, L.; Robinson, J.V.; Tropepe, V. Restrictions on the importation of zebrafish into Canada associated with spring viremia of carp virus. *Zebrafish*. 2016, 13, S153-S163.